Multilayer Thin Films by Layer-by-Layer (LBL) Assembly of Functional Polyelectrolytes: Their Optical and Electrochemical Properties.

Dissertation

Zur Erlangung des Grades
"Doktor der Naturwissenschaften"
am Fachbereich Chemie, Pharmazie und Geowissenschaften
der Johannes-Gutenberg-Universität in Mainz

von M.Sc. Kyungsun Choi

geboren in Seoul, Korea

Mainz 2006

PUBLICATIONS

[1]   "Amphotropic LC Polymers and Their Multilayer Build-up", K. Choi, R. Mruk, A. Moussa, A. M. Jonas, R. Zentel, *Macromolecules* **2005**, 38, 9124.

[2]   "Electrochemical and Electrochromic Properties of Layer-by-Layer Polymer Films", K. Choi, R. Zentel, *Polymer Preprints*. **2006**, 47, 1, 386.

[3]   "Multilayer Thin Films by Layer-by-Layer Assembly of Hole and Electron Transport Polyelectrolytes: Their Optical and Electrochemical Properties.", K. Choi, R. Zentel, *Macromol. Chem. Phys*. **2006**, 207, 1870.

[4]   "High Contrast Ratio and Rapid Switching Organic Polymeric Electrochromic thin films Based on Triarylamine derivatives from Layer-by-Layer Assembly". K. Choi, S. Yoo, Y. E. Sung, R. Zentel, *Chem. Mater*. **2006**, accepted.

[5]   "Vacuum-deposited Triarylamine Polymer Thin-Film and Its Structure and Electronic Properties as Hole Transporting Layer". K. Choi, J. Kwak, C. Lee, H. Kim, K. Char, D. Kim, R. Zentel, *Chemical Vapor Deposition*. **2006**, submitted.

POSTERS

[1]   "Electrochemical and electrochromic properties of Layer-by-Layer polymer films" K. Choi, R. Zentel, 231st ACS National Meeting, Atlanta, oral presentation session, March 2006, U. S. A.

[2]   "Multilayer Thin Films by Layer-by-Layer Assembly of Hole and Electron Transport Polyelectrolytes: Their Optical and Electrochemical Properties" K. Choi, R. Zentel, September 2006, CDCh, Mainz, Germnay.

TABLE OF CONTENTS

1. Introduction

Nanoscience is the world of atoms, molecules, macromolecules, quantum dots, and macromolecular assemblies and it aims at manipulating atoms, molecules and nanosize particles in a precise and controlled manner.[1] It is dominated by surface effects such as van der Waals force attraction, hydrogen bonding, electronic charge, ionic bonding, covalent bonding, hydrophobicity, hydrophilicity, quantum mechanical tunneling and the virtual exclusion of macro-scale effects such as turbulence and inertia. For example, the vastly increased ratio of surface area to volume opens new possibilities in surface-based science, such as catalysis. The fascination with nanotechnology stems from these unique quantum and surface phenomena that matter exhibits at the nano-scale, making possible novel applications and interesting materials.

One promise of nanoscience is improvement in thin-film structures with increased surface area of a material. Nano-scale control of the structure of organic/polymeric materials is a prerequisite to the fabrication of sophisticated functional devices. In this dissertation, so-called layer-by-layer (LBL) assembly technique is particularly used as simple system wherein nano-scale control of the structure in one direction is easily attainable. The ionic self-assembly technique, introduced by Decher in 1991 (G. Decher, Macromol. Chem. Macormol. Symp., 1991, 46, 321-327) provides an elegant way of controlling the composition of the resulting assemblies and the thickness of an individual layer on the nanometer scale. This method can easily be adapted for automated fabrication, and is applicable to any substrate shape. The thickness of a single polyelectrolytes layer is of the order of several Angstroms and, therefore, the total film thickness can be precisely controlled by the number of adsorbed layers. Large varieties of charged materials, including almost all kinds of polyions, dyes, organic/inorganic particles, proteins, viruses, and other biosystems have been incorporated into multilayer assemblies using this technique. These thin film assemblies have potential applications in nonlinear opticl materials, conductive films, permselective gas membranes, light emitting device, sensors, and ets.

Chapter 1 gives an overview about LBL self-assembly technique, suggesting that this technique easily creates high-performance material structures. The scientific interest of the LBL technique is based on the possibility of designing and manipulating molecular

architectures composed of a number of functional materials and studying physical phenomena on a molecular level.

1.1. Layer-by-Layer (LBL) Assembly

With nanotechnology, a large set of materials with distinct properties (optical, electrical, or magnetic) can be fabricated as thin nano-scale films. The multilayers are particularly simple systems wherein nanoscale control of the structure in one direction is easily attainable. There are different ways to build organic or hybrid organic/inorganic multilayers, among which the Langumir-Blodgett deposition technique[2] and chemical self-assembly[3] (using e.g., functional silanes[4], thiols[5], or α,ω-biphosphonic acids[6]) were mostly known one decade ago. Layer-by-layer (LBL) self-assembly, also known as electrostatic self-assembly (ESA), is the most recent addition to this collection of techniques and a very promising one indeed, owing to its versatility, simplicity and environmental friendliness.[7,8] However, by contrast with older methods, LBL provides essentially amorphous films, with profuse interpenetration of neighbouring "layers". This may certainly be seen as one of the advantages of the technique, since it avoids defect propagation from layer to layer, a nagging problem of other multilayer construction techniques.[9] In addition, it is a simpler technique involving simple equipment and preparation and can be applied to larger substrate dimensions. A large variety of water-soluble macroions or polyions can be used. The individual layers can have distinct molecular thicknesses and ordering.[10]

1.1.1. Basic Mechanism of LBL Assembly

The LBL multilayers are simply formed by the alternating deposition of oppositely charged polyelectrolytes such that the charge oscillates between positive and negative with each layer deposition. While electrostatic attraction between the oppositely charged polyelectrolytes is generally thought to drive the depositions, the amount and conformation of adsorbed chains are dramatically dependent on processing parameters, particularly ionic strength and pH of the deposition baths, as well as the charge densities of both polyelectrolyte components. A number of articles have explored the effects of molecular structure, substrate, charge density,

ionic strength, deposition pH and rinsing conditions on multilayer stability.[11,12] They concluded that multilayer stability is largely governed by polymer charge density and solution ionic strength, with high charge densities and low ionic strengths favoring multilayer formation. Furthermore, the driving forces for the LBL assembly need not be electrostatic interaction. Other forces, such as hydrogen bonding,[13,14] coordination bonding,[15,16] charge transfer,[17] molecular recognition,[18] etc. can also be used as the driving force for the assembly process.

Although the LBL technique is based on electrostatic attraction between positively and negatively charged species, the primary driving force is presumably entropy, not enthalpy.[19] The complexation of the polyions by a charged surface liberates undissociated low molar mass counterions, thus increasing the entropy of the system. An additional entropic gain may derive from the liberation of solvent molecules from the solvation shell of the polymer-bound ionic groups. During consecutive adsorption steps, the substrate is deposited with the oppositely charged polymer solutions and then between these two steps, the growing films are normally rinsed with pure solvent, to remove adhering polymer solution. This washing step may have several additional consequences.

The equalibria considered in this dissertation are variations of place-exchange reactions. In its most generic form, the interaction between charged polymer segments is represented by Figure 1.1.1. Upon complexation, polyelectrolyte segments form ion pairs and release their counterions. Electrostatic neutrality is maintained and no chemical bonds are formed. The term "ion pairing" is used to describe an energetically favorable pairing of polymer segments, drivened by the loss of water and counterions. From the perspective of a single polyelectrolyte segment, an appositely charged segment and a counterion compete to balance the charge. There are two arenas where this competetion for charge takes place. The first is in the initial formation of the polylectrolyte complexation. Individual solution phases of macromolecules come together, expelling their counterions as they complex. For a polyelectrolyte adsorbing to an oppositely charged surface, the surface counterions are displaced by adsorbing polymer segments. In the second arena, the chemical potential of salt in solution can cause swelling or infiltration of ions into a bulk polyelectrolyte complex after it has been formed. For assembled multilayers, there is a clear phase change on going from complexed polymer to solution.

On consideration of the equilibria above, it is clear that elecroneutralization is the dominant mechanism,[20] but an analysis of the overall driving force must include consideration of all charged species. The situation cannot be described simply by vacuum electrostatic between naked, isolated charges, which would yield emormous free energy changes. The driving force is ion pairing between polyelectrolyte segments, driven by release of counterions and water. Additional salt ions modify the overall free energy of interaction by competing for polymer charge. Given this, the mechanism is better defined as competitive ion pairing.
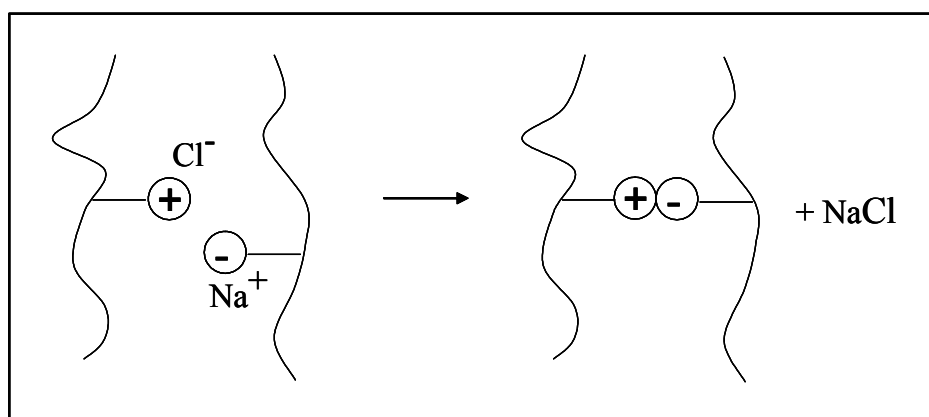
Figure. 1.1.1. Complexation between positively and negatively charged polyelectrolyte segments releasing counterions.

A model of the film formation by adsorption of charged polyionic macromolecules on an oppositely charged surface could help for better understanding of whole adsorption process. Tsukruk et al. has investigated the LBL process by the model concept with both Poly(styrenesulfonate), PSS and Poly(allylamine), PAA molecular layers versus deposition time, *t*. (Figure 1.1.2., *Macromolecules* **1997**, 30, 6615) It is speculated that assembly of polyions on charged surface is indeed a two stage process (fast and slow). At the very initial stage of film formation, within the first 1-2 min of self-assembly, charged PSS polymer chains are adsorbed inhomogeneously, mainly on selected sites of oppositely charged substrates with high concentrations of local charges (scratches, holes, edges, and foreign microparticles). Apparently at this stage of deposition, chains are tethered to the surface by only a few segments and thus virtually preserve their coiled conformation. And then polymer

chains are relaxed to a dense packing during the long second stage of self-assembly. Presumably, a stable homogeneous polymer monolayer which covers the original surface is formed only after complete "relaxation" of absorbed macromolecules. Concerning the deposition time, t, a longer deposition time allows macromolecules to equilibrate and form a complete monolayer. Polymer islands are gradually spread out over the surface: their height decreases to 1-1.5 nm for adsorption times after 10-30 min. This process results in homogeneous coverage of the surface with flattened macromolecular chains.
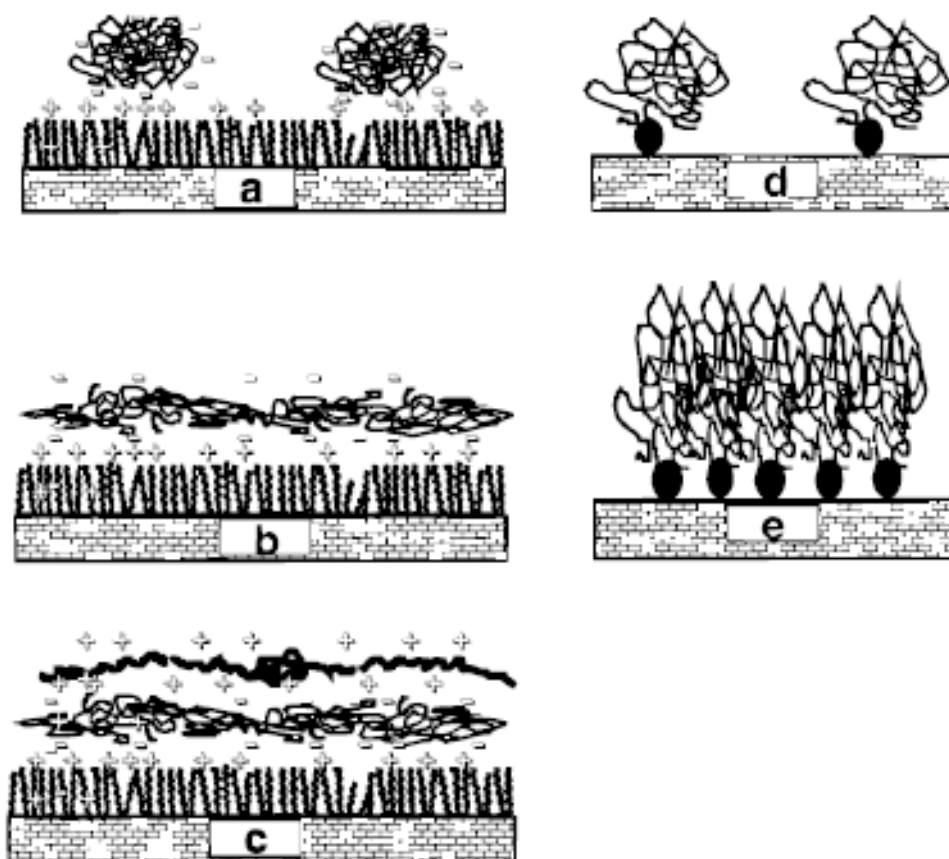
Figure 1.1.2. Models of surface microstructure for the polyionic molecular layers. (a) PSS at the shortest deposition time (<5 min). (b) PSS at the longest deposition time (>10 min). (c) PSS/ PAA complete bilayer. (d) Comparison with polymer brushes in the initial stage of tethering by one sticky end. (e) Polymer brushes in a dense state.

1.1.2. Multilayer Structure

The practical set-up for the multilayer build-up may be extremely simple, e.g. a solid support with a charged surface is exposed to the solution of a polyion of opposite charge for a short time and then just dipping the support into beakers filled with the polymer solutions. (Figure 1.1.3) The amount of adsorbed material is self-limiting and surplus polymer solution adhering to the support is removed by simple washing step. Under proper conditions, polymeric material with more than the stoichiometric number of charges (relative to the substrate) is adsorbed, so that the sign of the surface charge is reversed. In consequence, when the substrate is exposed to a second solution containing a polyion of opposite charge, an additional polyion layer is adsorbed. But this reverses the sign of the surface charge again. Consecutive cycles with alternating adsorption of polyanions and polycations result in the stepwise growth of polymer films. This deposition procedure is cycled to obtain desired thickness multilayers.
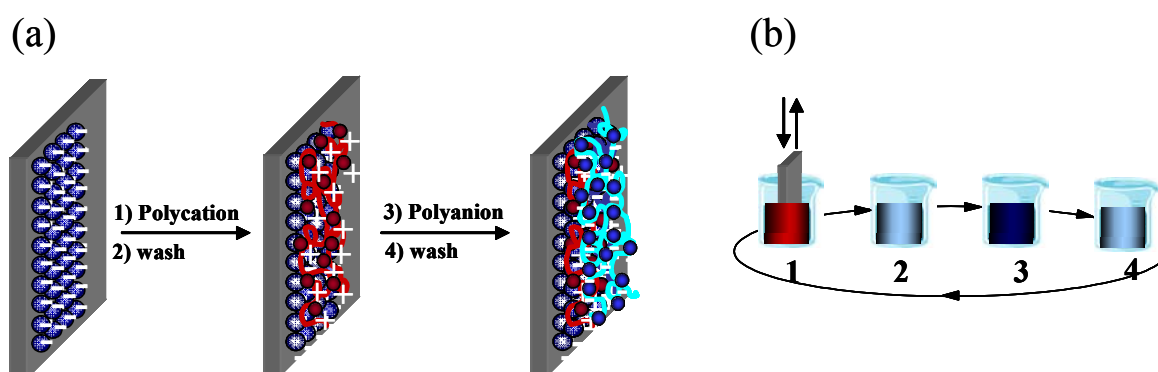
Figure 1.1.3. (a) Simplified molecular concept of the adsorption steps depicting film deposition. (b) Schematic of the film deposition process using glass slide and beakers.

In 1991, Decher has investigated multilayer structure composed of 10 bilayers with the film model as depicted in Figure 1.1.4. In a simplified polyelectrolyte multilayer structure composed of 10 layers, each layer is represented by an arbitrarily chosen sinusoidal concentration profile. The 50 % overlap of layers of equal charge has the consequence that at

any point inside the film (the substrate-film and film-air interfaces are different), the sum of the concentration of equal ionic groups is unity in both the cationic and anionic case, as represented by the lines composed of blue dots (concentration profile of anionic groups) and red dots (concentration profile of cationic groups). The line composed of green dots represents the concentration profile for a label applied to every fourth layer and shows that chemical functional groups (or labels) can be precisely positioned at certain distances from the substrate or with respect to each other. Thus, Figure 1.1.4 represents a film model in which the high overlap of layers of equal charge allows for a 1:1 stoichiometry of anionic and cationic groups within the film and provides the base for a true layer structure.
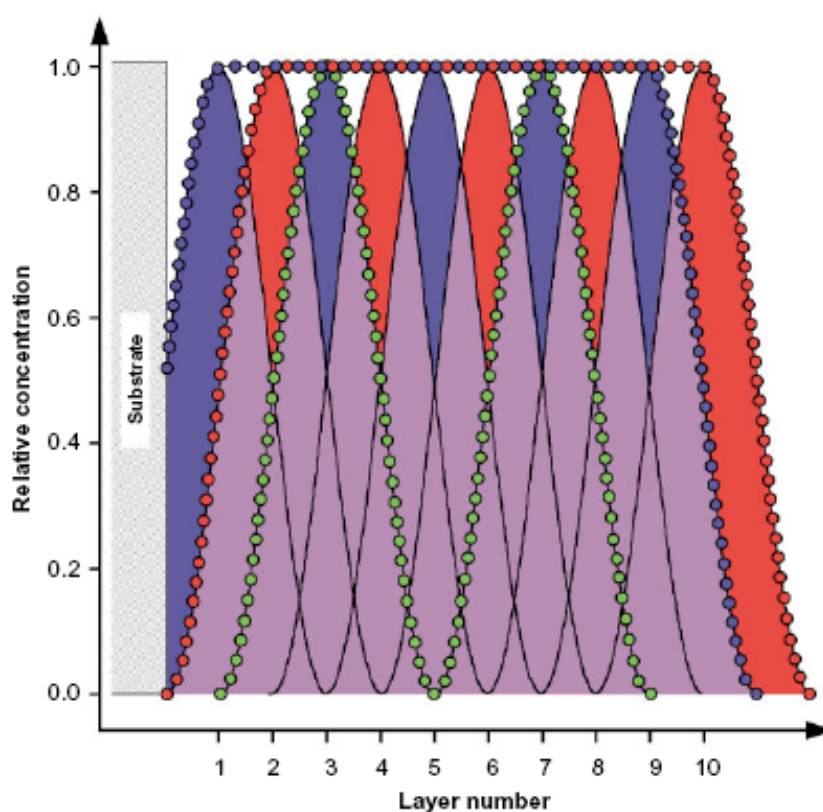
Figure 1.1.4. Schematic of a polyelectrolyte multilayer composed of 10 layers [(A/B/A/B)$_n$ architecture 5 deuterium labels in layers 3 and 7].

Usually, multilayer films prepared by the LBL method show a strong interpenetration between the oppositely charged polymer layers. Extensive interpenetration of adjacent

polyelectrolyte layers is an inherent property of these multilayer systems, and information about the extent of interpenetration is important for the generation of layered superstructures.[20] X-ray and neutron reflectometry measurements of multilayers have shown that a single layer overlaps approximately over four adjacent layers on both sides. The new polyelectrolyte layer can, therefore, interact with material seven to eight layers below the film surface.[21] In these cases, the physical extent of interpenetration is approximately 7-15 nm.

1.1.3. Various LBL Assemblies (Solution-dipping, Spin-coating and Spraying Methods)

In a variation of the deposition method, the spin-coating and spraying methods were introduced more recently. Actually, well known LBL assembly developed by Decher is so called solution-dipping LBL method. The practical set-up of this method is extremely simple as described previously; at each time, the substrate is dipped into the polyanion and polycation solutions, and then the substrate is rinsed with plenty of water between these two steps. These deposition procedures are then cycled to obtain desired number of bilayers and the multilayered films are dried under nitrogen gas purging at the end of their fabrication. However, one disadvantage of the technique is a rather long time required to assemble a monomolecular film that lasts in general between 1 min and 1 h depending on adsorbing systems, typically 10-20 min.

As one of the variations, spin-coating LBL method was demonstrated by Hong[22,23] and also by Wang.[24] The spin-coating method has the advantage that only small amounts of liquids are needed to coat large surface areas. In principle, there are four distinct stages to the spin coating process. The first stage is the deposition of the coating fluid onto the substrate. The second stage is when the substrate is accelerated up to its final and desired rotation speed. The third stage is when the substrate is spinning at a constant rate and fluid viscous forces dominate fluid thinning behaviour. Finally, the fourth stage is when the substrate is spinning at a constant rate and solvent evaporation dominates the coating thinning behaviour. Because of this spinning process, different adsorption mechanism occurs between the solution-dipping and the spin-coating methods.

In the case of the conventional solution-dipping method, polyelectrolyte chains are allowed to diffuse toward the substrate under the influence of the electrostatic interaction and then the adsorbed chains rearrange themselves on the surface. On the other hand, in the spin-coating process, the adsorption and rearrangement of adsorbed chains on the surface, and the elimination of weakly bound polymer chains from the substrate are almost simultaneously achieved at a high spinning speed for a short time. Fast elimination of water in the spinning process significantly increases the molar concentration of the polyelectrolyte solution during the short deposition time.[25] This increase in the polyelectrolyte concentration yields thick layers, despite the thin film formation typically provided by the centrifugal force and air shear force.[26-28] It also increases the electrostatic attraction between oppositely charged polymers because the presence of water molecules in the assemblies generally screens the electrostatic attraction. However, this method is restricted with respect to substrate size and planarity.[29-32] Figure 1.1.5 schematically represents the driving forces caused by the spinning process.
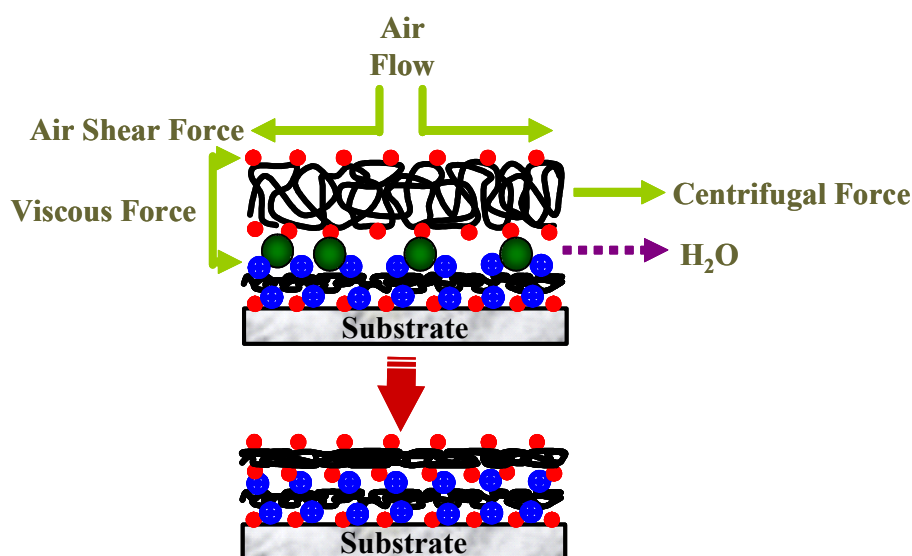
Figure 1.1.5. A side view schematic depicting the build-up of multilayer assemblies by consecutive spinning process of anionic and cationic polyelectrolytes. (K. Char. *Adv. Mater.* **2001**, 13, 14, 1076)

As the second variation of the LBL assembly, the spraying method was introduced by Schlenoff.[33] The influence of various parameters such as spraying time, polyelectrolyte concentration, and effect of film drying during multilayer construction was investigated. The

spraying method is convenient, fast, and more generally applicable for the coating of large surfaces. When the rinsing solution is replaced by the one containing the polyelectrolyte of opposite charge using mild agitation only, the solution-dipping method forms a zone with very low polyelectrolyte concentration ("depletion zone") close to the surface of the substrate. Depending on the solution viscosity and the diffusion constant of the polyelectrolyte, the depletion zone is expected to vary in thickness. The depletion zone possesses, thus, a gradient of polyelectrolyte concentration. It takes typically several tens of seconds or even minutes before the adsorption becomes homogeneous over the whole surface and the adsorption process becomes well controlled.

On the other hand, the spraying method provides homogeneous films (e.g., extremely short contact times) over large areas. Because drainage constantly removes a certain quantity of the excess materials arriving at the surface, one can even skip the rinsing step and, thus, speed up even further the whole build-up process. Interestingly, films prepared by dipping are always thicker than films prepared by spraying although in both cases it is safe to assume that enough material is provided to approach the plateau of adsorption. Therefore, spraying method allows building films even much faster and thinner films than the conventional solution-dipping method during repeated re-spraying cycles or re-dipping cycles. However, the effects of rinsing and the differences in film thickness between dipping and spraying are not fully understood at the present time. Figure 1.1.6 represents the experimental set-up for multilayer film deposition by the spraying method.

(a)

(b)
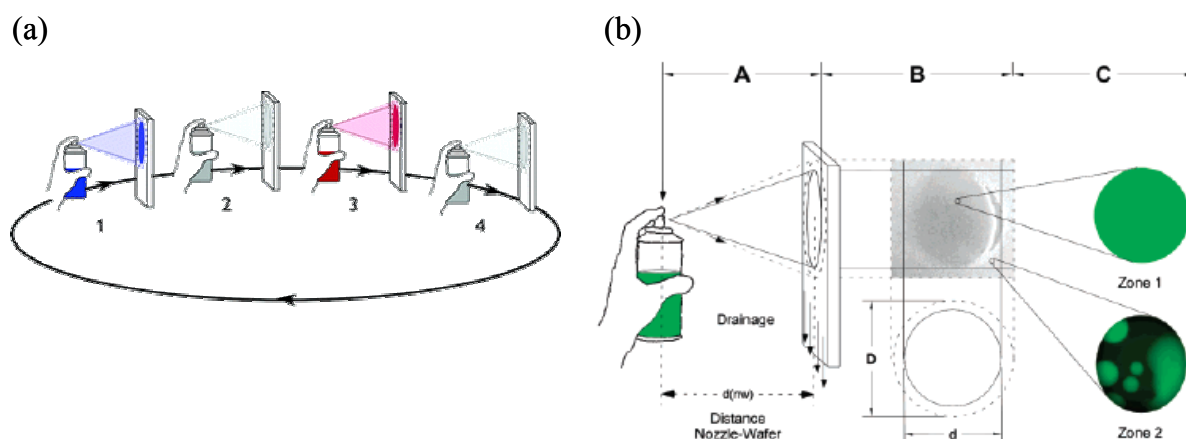
Figure 1.1.6. Experimental set-up for multilayer film deposition by the spraying method. (a) Concept of the film deposition process (b) A: Perpendicular spray of polyelectrolytes on a vertically oriented substrate indicating the spray cone, the distance between the nozzle and the receiving surface, and the direction of the draining liquid. B: Spray on a sheet of paper that changes its color as a function of the quantity of water delivered. C: Fluorescent images taken by fluorescence microscopy of a multilayer film. (G. Decher, *Langmuir* **2005**, 21, 7558)

1.2. Materials for LBL Assembly

Organic semiconductors and conjugated polymers are currently of wide interest for applications in electronic and optoelectronic devices including light-emitting diodes,[34,35] thin film transistors,[36-38] photovoltaic cells[39,40] and electrochromic devices.[41,42] The conjugated polymers have the advantages of allowing an easy and low-cost manufacture of large area displays using solution-processing of film-forming polymers. The vast majority of synthetic effort and structure-property studies in these fields have been devoted to organic and polymeric semiconductors having p-type (electron donor, hole transport)[43,44] and n-type (electron acceptor, electron transport)[45-47] properties.

Numerous materials have been developed for the p-type (electron donor, hole transport) materials. Most of those materials are arylamine derivatives[48,49] for the purpose of developing photo- and electro-active amorphous molecular materials. These materials are a novel class of

electron rich molecules consisting of a fully conjugated π-electron system and they are designed to make an amorphous thin film. These arylamine derivatives show high hole drift mobility (on the order of 10^{-3} /Vs for xerography). Molecular structures of the p-type (electron donor, hole transport) materials are illustrated in Figure 1.2.1.

TPD   TTB   NPD

TPTE   PYR-D2
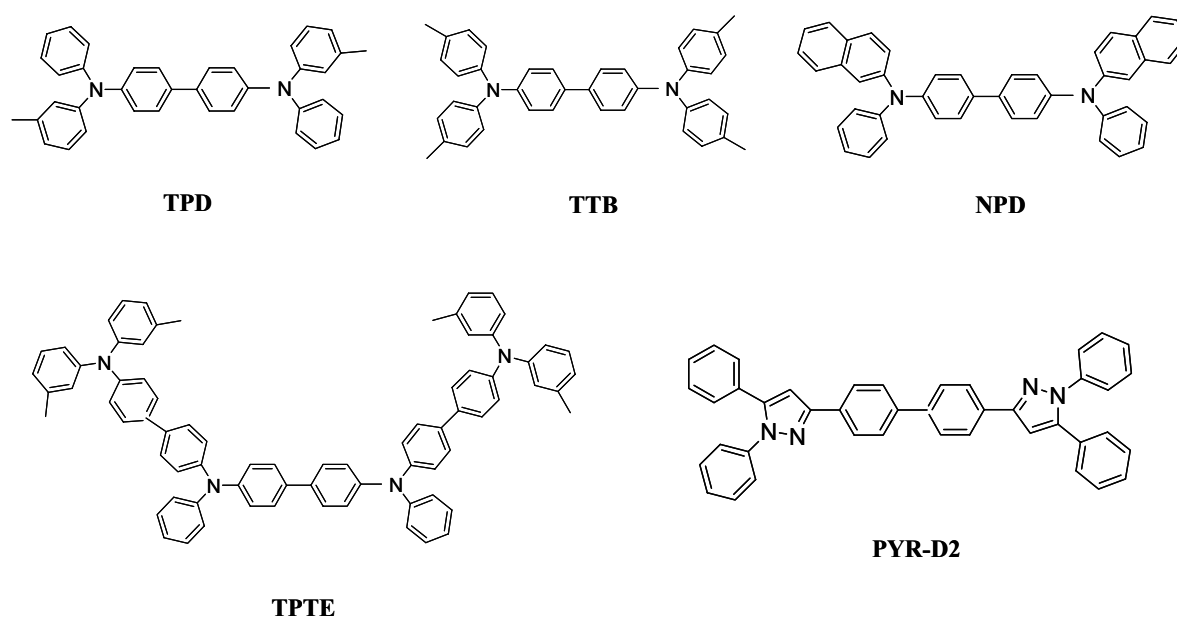
Figure 1.2.1. Molecular structures of the p-type (electron donor, hole transport) materials.

The n-type (electron acceptor, electron transport) property has been observed in fluorinated oligothiophenes,[50] perfluorinated oligophenylenes,[51] fluorinated phthalocyanines,[52] naphthalene and perylene diimides,[53] and silole compounds.[54] Compared to p-type semiconductors, the number of n-type semiconductors is still limited and their device performances are not satisfactory. The development of good n-type materials is crucial and to obtain high electron mobility, organic semiconductors should have proper LUMO energy levels near the work function of electrodes. Structure and half-wave reduction potentials of the well known n-type materials are shown in Figure 1.2.2. However, well known p-type and n-type organic and polymeric semiconductors with free ionic groups are not applicable with oppositely charged polymer by the LBL assembly method for the electronic devices. Because the ionic conductivity would lead to a short circuit in the devices.[55] This problem can be

solved, in principle, by the formation of polyelectrolyte complexes of the ionic semiconducting polymer and an oppositely charged polymer.
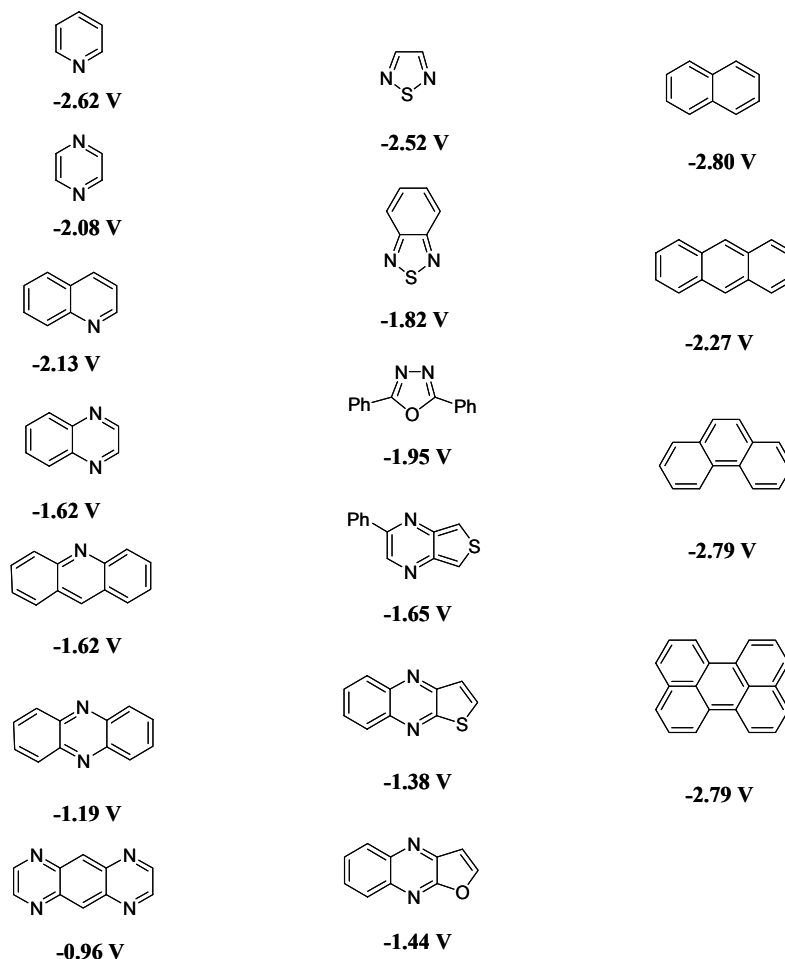
Figure 1.2.2. Structure and half-wave ($E_{1/2}$) reduction potentials (vs SCE) of aromatic hydrocarbons and heterocycles (Samson A. Jenekhe, *J. Am. Chem. Soc.* **2003**, 125, 13548)

The LBL assembly has been used with a wide variety of charged materials ranging from inorganic to organic and low molecular weight to polymeric materials due to the technique's flexibility and ease of use.[11(b)] Among all charged species, assemblies of electro- and photo-active semiconducting materials have attracted considerable attention. These assemblies with p-type and n-type materials will provide models for the investigation of nanoarchitecture and function in one self-assembly system. It is one of the ultimate goals of scientists and the best

way to fabricate nanosized devices and sensors. Well known electro- and photo-active building blocks used for LBL are shown in Figure 1.2.3.[56]
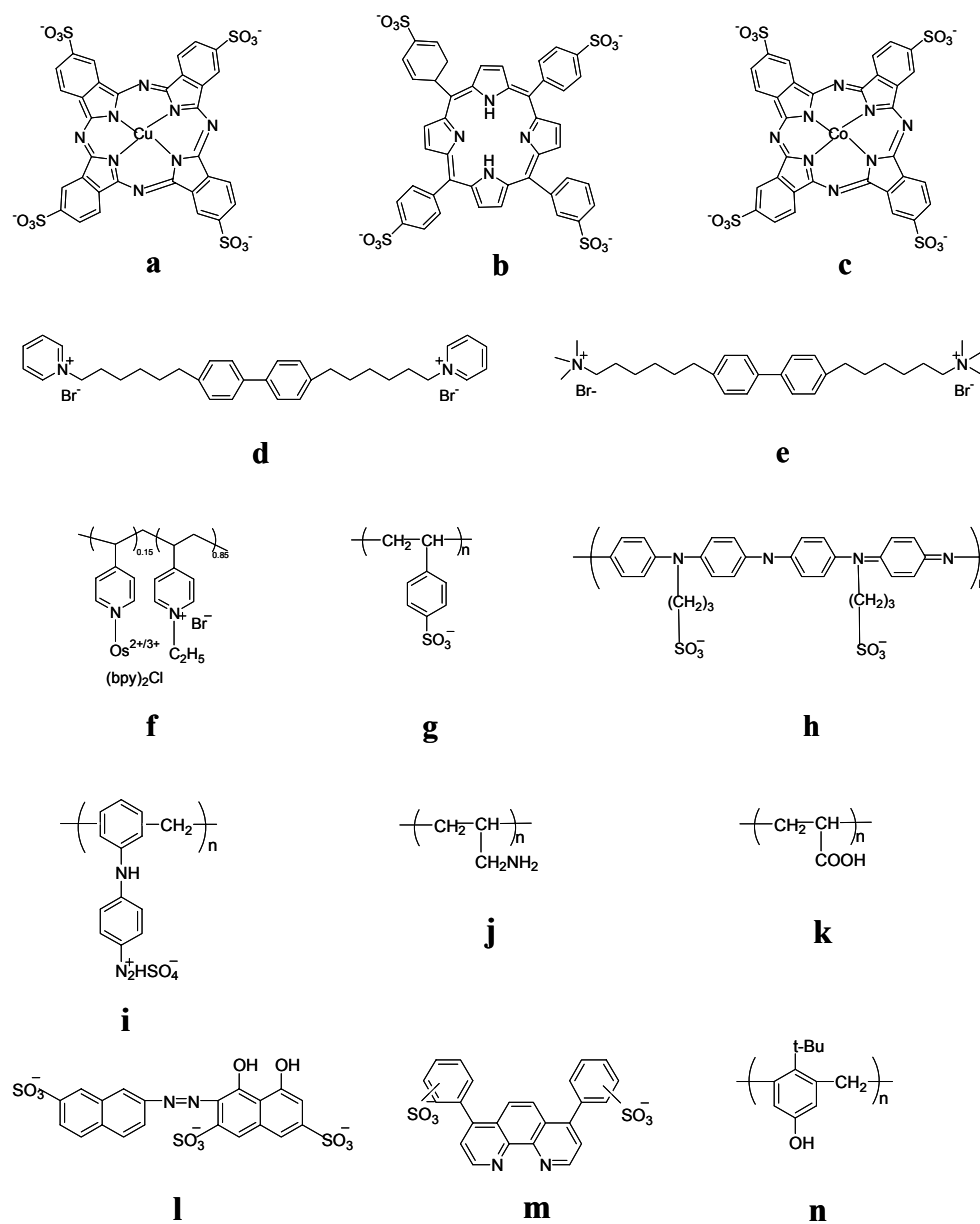
Figure 1.2.3. The electro- and photo-active building blocks for LBL assembly. (a) CuTsPc, (b) tpps₄, (c) CoTsPc, (d) PyC₆BPC₆Py, (e) NC₆BPC₆N, (f) PVP-Os, (g) PSS, (h) PAPSAH, (i) DAR, (j) PAH, (k) PAA, (l) SNAN, (m) BST and (n) Pr.

1.3. Functional LBL Assemblies with Electroactive Properties

The LBL fabrication of molecularly organized film has received tremendous attention in recent years as a simple, effective and versatile method to prepare uniform and ultrathin structures. Since composition, thickness and orientation of each layer can be effectively manipulated using this technique, it provides a route for the formation of various structures layered at the molecular level. These manipulations at the molecular level offer many potential advantages in device applications such as active components in nonlinear optical devices (NLO),[57] employing materials with selective chemical responses for sensor applications,[58] stable charge-separated assemblies for photovoltaics,[59] electrochromics (ECs)[60] and organic light-emitting diodes (OLEDs).[61] In detail, electrochromic devices (ECDs) and light emitting devices (LEDs) with LBL multilayered structure will be discussed.

1.3.1. Electrochromic Devices (ECDs)

Electrochromism is broadly defined as a reversible optical change in a material induced by an external voltage, with many inorganic and organic species showing electrochromism throughout the electromagnetic spectrum.[62] The phenomena of electrochromism was theoretically suggested by J. R. Platt[63] in 1961 and the first examples of electrochromic materials and devices were demonstrated by Deb et al.[64] when he started to work on amorphous and crystalline metal oxides at Cyanamid Corp. Among electrochromic materials, transition-metal oxides, especially the high band gap semiconductor tungsten oxide, WO_3, have received extensive attention over the past 30 years.[65] Initially transparent in the visible region, cation intercalation (reduction) of WO_3 to M_xWO_3 (M can be hydrogen or an alkali metal) leads to strong absorption bands in the visible region, making it a cathodically coloring material. Many other inorganic materials have been studied for their electrochromic properties such as Prussian Blue, oxides of V, Mo, Nb, and Ti (cathodically coloring), and oxides of Ni, Co, and Ir (anodically coloring).[66] Other electrochromic materials include organic small molecules, such as the bipyridiliums (viologens)[67] have been observed, which are a class of materials that are transparent in the stable dicationic state. More recently, composite systems, where organic molecules are adsorbed on mesoporous nanoparticles of doped metal oxides, have shown improved electrochromic properties.[68]

The most common applications of electrochromic materials include a variety of displays, smart windows, optical shutters and mirror devices. Pilkington introduced its first commercial electrochromic smart window product on glass in late 1998, while Sage Electrochromics has developed a switchable (electronically tintable) window called SageGlass. Additionally, researchers from Lawrence Berkeley Laboratories have installed and tested smart windows for office rooms in Oakland, CA, and the National Renewable Energy Laboratories (NREL) has ongoing research on developing prototypes of vertically integrated, photovoltaic powered electrochromic displays. NTERA's NanoChromics technology allows for fabrication of flexible display devices benefiting from high surface area of nanostructured metal oxides blended with organic electrochromes. Finally, Cidetec of North Spain has introduced polymer-based electrochromic false nails; probably the oddest application the field has encountered.[69]

There are three main types of electrochromic materials in terms of their electronically accessible optical states. The first type includes materials with at least one colored and one bleached state. These materials are especially useful for absorption/transmission-type device applications such as smart windows and optical shutters. Typical examples of this area are metal oxides, viologens and polymers such as poly(3,4-ethylenedioxythiophene) (PEDOT).[60] A second class of materials consists of electrochromes with two distinctive colored states. These electrochromic materials lack a transmissive state but are useful for display-type applications where different colors are desired in different redox states. Polythiophene is a good example of this type, where the thin films of this polymer switch from red to blue upon oxidation. A third class includes the growing interest in the electrochromic field, where more than two color states are accessible depending on the redox state of the material. This is the area where conjugated polymers have found the most interest due to their versatility for making blends, laminates and copolymers. Additionally, there are inherently multicolor electrochromic polymers such as PANI or poly(3,4-propylenedioxypyrrole) (PProDOP).[70]

Electrochromics are particularly well suited to large area displays because of their low power consumption and forgiving manufacturing tolerances. This electrochromics research increasingly looks to polymer thin films for advancement. Color switching in an electrochromic polymer is caused by changes to its electron excitation energy profile following reduction or oxidation; specific examples are the formation of discrete charge-

transfer complexes in poly-(viologens),[71] or the doping/undoping of conducting polymers such as poly(thiophenes).[72,73]

An absorption/ transmission-type electrochromic device operates by reversible switching of an electrochromic material between a colored (absorptive) and a transmissive (bleached) state on a transparent and conducting substrate. To achieve high contrast values in such a device, two complementary polymers are used, namely, a cathodically coloring polymer and an anodically coloring polymer, deposited onto transparent electrodes (e.g., ITO/glass, ITO/PET, or PEDOT-PSS/PET), and separated by an electrolyte (viscous gel or solid) to allow ion transport as shown in Figure 1.3.1.
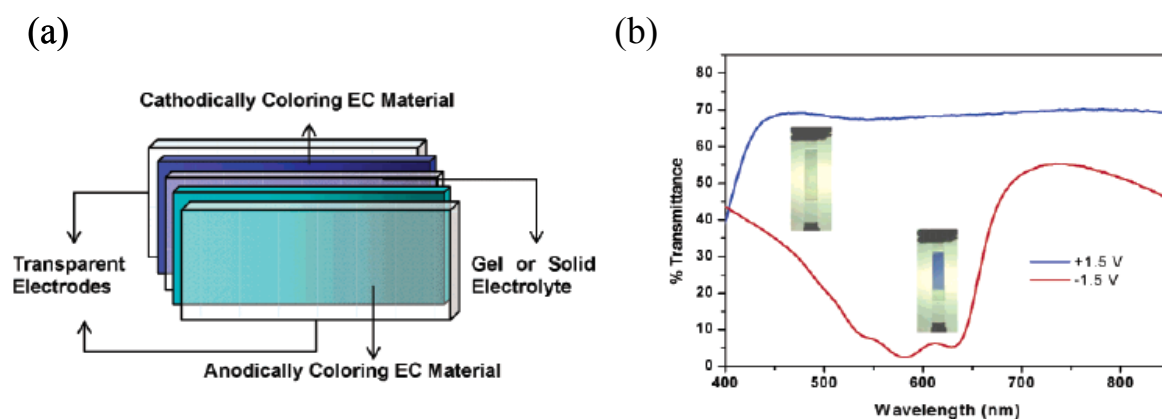
(a)　　　　　　　　　　　　　　　(b)

Figure 1.3.1. (a) Schematic representation of an absorption/ transmission-type device. (b) Percent transmittance spectra of an absorption/transmission electrochromic device composed of the complementary polymers PProDOT-Me$_2$ and N-PrSPProDOP. (J. R. Reynolds, *Chem. Mater.* **2004**, 16, 4401)

As is typical for most electroactive polymers, electrochromic polymers are customarily deposited on substrates by spin-coating, electropolymerization, or surface polymerization by chemical means. An alternative, innovative approach to film formation is the LBL assembly technique. DeLongChamp and Hammond have used the LBL assembly method to deposit soluble electrochromic polymers electrostatically on ITO electrodes and have fabricated complementary electrochromic devices by pairing PEDOT and PANI.[60] The LBL technique is the ideal tool for tailoring the properties of electroactive polymer films on the nanometer

scale. Electronically conductive LBL films of exceptional homogeneity and high conductivity have been fabricated and the multilayer thin films exhibit a fast and reversible redox switching behavior in aqueous media.[74,75] In Figure 1.3.2., electrochemical and spectrophotometric characterization such as optical switching and the spectroelectrochemistry of the multilayers are shown. The LBL assembly was composed with two readily available cathodically coloring electrochromic polymers: poly(hexyl viologen) (PXV) and the poly(3,4-ethylenedioxythiophene):poly(styrene sulfonate) (PEDOT:SPS) colloid. These results validate an LBL assembly based intermixing strategy for the design of multiple-color electrochromic electrode films.
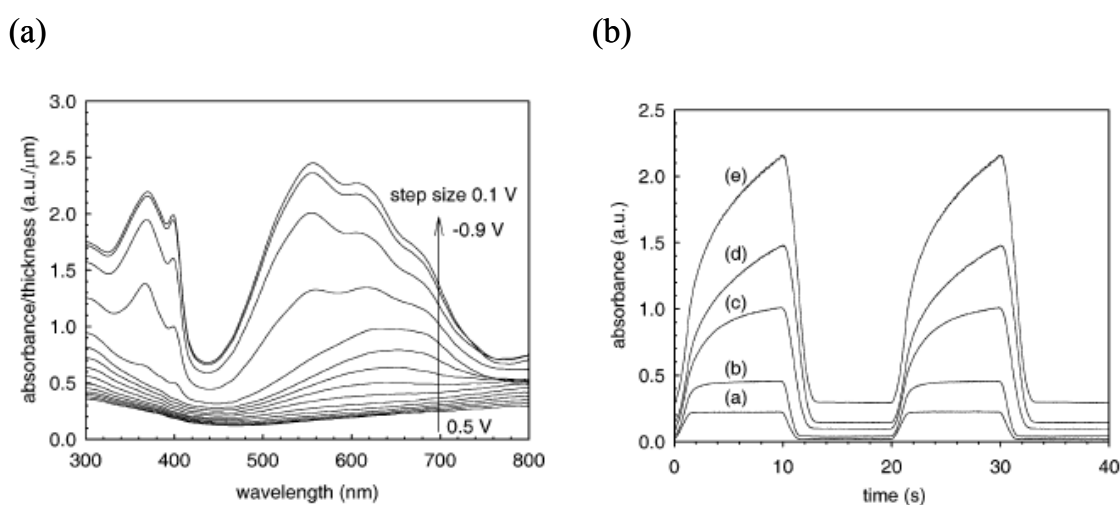
(a)   (b)

Figure 1.3.2. (a) Spectroelectrochemistry of (PXV/PEDOT:SPS)$_{40}$. Spectra were taken from 0.5 V to -0.9 V. (b) Potential step absorptometry of PXV/PEDOT:SPS films. Films of 20-, 30-, 40-, 50-, and 60-layer pairs were tested, corresponding to plots (a)-(e), respectively.

1.3.2. Light emitting Devices (LEDs)

The development of organic light emitting diodes (OLEDs) based on both vacuum deposited small molecules and spin-coated conjugated polymers continues to be an actively pursued area of research.[76] OLEDs have potential advantages of being large in area, full color and low cost. To get these advantages, however, new techniques for manipulating these novel light emitting materials into uniform thickness, large area thin films and thin film heterostructures are needed. In order to discuss the LBL assemblies for LEDs, it is necessary to briefly

describe the corresponding cell configurations and light emitting phenomena. The typical cell structure for a multi-layer OLED is: an anode (indium tin oxide (ITO) on glass substrate) / a hole transporting layer / a light-emitting layer / an electron transporting layer / a cathode (a low work function metal) in Figure 1.3.3.(a). In addition, the electron-hole recombination is represented in Figure 1.3.3.(b). It is believed that electroluminescence is generated from the radiative decay of singlet excitons which are produced by the recombination of the opposite charged carriers in the luminescent organic/polymeric layer in sandwiched structured LEDs. The opposite charges are separately injected from the two contacts under a bias voltage. The luminescent efficiency of the device is determined by the amount of charge carrier injection, the probability of the capture of the charges and the ratio of the singlet excitons formed. It is known that most of the conjugated polymers used as light-emitting materials tend to be p-type polymers with much greater tendency for injecting and transporting holes than for electrons. Therefore, the imbalance of rates for electron and hole injection from the negative and positive contacts becomes the obstacle for improving the electroluminescent efficiency.

(a) (b)
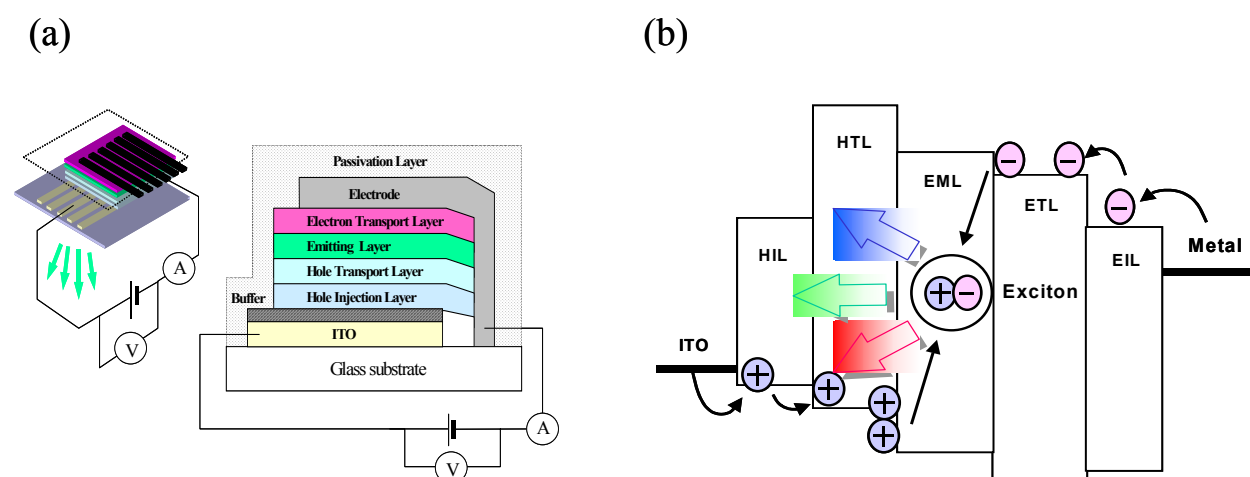
Figure 1.3.3. (a) Multilayer structure of OLED. (b) Electron and hole recombination process.

Polymer LEDs now shows attractive device characteristics, involving efficient light generation and there are several development programs now to establish procedures for manufacture. The conjugated Polymers have the advantage of allowing of easy, lack of crystallization, low-cost manufacture of flexible displays, possibly large-area, and using solution-processing of film-forming polymers. Usually polymer thin films are prepared from

organic materials in solution by solution-dipping or spin-coating method onto transparent conductive oxide (TCO)-coated glasses. Recently, M. F. Rubner (*J. Appl. Phys.*, **1996**, 80, 7, 1) has used the LBL assembly method to develop new processing techniques that can be utilized to manipulate organic systems at the molecular level.[77] The idea is that the ability to manipulate the manner in which molecules organize at the molecular and supermolecular level will make it possible to likewise control and tailor specific properties at this nanoscale level. Thus, it should be possible to control, at the molecular level, many of the critical elements that determine efficient device operation such as the mechanism and efficiency of carrier injection at the electrodes and the spatial location of the carrier recombination zone. The performance of the devices depends on the type of layer that is in contact with the Al top electrode thereby making it possible to manipulate device efficiency at the molecular level. Figure 1.3.4 shows thin film light emitting diodes based on the conjugated polymers via the use of a simple LBL molecular-level processing scheme and their Light–voltage and current–voltage curves.
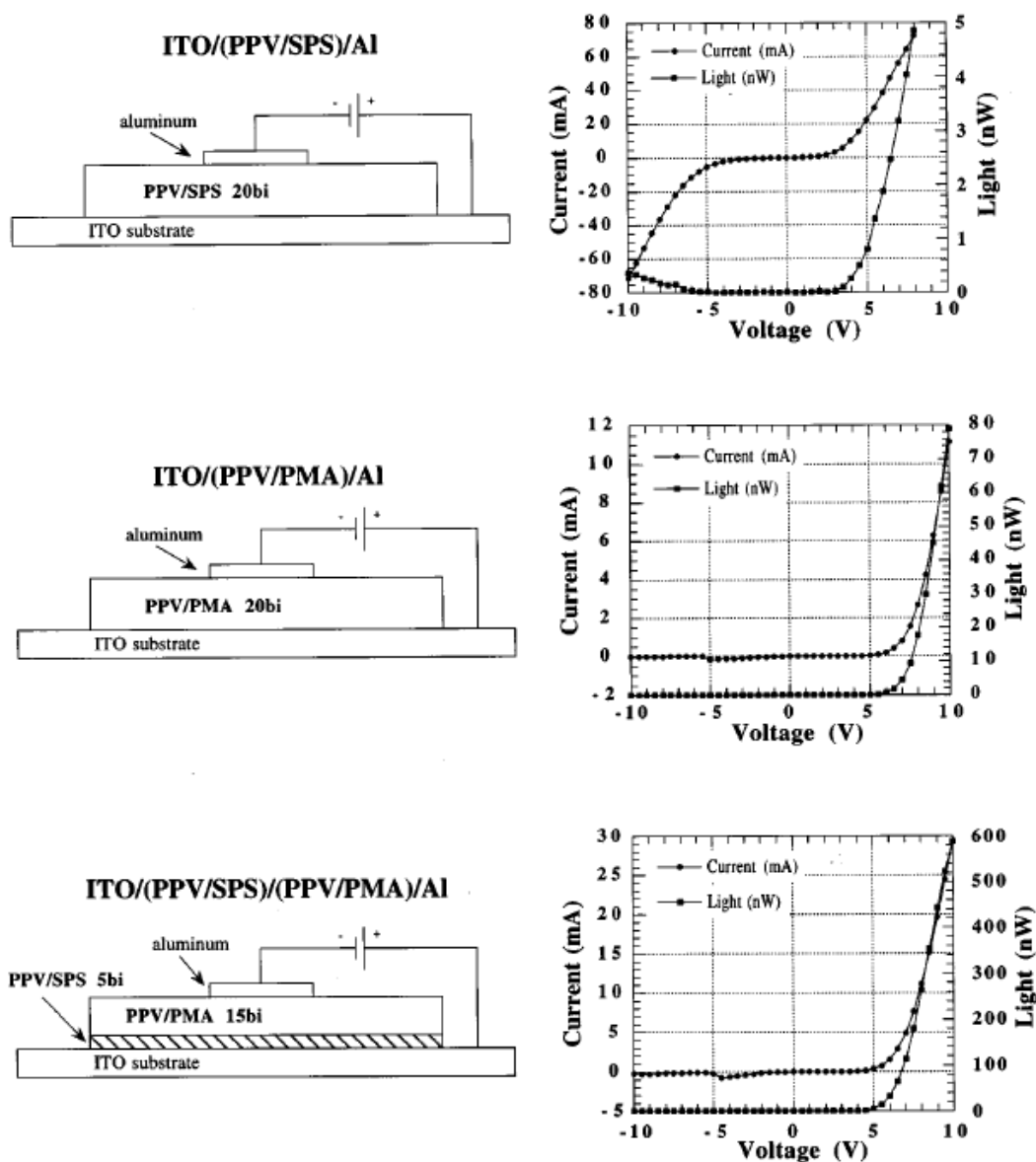
Figure 1.3.4. Light–voltage and current–voltage curves obtained from light emitting devices of ITO / (SPS/PPV)$_{20}$ / Al(top), ITO / (PMA/PPV)$_{20}$ / Al(middle), and ITO / (SPS/PPV)$_5$ / (PMA/PPV)$_{15}$ / Al (bottom).

Interestingly, the polymer LEDs are reported recently with the concept of the vacuum deposition method.[78] Although excellent results were achieved by spin-coating method for polymer solution, there are a number of problems that can arise. It could be difficult to find suitable solvents to prepare thin films (50-400 nm) that are free from pinholes. Moreover, if there are suitable solvents without any pinholes on the surface, mutually exclusive solvents

for the different polymer layers in a multilayer device are also difficult to engineer. As a next problem, oxygen and other contaminants (e.g., dust) are difficult to exclude from the solutions used to make films and solvent not fully removed from the films after deposition. They can cause formation of voids and chemical reactivity with the electrodes and finally it could be minimized device performance. Vapor deposition method provides a clean environment; it is solvent free and well suited to sequential depositions in hetero-structured multilayer system. Moreover, the device fabrications by the vacuum deposition method allows a whole processing in the same run without vacuum breaking from the polymer materials to the metal upper electrode.

To conclude, nanostructures, especially with functional polymers, open the door for the coming era of nanotechnology in various device applications. By controlling the structure at nano-scale and polymer properties within solid film state, multilayer thin films can have applications in photo-detectors, light-emitting diodes, displays and sensors, as well as in solar cells. Moreover, there is a need to develop new semiconducting polymers which are well soluble in water/alcohol as environmental-friendly materials. In this thesis, we introduce the LBL assembly to fabricate well defined multilayers, which composed of cationic and anionic LC amphotropic ionomers, p-type and n-type semiconducting polyelectrolytes with an internal structure.

1.4. References

(1) The United States' National Nanotechnology Initiative website

(2) M. C. Pettty, Langumir-Blodgett films: An Introduction, Cambridge University Press, Cambridge, **1996**.

(3) Ulman, *Chem. Rev.* **1996**, 96, 1553.

(4) L. Netzer, J. Sagiv, *J. Am. Chem. Soc.* **1983**, 105, 674.

(5) S. D. Evans, A. Ulman, K. E. Goppert-Berarducci, L. J. Gerenser, *J. Am. Chem. Soc.* **1991**. 113, 5866.

(6) H. Lee, J. Kepley, H-G. Hong, T. E. Mallouk, *J. Am. Chem. Soc.* **1988**. 110, 618.

(7) G. Decher, J. D. Hong, Ber. Bunsen-Ges. *Phys. Chem.* **1991**, 95, 1430.

(8) (a) P. Bertrand, A. M. Jonas, A. Laschewsky, R. Legras, *Macromol. Rapid. Commun.* **2000**, 21, 319. (b) G. Decher, M. Eckle, J. Schmitt, B. Struth, *Curr. Opin. Colloid Interface Sci.* **1998**, 3, 32. (c) G. Decher, *Science* **1997**, 277, 1232.

(9) Laschewsky, *Eur. Chem. Chronicle* **1997**, 2, 13.

(10) (a) Korneev, D.; Lvov, Y.; Decher, G.; Schmitt, J.; Yaradaikin, S. *Physica B* **1995**, 213/214, 954. (b) Kellogg, G.; Mayes, A.; Stockton, W.; Ferreira, M.; Rubner, M.; Satija, S. *Langmuir* **1996**, 12, 5109.

(11) (a) Shiratori, S. S.; Rubner, M. F. *Macromolecules* **2000**, 33, 4213. (b) See, for example: Decher, G. *Science* **1997**, 277, 1232. (c) Yoo, D.; Shiratori, S.; Rubner, M. F. *Macromolecules* **1998**, 31, 4309.

(12) (a) Dubas, S. T.; Schlenoff, J. B. *Macromolecules* **2001**, 34, 3736. (b) Dubas, S. T.; Schlenoff, J. B. *Macromolecules* **1999**, 32, 8153. (c) Schoeler, B.; Kumaraswamy, G.; Caruso, F. *Macromolecules* **2002**, 35, 889. (d) Steitz, R.; Jaeger, W.; v. Klitzing, R. *Langmuir* **2001**, 17, 4471.

(13) L. Y. Wang, Z. Q. Wang, X. Zhang, J. C. Shen, *Macromol. Rapid Commun.*, **1997**, 18, 509.

(14) W. B. Stockton, M. Rubner, *Macromolecules*, **1997**, 30, 2717.

(15) H. M. Xoing, M. H. Chen, Z. Zhou, X. Zhang, J. C. Shen, *Adv. Mater.*, **1998**, 10, 529.

(16) M. Schütte, D. G. Kurth, M. R. Linford, H. Cölfen, H. Möhwald, *Angew. Chem. Int. Ed. Engl*, **1998**, 37, 2891.

(17) Y. Shimazaki, M. Mitsuishi, S. Ito, M. Yamamoto, *Langmuir*, **1997**, 13, 1385.

(18) J. Anzai, Y. Kobayashi, N. Nakamura, M. Nishimura, T. Hoshi, *Langmuir*, **1999**, 15, 221.

(19) P. Bertrand, A. Jonas, A. Laschewsky, R. Legras, *Macromol. Rapid Commun*. **2000**, 21, 319.

(20) Hong, H.; Steitz, R.; Kirstein, S.; Davidov, D. *Adv. Mater*. **1998**, 10, 1104.

(21) Caruso, F.; Lichtenfeld, H.; Donath, E.; Möhwald, H. *Macromolecules* **1999**, 32, 2317.

(22) Cho, J., Char, K., Hong, J. D., Lee, K. B., *Adv. Mater*., **2001**, 13, 1076.

(23) Lee, S. S., Hong, J. D., Kim, C. H., Kim, K., Koo, J. P., Lee, K. B., *Macromolecules*, **2001**, 34, 5358.

(24) Chaarelli, P. A., Johal, M. S., Casson, J. L., Roberts, J. B., Robinson, J. M., Wang, H. L., *Adv. Mater*., **2001**, 13, 1167.

(25) D. E. Bornside, *J. Electrochem. Soc*. **1990**, 137, 2589.

(26) S. Middleman, *J. Appl. Phys*. **1987**, 62, 2530.

(27) T. J. Rehg, B. G. Higgins, *Phys. Fluids* **1988**, 31, 1360.

(28) F. Ma, J. H. Hwang, *J. Appl. Phys*. **1990**, 68, 1265.

(29) Chiarelli, P. A.; Johal, M. S.; Casson, J. L.; Roberts, J. B.; Robinson, J. M.; Wang, H.-L. *Adv. Mater*. **2001**, 13 (15), 1167.

(30) Cho, J.; Char, K.; Hong, J.-D.; Lee, K.-B. *Adv. Mater*. **2001**, 13 (14), 1076.

(31) Lee, S.-S.; Hong, J.-D.; Kim, C. H.; Kim, K.; Koo, J. P.; Lee, K.-B. *Macromolecules* **2001**, 34 (16), 5358.

(32) McAloney, R. A.; Goh, M. C. *J. Phys. Chem. B* **1999**, 103 (49), 10729.

(33) Schlenoff, J. B., Dubas, S. T., Farhat. T., *Langmuir*, **2000**, 16, 9968.

(34) Tang, C. W.; Van Slyke, S. A. *Appl. Phys. Lett*. **1987**, 51, 913.

(35) Kolosov, S.; Adamovich, V.; Djurovich, P.; Thompson, M. E.; Adachi, C. *J. Am. Chem. Soc*. **2002**, 124, 9945.

(36) Katz, H. E.; Bao, Z. *J. Phys. Chem. B*. **2000**, 104, 671.

(37) Katz, H. E.; Bao, Z.; Gilat, S. L. *Acc. Chem. Res*. **2001**, 14, 359.

(38) Dimitrakopoulos, C. D.; Malenfant, P. R. L. Adv. Mater. 2002, 14, 99.

(39) Brabec, C. J.; Sariciftci, N. S.; Hummelen, J. C. *Adv. Funct. Mater*. **2001**, 11, 15.

(40) Yu, G.; Gao, J.; Hummelen, J. C.; Wudl, F.; Heeger, A. J. *Science*. **1995**, 267, 1969.

(41) Sapp, S. A.; Sotzing, G. A.; Reynolds, J. R. *Chem. Mater*. **1998**, 10, 2101.

(42) Kumar, A.; Welsh, D. M.; Morvant, M. C.; Piroux, F.; Abboud, K. A.; Reynolds, J. R. *Chem. Mater*. **1998**, 10, 896.

(43) Mitschke, U.; Bauerle, P. *J. Mater. Chem*. **2000**, 10, 1471.

(44) Kraft, A.; Grimsdale, A. C.; Holmes, A. B. *Angew. Chem. Int. Ed*. **1998**, 37, 402.

(45) Strukelj, M.; Papadimitrakopoulos, F.; Miller, T. M.; Rothberg, L. *J. Science.* **1995**, 67, 1969.

(46) Dimitrakopoulos, C. D.; Malenfant, P. R. L. *Adv. Mater*. **2002**, 14, 99.

(47) Babel, A.; Jenekhe, S. A. *Adv. Mater*. **2002**, 14, 371.

(48) K, W. Klupfel, O. Sus, H. Behmenburg, and W. Neugebauer, US 3, 180, 730, (1965)

(49) T, B. Brantly, L.E.Contois and C.J.Fox, US, **1971**, 3, 567, 450.

(50) (a) Fachetti, A.; Mushrush, M.; Katz, H. E.; Marks, T. J. *Adv. Mater*. **2003**, 15, 33. (b) Sakamoto, Y.; Shingo, K.; Suzuki, T. *J. Am. Chem. Soc*. **2001**, 123, 4643. (c) Fachetti, A.; Deng, Y.; Wang, A.; Koide, Y.; Sirringhaus, H.; Marks, T. J.; Friend, R. H. *Angew. Chem., Int. Ed*. **2000**, 39, 4547.

(51) Sakamoto, Y.; Suzuki, T.; Miura, A.; Fujikawa, H.; Tokito, S.; Taga, Y. *J. Am. Chem. Soc*. **2000**, 122, 1832.

(52) Bao, Z.; Lovinger, A. J.; Brown, J. *J. Am. Chem. Soc*. **1998**, 120, 207.

(53) (a) Katz, H. E.; Lovinger, A. J.; Johnson, J.; Kloc, C.; Siegrist, T.; Li, W.; Lin, Y.-Y.; Dodabalapur, A. *Nature* **2000**, 404, 478. (b) Gregg, B. A.; Cormier, R. A. *J. Am. Chem. Soc*. **2001**, 123, 7959.

(54) Murata, H.; Malliaras, G. G.; Uchida, M.; Shen, Y.; Kafafi, Z. H. *Chem. Phys. Lett*. **2001**, 339, 161.

(55) R. Mruk, S. Prehl, R Zentel, *Macromol. Rapid Commun*, **2003**, 24, No. 17, 1014.

(56) G. Decher, J. B. Schlenoff, Multilayer thin film, Wiley-VCH, p 302.

(57) (a) Piscevic, D.; Knoll, W.; Tarlov, M. *J. Supramol. Sci*. **1995**, 2, 99. (b) Li, D.-Q.; Ratner, M. A.; Marks, T. J.; Zhang, C. H.; Yang, J.; Wang, G. K. *J. Am. Chem. Soc*. **1990**, 112, 7389.

(58) Rubinstein, I.; Steinberg, S.; Tor, Y.; Shanzer, A.; Sagiv, *J. Nature (London)* **1988**, 332, 426.

(59) Vermeulen, L. A.; Thompson, M. E. *Nature (London)* **1992**, 358, 656.

(60) Dean M. DeLongchamp, Mark Kastantin, Paula T. Hammond, *Chem. Mater*. **2003**, 15,b 1575. (b) Dean M. DeLongchamp, Paula T. Hammond, *Adv .Mater*, **2001**, 13, 19, 1455. (c) Dean M. DeLongchamp, Paula T. Hammond, *Chem. Mater*. **2004**, 16, 4799. (d) C. A. Cutler, M. Bouguettaya, J. R. Reynolds. *Adv .Mater*. **2002**, 14, 9, 684.

(61) Fou, A. C.; Onisuka, O.; Ferreira, M.; Rubner, M. F. *J. Appl. Phys*. **1996**, 79, 7501.

(62) Monk, P. M. S.; Mortimer R. J.; Rosseinsky, D. R. Electrochromism: Fundamentals and Applications; VCH: Weinheim,Germany, 1995.

(63) Platt, J. R. *J. Chem. Phys*. **1961**, 34, 862.

(64) Deb, S. K. *Appl. Opt., Suppl*. **1969**, No. 3, 192.

(65) (a) Granqvist, C. G. Sol. Energy Mater. Sol. Cells 2000, 60, 201. (b) Granqvist, C. G.; Avendano, E.; Azens, A. *Thin Solid Films* **2003**, 442, 201. (c) Faughnan, B. W.; Crandall, R. S.; Heyman, P. M. *RCA Rev*. **1975**, 36, 177.

(66) Habib, M. A. *Electrochem. Transition* **1992**, 51.

(67) Somani, P. R.; Radhakrishnan, S. *Mater. Chem. Phys*. **2003**, 77, 117.

(68) (a) Bach, U.; Corr, D.; Lupo, D.; Pichot, F.; Ryan, M. *Adv. Mater*. **2002**, 14, 845. (b) Corr, D.; Bach, U.; Fay, D.; Kinsella, M.; McAtamney, C.; O'Reilly, F.; Rao, S. N.; Stobie, N. *Solid State Ionics* **2003**, 165, 315.

(69) See the following Web sites: http://www.chem.ufl.edu/~reynolds, http://www.gentex.com, http://www.donnelly.com, http://www.dynamircorp.com/, http://eetd.lbl.gov/btp,http://www.sage-ec.com, http://www.nrel.gov/buildings/windows, http:// www.ntera.com, http://www.acreo.se, and http://www.cidetec.es.

(70) Dean M. W, John R, Reynolds, *Adv .Mater*. **1999**, 11, 16, 1379.

(71) Monk, P. M. S. The Viologens; John Wiley & Sons Ltd.: West Sussex, U.K., 1998.

(72) Sapp, S. A.; Sotzing, G. A.; Reynolds, J. R. *Chem. Mater*. **1998**, 10, 2101.

(73) Welsh, D. M.; Kumar, A.; Meijer, E. W.; Reynolds, J. R. *Adv. Mater*. **1999**, 11, 1379.

(74) Cheung, J. H.; Fou, A. F.; Rubner, M. F. *Thin Solid Films* **1994**, 244, 985.

(75) Ferreira, M.; Rubner, M. F. *Macromolecules* **1995**, 28, 7107.

(76) C. W. Tang and S. A. VanSlyke, *Appl. Phys. Lett*. **1987**, 51, 913.

(77) O. Onitsuka, A. C. Fou, M. Ferreira, B. R. Hsieh, M. F. Rubner, *J. Appl. Phys*. **1996**, 80 7, 4067.

(78) (a) Konstantin P. Gritsenko, Anatoly M. Krasovsky, Chem. Rev. 2003, 103, 3607. (b) C. H. Lee, G. W. Kang, J. W. Jeon, W. J. Song, C. Seoul. *Thin Solid Films*. **2000**, 363, 306.

2. Aim of the Work

In the introduction, we have discussed the layer-by-layer (LBL) assembly technique with various functional materials. Even though this assembly method is well known as the ideal processing technique to prepare thin film composites with fine control over morphology and composition, there is a general interest in obtaining multilayers with an internal structure. In principle, multilayers prepared by LBL method usually present a low degree of internal organization and show a strong interpenetration between the oppositely charged polymer layers. Because of this interpenetration, these multilayer films do not contain defined internal sublayers and this may be a limitation of the technique. Several attempts have been presented to use multilayers containing rigid ionic blocks for reduction of interpenetration, however, very particular conditions seem to be necessary. To get multilayer films with well-defined internal structure, we want to synthesize novel ionic liquid crystalline (LC) polyelectrolytes. The amphotropic LC polyelectrolytes, which preorganize in solution through a lyotropic LC phase (high mobility) prior to drying a thermotropic LC phase (bulk state); thereby, LBL multilayers with internal order may be achieved. In addition, we introduce not only the conventional solution-dipping LBL method but also spin-coating LBL method for assembly. With regard to the formation of an internal order, both types of fabricated multilayer films could show different behaviour

Concerning the functional materials for LBL assembly, organic semiconductors and conjugated polymers are currently of wide interest for applications in electronic and optoelectronic devices. Unfortunately, well known p-type (electron donor, hole transport) and n-type (electron acceptor, electron transport) materials with free ionic groups are not applicable for the use in electronic devices, as the ionic conductivity would lead to a short circuit in the device. This problem can be solved, in principle, by the formation of polyelectrolyte complexes of the ionic hole- or electron-transporting polymers and oppositely charged polymers by LBL method from dilute polymer solutions. Moreover, triarylamine, oxadiazole, thiadiazole and triazine have been most widely used as the hole- and electron-transporting materials in organic LEDs. There is even substantial and growing interest in using water/alcohol soluble conjugated polymers for chemical and biological applications, as these are environmentally friendly and low-cost solvents allow safe processing. Therefore, we

design water/alcohol soluble charged semiconducting polymers composed of triarylamine, oxadiazole, thiadiazole and triazine moieties for LBL thin film assembly.

The well defined and effective electroactive LBL films have been used for diverse electronic and optoelectronic devices. As the process is simple and inexpensive, it allows the incorporation of many different functional materials within a single film without the phase separation. For example, electrochromic devices prepared by LBL assembly can provide reasonable contrast without angle dependence and backlights. Most of the studies have been focused on inorganic/organic hybrid composites by a conventional solution-dipping LBL method; however, inorganic materials have difficulties in processing and slow response time. Furthermore, the solution-dipping technique requires a rather long time for the same number of bilayers. Based on these difficulties, we want to fabricate electrochromic films with triarylamine polymers by the spin-coating LBL method. Triarylamine polymers, which have high charge carrier mobility can be used as promising electrochromic materials and their dimers in nano-scale thin film geometry may be a concept to improve the switching time.

Usually, polymer thin films are prepared by solution-dipping or spin-coating method. Although excellent results were achieved this way, a number of problems can arise. It can be difficult to find suitable solvents to prepare thin films without pinholes and solvents may not be fully removed from the films after deposition. It causes formation of voids and chemical reactivity with the electrodes and finally minimizes the device performance. At that point, dry process such as vapor deposition under vacuum condition can be the perfect candidate to deposit the polymer films for LEDs. Polymers generally cannot be vaporized without decomposition. However, many polymers decompose to oligomers at elevated temperatures and resulting oligomers can be vaporized. Such evaporated oligomers could benefit from the advantages described above and they may give more stable amorphous structures compared to low molar mass materials. We have a triarylamine polymer, which has carboxylate and amide groups, it later can be imidized during heat treatment and degrades to oligomers. Therefore, we want to make high quality homogeneous films by the vacuum deposition method and introduce the films as hole transporting layers into the LEDs.

The chapters 3, 4, 5 and 6 in this dissertation are a compilation of publications containing various polymer thin films with newly synthesized functional polymers.

In brief, *Chapter 3* describes the LBL assembly of amphotropic LC ionomers, especially the control of molecular orientation and organization on the nanoscale. We have described the synthesis of new amphotropic LC ionomers, cationic and anionic LC ionomers are suitable materials to fabricate multilayers with an internal structure. The multilayers were deposited by both solution-dipping and spin-coating methods. Both methods showed quite linear and reproducible multilayer build-up performances, however, the UV/VIS, AFM, SPR, and XRR measurements indicated differences between multilayer samples prepared by both methods owing to the different mechanisms.

Chapter 4 illustrates the importance of multilayer thin films of hole and electron transport polyelectrolytes by LBL assembly. A series of newly synthesized p-type and n-type semiconducting polyelectrolytes were optically and electrochemically fully characterized. The fabricated electroactive thin films are promising candidates for various applications such as photodetectors, light-emitting diodes, displays and sensors, as well as in solar cells. The film thickness could be easily controlled at the molecular level and multilayer architecture does indeed make it possible to realize significant improvements in the device performance.

Chapter 5 reports on organic polymeric electrochromic thin films based on triarylamine derivatives from LBL assembly. The desire for cheap and simple displays with reasonable contrast in multiple colors has lead to investigation of electrochromic devices. Triarylamine polymers, which have high charge carrier mobility can be used as electrochromic materials and their LBL films were used as simple electochromic films. The assembled films revealed outstanding device characteristics in terms of high contrast ratio and rapid switching times.

Chapter 6 deals with vacuum-deposited triarylamine thin film and its structure and electronic properties. Concerning the making of polymer thin films, we have introduced a vacuum deposition method. During the vacuum deposition process, a secondary reaction is occurrs and the triarylamine polymer is degraded to oligomers at elevated temperatures. As one of the

potential applications, the fabricated films were used in light emitting devices as hole transporting layers.

Chapter 7 and *8* includes a brief summary, conclusions, methods and instrumentation used in this dissertation. The appendix is given in *Chapter 9*.

3. Amphotropic LC Polymers and Their Multilayer Build-up*

3.1. Introduction

The layer-by-layer (LBL) fabrication of molecularly organized film has received tremendous attention in recent years[1,2,11] as a simple, effective, and versatile method to prepare uniform and ultrathin structures. Since composition, thickness, and orientation of each layer can be effectively manipulated using this technique, it provides a route for the formation of various structures layered at the molecular level.[3-7] These manipulations at the molecular level offer many potential advantages in device applications such as active components in nonlinear optical devices (NLO),[4,8] employing materials with selective chemical responses for sensor applications,[7] stable charge-separated assemblies for photovoltaics,[9] and organic light-emitting diodes (OLED's).[10] Since the first report of Decher and coworkers in the early 1990s,[11] there have been numerous reports on the LBL deposition technique based on the electrostatic attraction between polycations and polyanions. Many types of charged molecules and nanoobjects seem are suitable for deposition by the LBL method, but the use of polyelectrolytes rather than low molecular weight polyelectrolytes is advantageous mainly because good adhesion of a layer to the underlying substrate or film requires a certain number of ionic bonds. So far, mostly commercially available polyelectrolytes have been studied, and only in rare cases were functional polyelectrolytes prepared for this purpose.[17,18]

The electrostatic attraction between the oppositely charged polyelectrolytes and especially the entropy gain of the low molar mass counterions are generally thought to drive the depositions. The amount and conformation of adsorbed chains depend on dramatically processing parameters, particularly ionic strength and pH of the deposition solution, as well as the charge densities of both polyelectrolytes. A number of articles have explored the electrostatic parameter in order to delineate conditions of polyelectrolyte multilayer film formation and to correlate molecular and processing parameters with the final film structure.[12-15]

Concerning the multilayer build-up by the LBL technique, there is a general interest in obtaining multilayers with an internal structure.[19] However, multilayers prepared by LBL usually present a low degree of internal organization, and this may be a limitation of the technique. Well-organized multilayers would be advantageous for the applications mentioned,

especially for those requiring a vectorial transfer of energy, electrons, or matter or when a precise placement of active functional groups in confined layers is desired. Usually, multilayer films prepared by the LBL method show a strong interpenetration between the oppositely charged polymer layers. Because of this interpenetration, these multilayer films do not contain defined internal sublayers, and no Bragg peaks are observed by grazing angle specular scattering measurements (Xray reflectometry, XRR, or neutron reflectometry, NR).[19,20] Several attempts have been presented to use multilayers containing rigid ionic blocks for reduction of interpenetration in order to observe Bragg peaks. However, very particular conditions seem to be necessary, but still the appearance of Bragg peaks is exceptional.[19-23]

To get multilayer films with well-defined internal structure, we have studied multilayers of ionic liquid crystalline (LC) polyelectrolytes by LBL.[24,25,36] However, even in the case when both anionic and cationic LC ionomers showed a smectic phases as neat materials in their bulk state, no Bragg peaks could be detected for the multilayers prepared by the LBL technique.[36] This might be explained by the fact that thermotropic liquid crystals show only liquid-crystalline properties in bulk and not in solution. Accordingly, LC ionomers do not show any liquid-crystalline properties during the adsorption from solution. After ion pairing, the formation of the liquid-crystalline order is not possible because of the low mobility inside the polyelectrolyte complex. As a consequence, it seems desirable to investigate novel LC polyelectrolytes, which preorganize in solution through a lyotropic LC phase (high mobility) prior to drying a thermotropic LC phase (bulk state); thereby, LBL multilayers with internal order may be achieved. After the removal of the solvent, these lyotropic phases change into thermotropic phases, which can stabilize the internal structure within the dried multilayer film.

In this paper, we describe the synthesis of such new LC ionomers, possessing an amphotropic character.[37] The polymers show both thermotropic phases in bulk and lyotropic phases in concentrated solution. They can be used for the multilayer build-up by LBL (solution-dipping) and self-assembly spin-coating (spin-coating) method.[27] X-ray reflectivity measurements indicate internal layering in multilayer films, and angular dependent UV/VIS measurements present a preferred orientation of the mesogens perpendicular to the surface.

3.2. Results and discussion

Synthesis of the Amphotrophic Polymers. The chemical structures and reaction schemes of the LC polymers and ionomers prepared in this study are shown in Schemes 3.1 and 3.2. The new LC ionomers **P2** and **P3** were synthesized by a reaction of a biphenyl functionalized amine and ionic amines with a reactive precursor polymer (Scheme 3.2). The side groups (ionic groups and mesogens) are attached to the main chain by amide bonds which are stable against hydrolysis. The mesogens consist of a long alkyl chain to increase the amphiphilicity of the structure. Branched alkyl chains are used to prevent side-chain crystallization. A larger variety of polymers, which are synthesized under the variation of concentration of mesogens and ionic groups, were briefly described elsewhere.[26] Here we selected homopolymer **P1**, the anionic LC ionomer **P2**, and the cationic LC ionomers **P3a,b**. First, the mesogen containing primary amine **4** had to be synthesized, as shown in Scheme 3.1. Phthalimide potassium, which was transformed into the corresponding N-(6-bromohexyl)- phthalimide **1**. The phenol **2** was obtained by reaction of 4,4'-dihydroxybiphenyl and racemic p-toluenesulfonic acid-2-octyl ester. Compounds **1** and **2** were afterward reacted to obtain the phthalimide protected primary amine **3**. In the final step, the protection group was then cleaved by treatment with hydrazine hydrate in ethanol, yielding 60 % of **4**.

**Scheme 3.1.** Synthesis of the Mesogen-Containing Primary Amine.
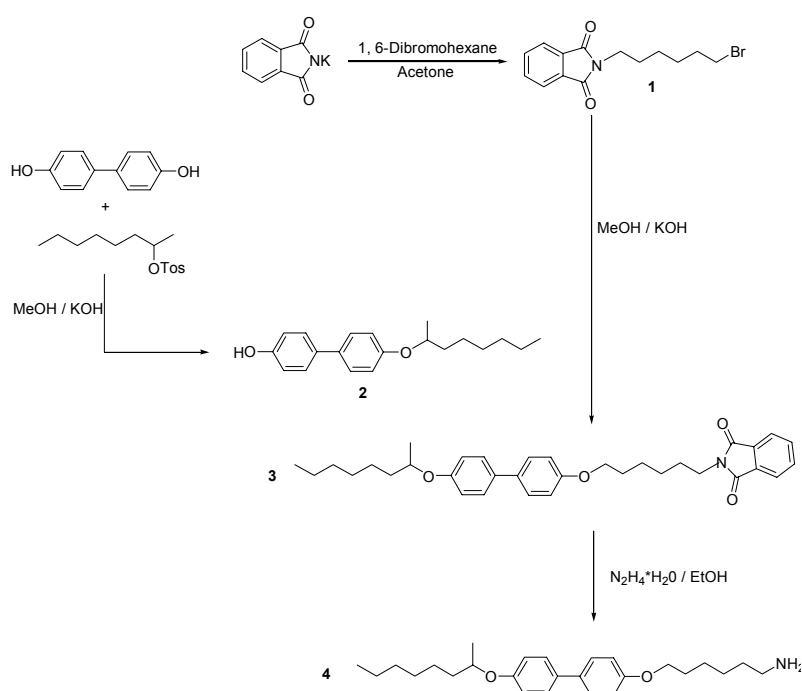
The synthesis of the polymers started with the polymerization of N-acryloyloxysuccinimide.[28-30] To determine the molecular weight, the reactive ester polymer was reacted with an excess of N-methylhexylamine. The resulting polymer was analyzed by GPC with THF as eluent; a Mn of 28 000 g/mol and a Mw of 49 000 g/mol were found.[37]

For the synthesis of the LC polymers (Scheme 3.2), the reactive ester polymer was reacted, at first, with the primary amine **4** (slight excess for homopolymer **P1** and varying amounts for the LC ionomers **P2** and **P3**). The completeness of the reaction was checked by thin-layer chromatography. For the synthesis of the LC ionomers **P2** and **P3**, afterward, an excess of 4-aminobutyric acid methyl ester hydrochloride or 4-amino-1-triethylphosphoniumbutane dihydrochloride was added, respectively. The resulting nonionic polymer was precipitated and dried. Finally, the anionic ionomer **P2** was created by hydrolysis of the ester group (Scheme 3.2 and Experimental Section), and in the case of the cationic side chains of the polymer, **P3** was already ionic. The incorporation of biphenyl-containing side chains in polymer **P2** was confirmed by UV/VIS spectroscopy measurements. 50 % of the polymer side chains contain biphenyl mesogens, corresponding to the amount of the biphenyl-containing primary amine used for the polymer analogous reaction.

Scheme 3.2. Structures of Mesogen-Containing Polymers (s: Smectic Phase; i: Isotropic Phase).
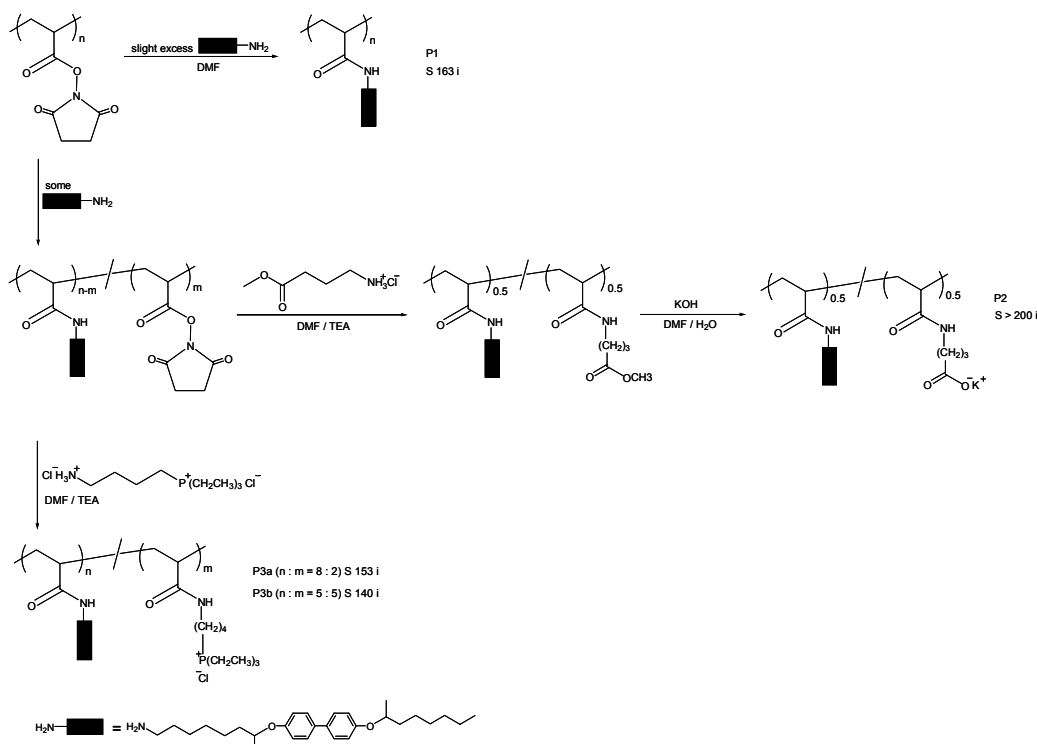
Liquid Crystalline Behavior. The LC phases of **P1-P3** were characterized by polarizing microscopy, differential scanning calorimetry (DSC), and X-ray reflectivity measurements. The polymer melts and especially the ones from the LC ionomers **P2** showed a rather high viscosity, which might be explained by the fact that H-bonding of amide groups reduces mobility. For **P2** and **P3** in addition the formation of ion pairs has to be considered (see ref 36 for similar observations), which are especially strong for the carboxylate groups. Nevertheless, LC phases with smectic textures (batonetts)[41] were observed for all polymers by polarizing microscopy after prolonged annealing (see Figure 3.1(a)). For **P1** the clearing temperature was 163 °C. In the series of the cationic LC ionomers (**P3a,b**), the decreasing temperature decreased with increasing amount of the bulky triethylphosphonium groups (see ref 36 for similar behavior). A different effect was observed for **P2**. The clearing point was higher than 200 °C and occurred at decomposition. This happens presumably because of a strong tendency of the small carboxylate groups to demix from the hydrophobic mesogens (see X-ray measurements and Figure 3.2). As a result, this segregation stabilizes the smectic phase. The phase transition temperatures are included in the reaction scheme 3.2.
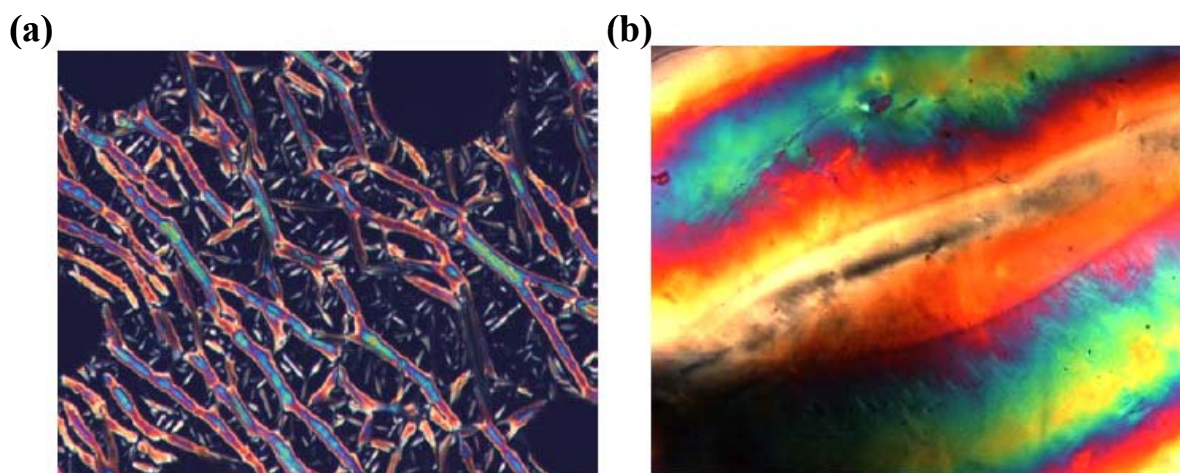

Figure 3.1. Polarizing microscopy image of (a) A thermotropic phase of **P1** (163 °C) and (b) a lyotropic phase of **P3b** (50 °C) with ethylene glycol.

X-ray reflectivity measurements showed a smectic layer spacing of 48.5 Å for **P1** and of 72 Å for the LC ionomer **P2** in bulk state. Based on the molecular model presented in Figure 3.2(a), these spacings correspond to an interdigitated smectic structure for the homopolymer **P1** (smectic layer thickness is about 1.6 times the length of the mesogen, which is 30 Å) and a

bilayer structure for the LC ionomer **P2** (distance from end of mesogen to the ionic group is 39 Å).[42,43] The difference between the "ideal" bilayer length of 78 Å and the experimentally determined length of 72 Å can be explained due to partial coiling, some tilting of the mesogens, and/or a partial interdigitation of the ends of the alkyl chains. The bilayer structure is a result of the segregation between the hydrophilic ionic groups and the hydro-phobic mesogens. It is the precondition for the formation of a lyotropic phase in polar solvents. **P2** and **P3b** do not dissolve in water; only slight swelling can be observed, while preserving their liquid crystalline phase. To prove their potential to form lyotropic phases in polar solvents, ethylene glycol was used as polar solvent. Contact preparations in ethylene glycol show clearly the formation of lyotropic phases at high concentrations of **P2** and **P3b** (see Figure 3.1(b)). The observation of lyotropic phases has also been made for a large variety of other LC ionomers of similar structure.[26,37] As a result, **P2** and **P3b** are amphotropic polymers, which form both thermotropic smectic phases in the bulk and lyotropic phases in polar solvents, such as ethylene glycol.
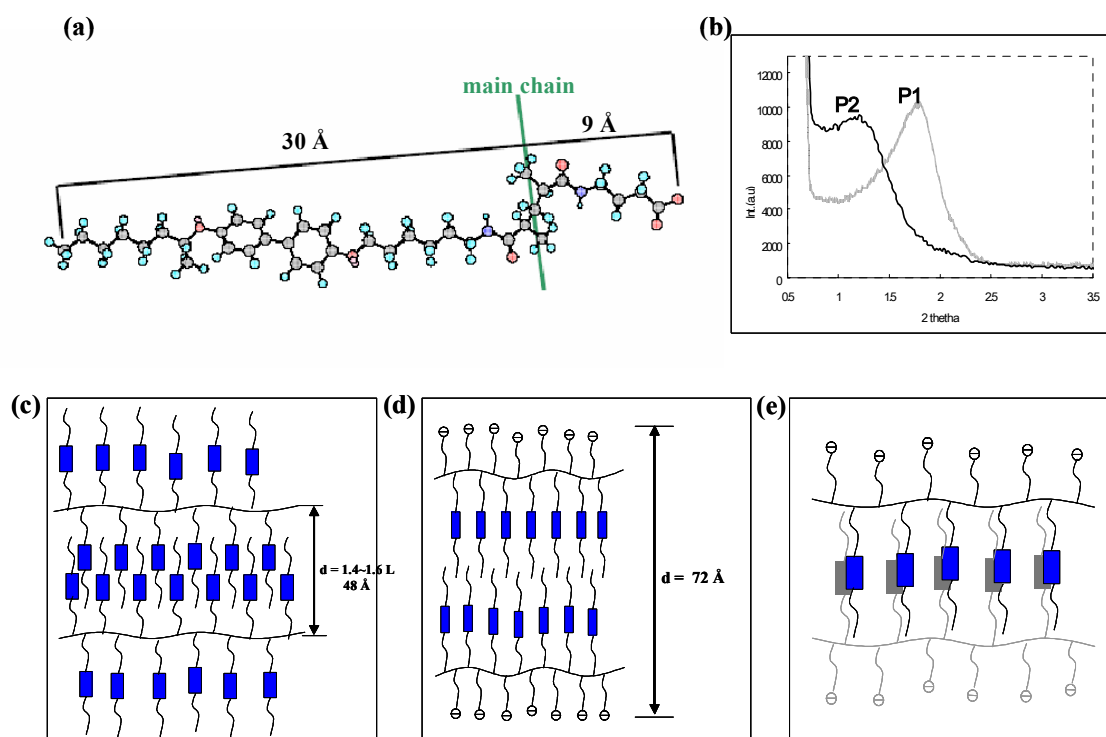
Figure 3.2. (a) Molecular model structure with distance of **P2** by using Chem 3D Ultra 7.0. (b) X-ray scattering diagram of **P1** (homopolymer) and **P2** (anionic LC ionomer) in bulk state (using Ni-filtered Cu KR radiation, $\lambda = 1.54$ Å). (c) Schematic representation of the smectic bulk structure of **P1** and (d) **P2**. (e) Interdigitated layer structure present in the multilayer.

Multilayer Build-up. After analysis of the phase behaviors of the LC ionomers **P2** and **P3b**, the multilayer build-up with oppositely charged polyelectrolytes was successfully examined using the method introduced by Decher.[11] For **P2**, a comparison between the LBL solution-dipping method and the subsequent spin-coating method[31-34] was done. For both processes, **P2** and **P3b** were dissolved in THF with the addition of some ethylene glycol or water (5:1 ratio), and in this solvent mixture, no lyotropic phases are formed. During the drying procedure, THF evaporates first, increasing the concentration of ethylene glycol or water to a range, where lyotropic phases can be expected. Before alternately depositing polymer **P2** (anionic LC ionomer) and poly(choline methacrylate) (PCM) or poly(2-acryloylamino-2-methylpropyl sulfonate sodium salt) (PAMPS) and **P3b** (cationic LC ionomer) onto the substrate, poly-(ethylenimine) (PEI) and PAMPS were predeposited two times as basis layers.

For a comparative study, multilayers were assembled using solution-dipping as well as spin-coating methods applying the same conditions. The preparation of multilayer assemblies based on the solution-dipping method was achieved by dipping the substrate alternately for 10 min in cationic aqueous solution of PCM and then in anionic polymer **P2** solution and rinsing three times with plenty of Milli-Q water for 1 min between these two steps. A similar procedure was adopted when assembling the multilayers by the spin-coating method. The polymer solution and the aqueous solution of PCM were poured onto a substrate, and then the substrate was spun at a speed of 4000 rpm for 15 s.

Figure 3.3(a) showed the multilayer build-up from LC ionommer **P2** investigated by UV/VIS; the increase of the maximum of the π-π* absorbance of the biphenyl mesogen at 267 nm as a function of the number of bilayers for both the solution-dipping and spin-coating multilayers, respectively. According to Figure 3.3(b), the deposition process was linear, indicating that the amount of material deposited per bilayer is completely reproducible from layer to layer. Similar behavior of the multilayer build-up using the spin-coating method was investigated as well. Thus, with both methods, it is possible to prepare multilayers, which grow constantly in thickness according to the number of bilayers. Figure 3.3(c) showed the difference in UV/VIS absorbance of multilayer films with alternating **P2** and PCM layers prepared by solution-dipping and spin-coating methods. It is obvious that the absorbance of the spin-coated films was about 20 times as high as those prepared by solution-dipping. This happens despite the fact that the spin-coated film was adsorbed onto only one side of a quartz substrate, while the film prepared by the solution-dipping method was adsorbed onto both sides of a quartz

substrate. This was in agreement with literature data.[27,31-33] With regard to the formation of an internal order, both types of films could be different: This significant difference of the absorption between the multilayers from the solution-dipping and the spin-coating method was caused by the different adsorption mechanisms. During the solution-dipping process, LC ionomer chains diffused toward the substrate, and then the adsorbed chains rearranged themselves on the surface. After evaporation of the THF, during the drying process, the concentration of polymers in the water phase increased, whereby the formation of a lyotropic phase was expected. This drying process was quite slow, and it can provide enough time to rearranged adsorbed LC ionomers and to oriented mesogens during the drying process. Subsequently, solution-dipping samples had preferably structured order due to the oriented mesogens, and it would be perpendicular to the surface.

On the other hand, the spin-coating method results in thicker films. In the spin-coating process, the adsorption and rearrangement of adsorbed chains on the surface and the elimination of weakly bound LC ionomer chains from the substrate are almost simultaneously achieved at a high spinning speed for a short time. A very fast elimination of the solvent yields thick layers. Quick solidification and polyelectrolyte formation compete with the ordering process. With regard to the formation of an internal order in the multilayer system, the film of the spin-coating method may possess less well-ordered internal structures than that of the solution- dipping method.
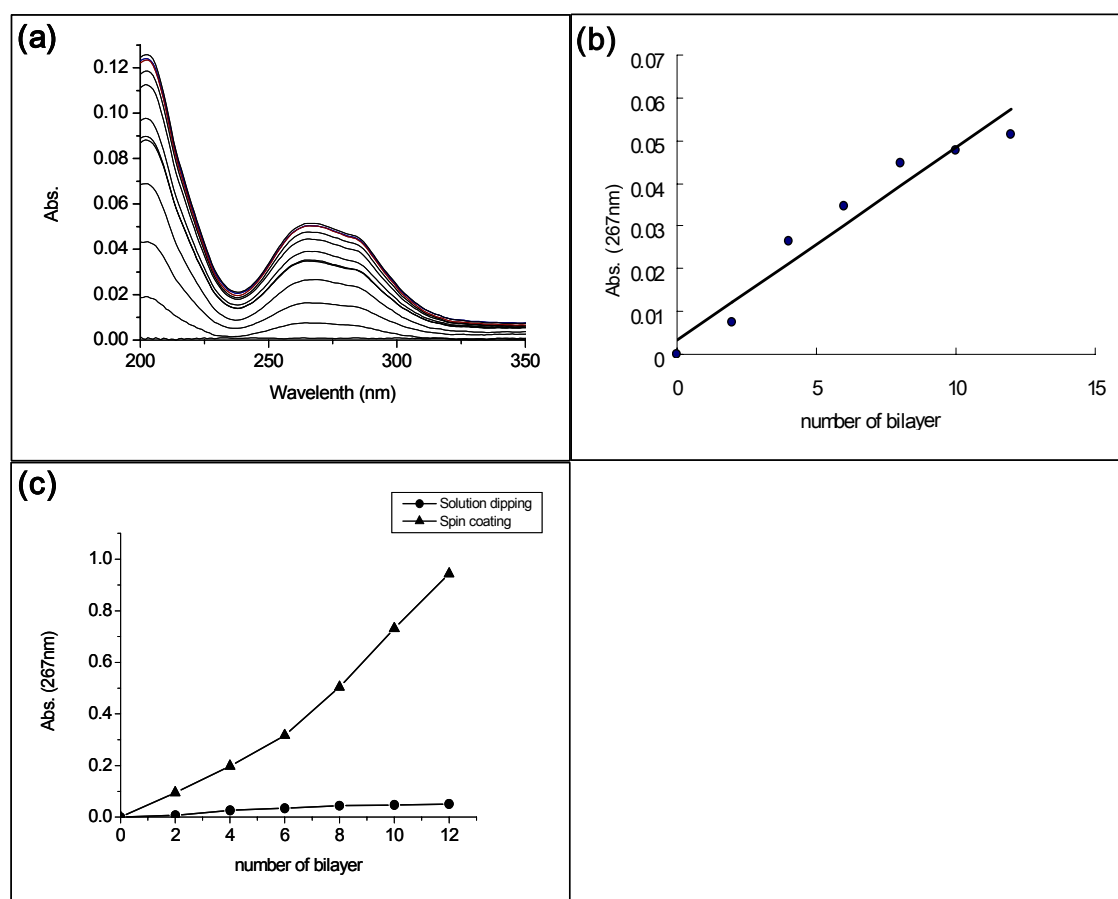
Figure 3.3. Multilayer build-up from LC-ionomer **P2**. (a) UV/VIS spectra measured during the multilayer build-up of **P2** and PCM by solution dipping. (b) Growth of the solution-dipping films at 267 nm. (c) Comparison of the growth of the multilayer films assembled by solution-dipping (●) and spin-coating (▲)

To investigate the difference between both types of multilayers in more detail, they were characterized by surface plasmon resonance (SPR, thickness), atomic force microscopy (AFM, roughness, topology), X-ray reflectometry (XRR, internal order), and angular dependent UV/VIS measurements to monitor the order within the multilayers. AFM images can give information about the surface coverage and roughness of the assembled multilayers. These AFM images were taken in air at room temperature in the tapping mode on multilayer samples prepared by solution-dipping and spin-coating on quartz (12 double layers each). The results are displayed in Figure 3.4.
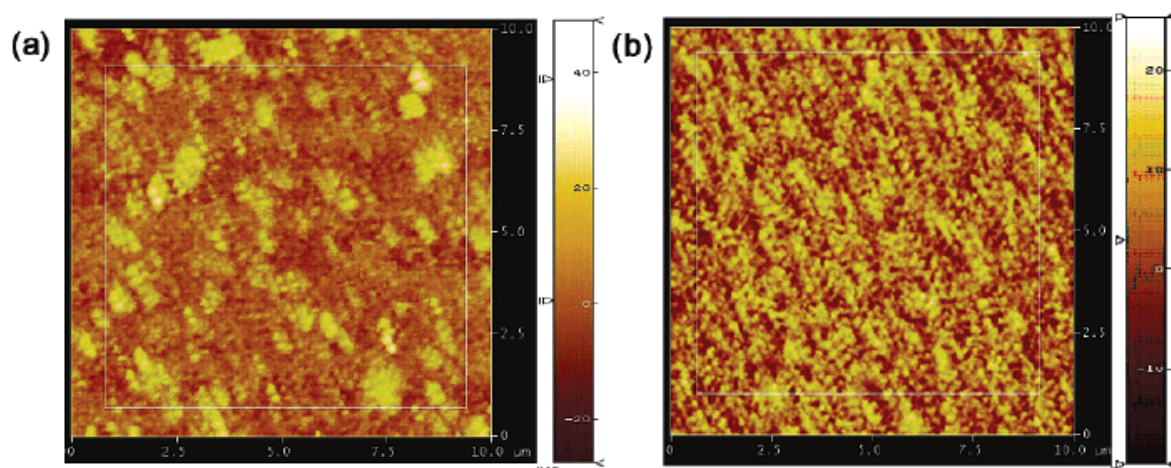
Figure 3.4. Tapping mode AFM images of 12 double layers of **P2** and PCM multilayer films prepared by (a) The solution-dipping method and (b) The spin-coating method

A clear difference can be seen between the solution-dipped (Figure 3.4(a)) and the spin-coated sample (Figure 3.4(b)). The solution-dipped sample showed relatively large flat plateaus, separated by sharp steps, whereas the spin-coated sample showed a smoother variation of the height and a finer structure. As a result, the surface roughness (standard deviation from average) of a solution- dipped film is about 5.9 Å and that of a spin-coated film only 3.7 Å. This demonstrates that the shear forces during the spinning process enhance the planarization of the multilayer film. On the other hand, the solution-dipped sample resembles the thin films of smectic liquid crystals,[38-40] which display also large plateaus separated by sharp layer steps.

To determine the thickness of the multilayer films, surface plasmon resonance (SPR) measurements were performed at various stages during the solution adsorption process (solution-dipping).[35] For the much thicker samples obtained by spin-coating method a proper evaluation was not possible. Examples of SPR curves are depicted in Figure 3.5. Measurements were performed after adsorption of each bilayer from THF/water mixture onto a thin gold film, which was brought into optical contact with a prism afterward. Then the reflectivity of the sample is monitored as a function of incident angle Θ (see Figure 3.5).
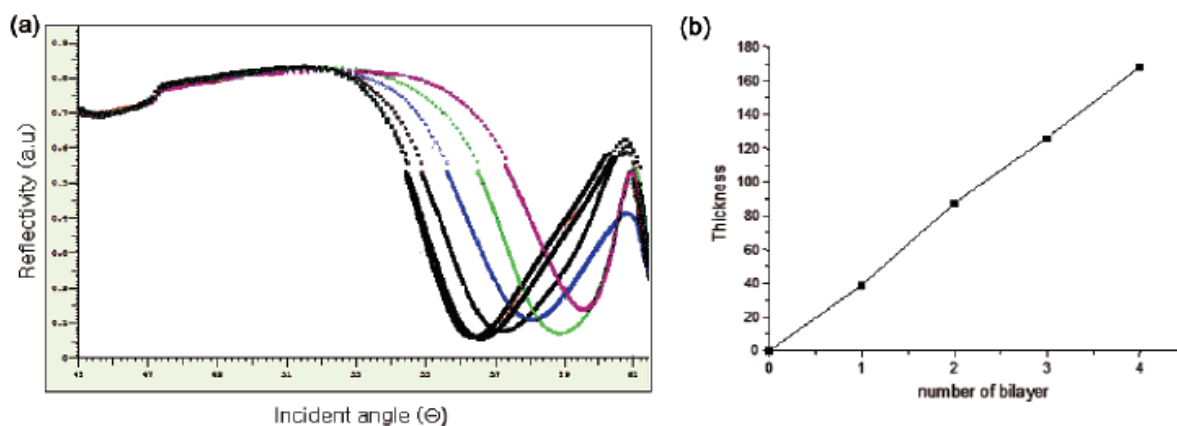
Figure 3.5. (a) Angular dependent SPR curves after different deposition cycles of the LC polymer **P2** and PCM by the solution-dipping method. (b) The film thickness according to the number of bilayers.

The shift in the SPR angle (minimum of curve) observed during the formation of the multilayer (**P2** and PCM) can be used to determine the film thickness, if the refractive index of the film is known. As a starting point, we assumed the refractive index of LC-ionomer **P2** to be 1.5, as generally used.[35] A value of about 6 Å was found for the initially adsorbed anionic layer of 3-mercaptopropionic acid used to functionalize the metal gold layer. The resulting evaluation (Figure 3.5(b)) showed a linear thickness increase with a thickness per bilayer (cationic layer (PCM) and anionic ionome layer (**P2**)) about 40 Å. This value per double layer is rather high compared to "usual" polyelectrolytes, but still it is in the range of values found for other LC ionomers.[24,25,36] This is a consequence of the low charge density of the rather hydrophobic LC ionomers.

The question to be answered is: Is there an influence of the liquid-crystalline phase on the adsorption process? SPR measurement gives only an averaged thickness of the adsorbed film. Following the arguments of the introduction (difficulty of complete reorganization of polyelectrolyte multilayer assembly; preorganization in lyotropic phase), there should be a relation between the smectic structure and the thickness of the adsorbed layer. On the basis of the X-ray results of **P2** and the molecular model (see Figure 3.2), a thickness of about 80 Å would have been expected per adsorbed double layer of LC ionomer and polycation (an anionic smectic double layer of **P2** and some thickness for the cationic PCM layer). However, the thickness of the double layer adsorbed from solution is only half as thick (40 Å, SPR).

Concerning the alternating deposition sequence in multilayer buildup between **P2** and PCM, the **P2** layer must expose negative charges to both sides as presented in Figure 3.2(e). A possibility to combine a thickness of 40 Å per double layer, fabricated between polycation and polyanion, and a smectic structure is the assumption of the adsorption of fully interdigitated monolayers of **P2** (see Figure 3.2(e)). That is to assume a structure in the multilayer, which is different from the double layers stable in the melt. Such fully interdigitated monolayers result if mesogens are originating from different polymer chains interdigitate, as found for homopolymer **P1**. The mesogens may pack well in such an arrangement, but the distance between the ionic groups must be increased compared to the situation in bulk (Figure 3.2). This might be possible in the lyotropic phase due to the presence of solvent.

To determine of the order within the multilayer assembly, X-ray reflectivity measurements were made. For these measurements, samples were made differently that they consisted of 16 bilayers, and they were assembled on a polished silicon wafer. The results obtained from solution-dipped and spin-coated samples are displayed in Figure 3.6.
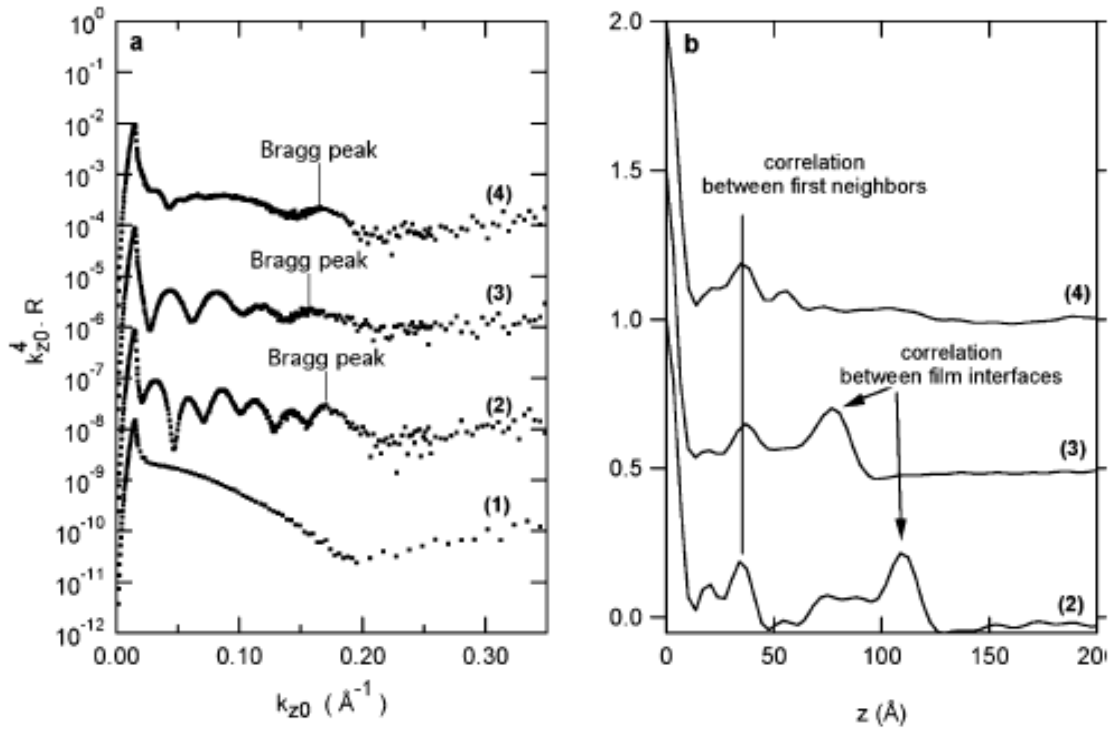
Figure 3.6. (a) X-ray reflectivity of different multilayer films: (a-1) basis double layer prepared with PEI and PAMPS; (a-2) 16 bilayers sample with **P2**/PCM prepared by the solution-dipping method; (a-3) annealed solution-dipping sample for 12 h at 150 °C; (a-4) 16 bilayers sample with **P2**/PCM prepared by the spin-coating method. k_{z0} is the vertical component of the incident photons in a vacuum. (b) Patterson function of samples shown in (a). In (a) and (b), the curves are shifted vertically for clarity.

The evaluation of the X-ray reflectivity measurements shows for all samples a weak Bragg peak at a k_{z0} value of about 0.17 Å^{-1}, suggesting an internal ordering. We assume that this is the second order of a Bragg peak located at about k_{z0} = 0.085 Å^{-1} and buried below Kiessig fringes. This would correspond to a layering of about 37 Å, in agreement with the values of the increment determined by SPR measurements. To check this hypothesis, we have computed the Patterson functions from the X-ray reflectograms, as described previously.[19] The Patterson function P(z) is proportional to the probability of finding in the film two interfaces spaced apart by a distance z. For all **P2**-based samples, a strong peak develops at 36 Å in the Patterson functions, indicating the existence of a periodic fluctuation in the film. Indications for correlation between second neighbours can also be seen in these functions. This inner periodic fluctuation is found independent of the preparation of the sample. It is,

however, better developed for the sample obtained by solution-dipping, and it decreases during annealing. Nevertheless, these experiments clearly demonstrate that layering exist in all **P2**-based films, albeit of limited spatial extent. Next, only samples obtained by solution-dipping show Kiessig fringes. These fringes transform in the Patterson function into a final peak whose position directly determines the film thickness. This shows that the films from the solution-dipping method are flat and smooth. However, the thickness of the films prepared by the solution-dipping method is much lower than expected, indicating incomplete growth on the silicon wafer. Interestingly, the film contracts upon annealing; its thickness decreasing from 109 Å to about 77 Å, testifying for substantial rearrangements occurring upon annealing. By contrast, the film prepared by spin-coating does not present Kiessig fringes or a strong final peak in the Patterson function. Since the outer surface of this film was shown to be very flat by AFM, the absence of Kiessig fringes most probably results from a very large film thickness, which prevents to get fringes due to the finite resolution of the X-ray reflectometer.

As a smectic layering exists, the mesogenic groups should be oriented perpendicular to the surface. UV/VIS dichroism offers a possibility to determine the order parameter of the mesogens by angular dependent UV/VIS measurements, using unpolarized light. These were done with the multilayer samples obtained by solution-dipping and spin-coating methods. The results are displayed in Figure 3.7. In addition, it must be noted that the measurements were repeated with same samples after 6 months. The samples were stored at room temperature without special precaution, and we can conclude that the samples do not change. This proves that a stable orientation in multilayer is achieved.
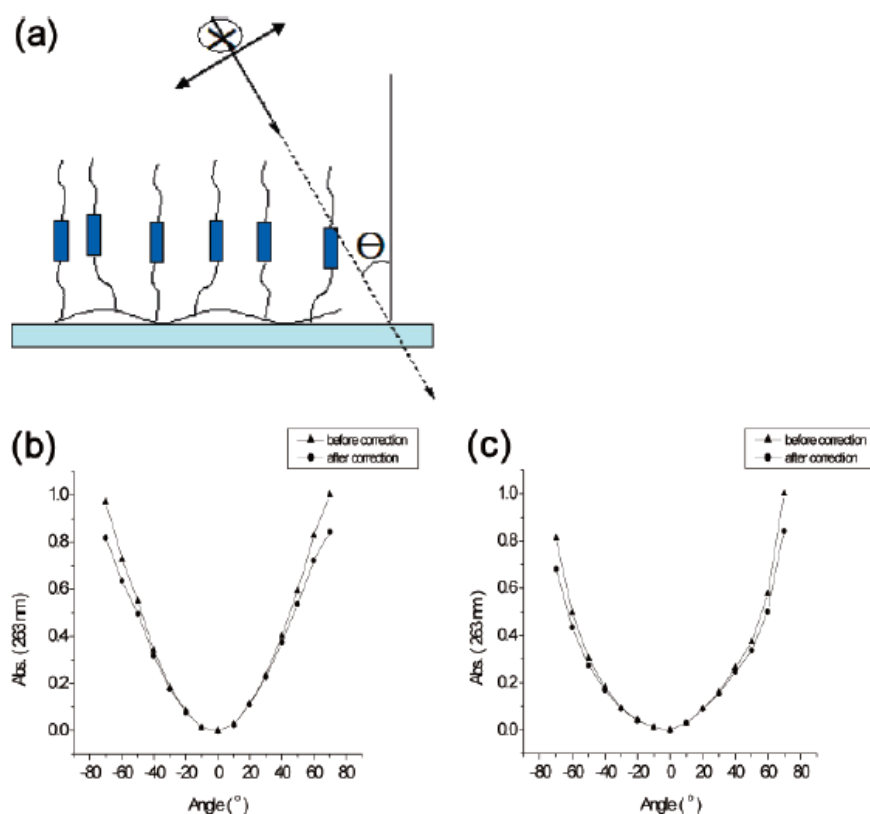
Figure 3.7. (a) Geometry scheme for the angular dependent UV/VIS measurement with unpolarized light, i.e., light polarized within the paper plane and perpendicular. Note that the absorption of light polarized perpendicular to the paper plane should not vary while changing the angle Θ. (b) Results of angular dependent UV/VIS measurement of 12 bilayers consisting of **P2** and PCM prepared by the solution-dipping method and (c) By the spin-coating method. For comparison of the both spectra the absorption perpendicular to the substrate $A^\perp$ was subtracted. $\blacktriangle$: primary data; $\bullet$: after thickness correction by factor **d**.

First, the measurements had to be corrected for the absorbance by a correction factor **d** (see Experimental Section). The corrected values showed a strong increase of the absorption on increasing the angle, too. As the biphenyl chromophores absorb light polarized along their long axis, this proved that the biphenyl units were oriented preferably perpendicular to the surface.

As the measurements were carried out with unpolarized light (Figure 3.7(a)), 50 % of the light is always polarized perpendicular to the long axis of the biphenyl chromophores independent of the angle. The absorption of the other 50 % of the light (polarized within the paper plane of Figure 3.7(a)) should follow eq 1. With this equation the angular dependence of both types of samples can be fitted for angles from -50° to +50°. From the fit, $A_\parallel$ (parallel absorbance) and

$A\perp$ (perpendicular absorbance) were obtained (see Experimental Part). Using these results, it was possible to estimate the nematic order parameter S (quality of the orientation of the long axis of the biphenyl chromophores perpendicular to the surface) using eq 2.[44] As a result, an order as high as S) 0.25 was obtained for the sample prepared by solution-dipping, and a value of only S) 0.07 was obtained for the sample obtained by spin-coating. In LC phases, typical order parameters between 0.3 and 0.6 are found for nematic phases and 0.6 and 0.8 for smectic phases.[43,44] Consequently, the value observed for the solution-dipped sample is very close to the value of monodomain liquid crystalline phases, and the value for the spin-coated sample corresponds only to "some" preferred orientation.

$$A(\Theta) = \sqrt{A_\parallel \sin^2 \Theta + A_\perp \cos^2 \Theta} \qquad (1)$$

$$S = \frac{A_\parallel - A_\perp}{A_\parallel + 2A_\perp} \qquad (2)$$

3.3. Conclusion

In this work, new amphotropic LC ionomers, which possess smectic thermotropic phases in bulk and lyotropic phases in solution, were synthesized. These LC ionomers could successfully be used for the multilayer build-up by solution-dipping and spin-coating methods. Although both methods showed quite linear and reproducible multilayer build-up performances by UV/VIS measurements, the AFM, SPR, and XRR measurements indicated differences between multilayer samples prepared by both methods. The differences between the solution-dipped and spin-coated samples can be rationalized by the different mechanisms. During the solution-dipping process, the charged LC ionomers diffused toward the substrate, and then adsorbed chains rearranged themselves as thin films. The amount of adsorption is controlled by charge compensation, and the whole deposition process (including final drying)

is quite slow. It gives enough time to orient mesogens in the lyotropic phases. After removal of the solvents, the lyotropic phases (in concentrated solution) change into thermotropic phases (in bulk), resulting in a stabilized internal structure. The orientation of the mesogens is well improved due to the liquid crystallinity. However, the amount of the adsorbed LC ionomers in most cases not be the exact amount needed to form the smectic layers; thus layer steps arise. As a result of a lyotropic phase, which is different from the thermotropic bulk phase (monolayers vs double layers), the films rearranged during annealing, decreasing the order and flatness of the films.

On the other hands, the spin-coating method gave much thicker films due to the fast elimination of the solvent and the high spinning process. In addition, spin-coated films possessed less internal order. The drying process happens very quickly, and it provides not enough time for the formation of the LC phase. Thus, the surface of the film was smoother because it does not fabricate the smectic layer. At the same time, the LC order, with respect to both layering and parallel orientation of the mesogens, was poorer compared to the solution-dipped sample.

The questions remaining are: What is the relation between the bulk phase of the LC ionomers and the structure present in the multilayers? And how is their long-term stability? At first, a direct comparison of the LC behavior of multilayers and the bulk or lyotropic phase of the LC ionomer is impossible because of the different composition. The LC ionomer contains low molar mass counterions in both bulk and lyotropic phase; on the other hand, the multilayer contains polymeric counterions (the polycation). Thus, from a thermodynamic point of view the phase behaviour should be different, and the LC phases of the multilayer have to be compared to that of a one to one mixture of LC ionomer and the polyelectrolyte. Now, the one-to-one composition from polycation and polyanions present in the multilayers corresponds to a polyelectrolyte complex, in which the viscosity is extremely high and the equilibrium is hardly reached. If e.g. LC ionomer and poly(choline methacrylate) (PCM, polycation) solutions are mixed, an unmeltable polyelectrolyte complex is formed immediately. So there is no equilibrium reference state for a bulk phase of the mixture, to which the multilayers can be compared. In addition, no equilibrium state is reached for the multilayer, too. On the contrary, the structure present during adsorption and drying (lyotropic phase, transition to thermotropic bulk phase) is frozen-in. This structure is, however, long-term stable. This can be shown e.g. by a repetition of the angular dependent UV/VIS

measurements done with samples stored at room temperature for 6 months, which reproduced the old parameters.

Consequently, we obtained multilayers with synthesized amphotropic LC ionomers, which are suitable materials to fabricate internal ordered multilayers. The multilayers deposited by the solution-dipping method show the order parameter closed to that of real liquid crystalline monodomains, and based on that parameter, the mesogens of the LC ionomers are oriented perpendicular to the substrate.

3.4. Experimental

LC Polyelectrolytes.

N-(6-Bromohexyl)phthalimide (1). A solution of 1,6-dibromohexane (44.8 g, 0.183 mol) in 300 mL of acetone was heated to reflux. Potassium phthalimide (17 g, 0.092 mol) was added in four portions over a period of 4 h. The resulting mixture was kept under reflux for an additional 24 h. After cooling to room temperature, the mixture was filtered and the solvent was evaporated. The crude product was purified by column chromatography (eluent petrol ether/ ethyl acetate 8:1), yielding 19.7 g (0.063 mol, 69 %) of colorless powder (melting point: 60 °C).

^{1}H NMR (CDCl$_3$, 200 MHz): δ = 7.77 (m, 2H, arom H), 7.70 (m, 2H, arom H), 3.66 (t, 2H, N-CH$_2$), 3.37 (t, 2H, Br-CH$_2$), 1.2-1.9 (m, 8H, aliphatic H).

(±)-4-Toluenesulfonic Acid 2-Octyl Ester. A solution of 90.6 mL (74.2 g/0.57 mol) of (±)-2-octanol in 300 mL of pyridine was cooled to 0 °C. Within 30 min, 104.9 g (0.55 mol) of p-toluenesulfonyl chloride was added. After that, the mixture was stirred for 20 h at room temperature. The reaction mixture was then poured on a mixture of 400 mL of concentrated hydrochloric acid and 600 mL of ice water. The resulting mixture was extracted three times with 300 mL of diethyl ether. The unified organic phases were dried over magnesium sulfate and filtered. After that, the solvent was evaporated in a vacuum. The reaction yielded 122.4 g of colorless oil that still contained ~10 wt % of unreacted (±)-2-octanol (equals 110.2 g/0.387

mol (±)-4-toluenesulfonic acid 2-octyl ester, yield: 70 %). The product was reacted without further purification.

^{1}H NMR (CDCl$_3$, 200 MHz): δ = 7.73 (d, 2H, arom H, meta to CH$_3$), 7.27 (d, 2H, arom H, ortho to CH$_3$), 4.53 (m, 1H, RCH$_2$-OR), 2.39 (s, 3H, Ar-CH), 1.0-1.7 (m, 13H, aliphatic H + remaining reactant), 0.80 (t, 3H, R-CH$_3$ + remaining reactant).

(±)-4'-(1-Methylheptyloxy)biphenyl-4-ol (2). A solution of 16.9 g (0.3 mol) of potassium hydroxide and 57.6 g (0.3 mol) of 4,4'- dihydroxybiphenyl in 750 mL of methanol was heated to reflux under a nitrogen atmosphere. After that, a solution of 95.6 g (0.3 mol) of (±)-4-toluenesulfonic acid-2-octyl ester prepared according to ref 37 in 160 mL of methanol was added in small portions during 8 h. The reaction mixture was then refluxed for another 40 h, and the solvent was removed in a vacuum. The residue was stirred for 1 h with 2 N hydrochloric acid, filtered, and washed twice with water and once with a small amount of ethanol. The crude product was purified by column chromatography (petrol ether/ethyl acetate 8:1). The reaction yielded 25.3 g (0.084 mol, 28 %) of colorless solid (mp: 76 °C).

^{1}H NMR (CDCl$_3$, 200 MHz): δ = 7.41 (m, 4H, arom H, meta to O), 6.88 (m, 4H, arom H, ortho to O), 4.36 (m, 1H, RCH$_2$OR), 3.32 (bs, 1 H, OH), 1.1-1.8 (m, 13H, aliphatic H), 0.87 (t, 3H, CH$_3$).
^{13}C NMR (CDCl$_3$, 50.3 MHz): δ = 157.4 (1C, arom C, ipso to -OR), 154.6 (1C, arom C, ipso to OH), 133.8 and 133.2 (2C, arom C, para to O), 127.9 and 127.7 (4C, arom C, meta to O), 116.2 and 115.6 (4C, arom C, ortho to O), 68.5 (1C, RCH$_2$O), 36.5, 31.8, 29.3, 25.6, 22.6, 19.8, 14.1 (7C, aliphatic C).

(±)-N-{6-[4'-(1-Methylheptyloxy)biphenyl-4-yloxy]hexyl}- phthalimide (3). A mixture of N-(6-bromohexyl) phthalimide (14.05 g, 45 mmol), (δ)-4'-(1-methylheptyloxy)biphenyl-4-ol (13.57 g, 45 mmol), potassium hydroxide (2.7 g, 48 mmol), and a catalytic amount of KI in 100 mL of methanol was heated to reflux for 4 days under a nitrogen atmosphere. After cooling to 4 °C, a white solid precipitated which was isolated and washed with a small amount of cool methanol. The product yielded 10.3 g (19.5 mmol, 43 %) of a white solid (mp: 64 °C).

^{1}H NMR (DMSO, 200 MHz): δ = 7.83 (m, 4H, arom H of phthalimide), 7.46 (d, 4H, arom H, meta to O of biphenyl), 6.91 (d, 4H, arom H, ortho to O), 4.41 (m, 1H, O-CH), 3.92 (t, 2H, O-CH$_2$), 3.56 (t, 2H, N-CH$_2$), 1.1-1.8 (m, 21H, H-6-H-9, H-19, R-CH$_2$), 0.81 (t, 3H, R-CH$_3$).

^{13}C NMR (DMSO, 50.3 MHz): δ = 167.9 (2C, carbonyl), 157.6 + 156.8 (2C, arom C, ipso to O), 134.3 (2C, arom C of phthalimide), 132.1 +132.0 (2C, arom C, para to O), 131.5 (2C, arom C of phthalimide), 127.1 + 127.0 (4C, arom C, meta to O), 122.9 (2C, arom C of phthalimide), 115.8 + 114.7 (2C, arom C, ortho to O), 72.9 (1C, O-CH), 67.3 (1C, O-CH$_2$), 37.3 (1C, N-CH$_2$), 35.8 (1C, O-CH-CH$_2$), 31.2 + 28.6 + 28.4 + 27.7 + 25.9 + 25.1 + 24.8 + 21.9 (8C, aliphatic C), 19.5 (1C, OCHCH$_3$), 13.8 (1C, R-CH$_3$).

(±)-6-[4'-(1-Methylheptyloxy)biphenyl-4-yloxy]hexylamine (4). Hydrazine hydrate (1.03 g, 20.6 mmol) was added to a solution of (±)-N-{6-[4'-(1-methylheptyloxy)biphenyl-4-yloxy]hexyl}- phthalimide (10.2 g, 19.2 mmol) in 100 mL of ethanol. The mixture was kept under reflux for 16 h. After addition of 10 mL of concentrated HCl, the resulting solution was kept under reflux for 1 h. After cooling to 4 °C a white solid precipitated which was isolated. The solid was stirred for 30 min in 1 M aqueous NaOH. After filtration, the crude product was heated with 200 mL of CHCl$_3$ and 5 g of Na$_2$SO$_4$ under reflux for 2 h. Filtration after cooling and evaporation of the organic solvent, the reaction yielded 4.53 g (11.3 mmol, 60 %) of a white product.

^{1}H NMR (CDCl$_3$, 200 MHz): δ = 7.43 (m, 4H, arom H, meta to O), 6.91 (m, 4H, arom H, ortho to O), 4.35 (m, 1H, O-CH), 3.96 (t, 2H, O-CH$_2$), 2.71 (t, 2H, NH$_2$-CH$_2$), 1.2-2.2 (m + bs, 23H, aliphatic H, NH$_2$), 0.87 (t, 3H, R-CH$_3$).

Poly(N-acryloyloxysuccinimide) was prepared as described in ref 37.

^{1}H NMR (DMSO, 200 MHz): δ = 3.11 (1H, CH, main chain), 2.80 (4H, CH$_2$, side groups), 2.08 (2H, CH$_2$, main chain).

^{13}C NMR (DMSO, 50.3 MHz): δ = 169.8 (2C, RC(O)N), 162.3 (1C, RC(O)O), 35.7 (1C, CH, main chain), 30.7 (1C, CH$_2$, main chain), 25.4 (2C, CH$_2$, side chain).

LC Homopolymer P1. A sample of 255 mg (1.51 mmol repeating units) of poly(N-acryloyloxysuccinimide) was dissolved in 40 mL of DMF and heated to 50 °C. Subsequently, a solution of 720 mg (1.81 mmol repeating units) of primary amine in 10 mL of DMF was

added. The reacting mixture was stirred for 24 h at room temperature under a nitrogen atmosphere; afterward, the mixture was concentrated in a vacuum to 5 mL. The polymer was precipitated by pouring the solution into 100 mL of methanol. After centrifugation, the solvent was decanted, and the product was washed several times with methanol and dried. The reaction yielded 340 mg of a pale yellow solid.

^{1}H NMR (CDCl$_3$, 200 MHz): δ = 7.45 (4H, arom H, meta to O), 6.92 (4H, ortho to O), 4.27 (1H, O-CH), 3.99 (2H, NHR- CH$_2$), 3.25 (2H, NH-CH$_2$), 1.31-1.24 (12H, aliphatic H + main chain), 0.86 (3H, O-R-CH$_3$).

LC Ionomers P2. A sample of 501 mg (2.96 mmol repeating units) of poly(N-acryloyloxysuccinimide) was dissolved in 40 mL of DMF and heated to 50 °C. Subsequently, a solution of 587 mg (1.48 mmol repeating units) of primary amine in 10 mL of DMF was added for **P2**. The reacting mixture was stirred for 5 h at RT under a nitrogen atmosphere. It was checked by thin-layer chromatography that no free amine was left after this time. For **P2**, a solution of 454 mg (2.96 mmol) of the 4-aminobutyric acid methyl ester hydrochloride in 10 mL of DMF was then supplemented, and then 4 mL of triethylamine was added. The mixture was stirred for a further 24 h at 50 °C. Afterward, the mixture was concentrated in a vacuum to 10 mL. The polymer was precipitated by pouring the solution into 100 mL of methanol. After centrifugation, the solvent was decanted, and the product was washed several times with methanol and dried. The reaction yielded **P2** as bright-yellow solids.

^{1}H NMR (CDCl$_3$, 200 MHz): δ = 7.41 (4H, arom H, meta to O), 6.87 (4H, ortho to O), 4.31 (1H, O-CH), 3.89 (2H, O-CH$_2$), 3.61 (3H, COOCH$_3$), 3.21 (4H, NH-CH$_2$), 2.31 (2H, CH$_2$-CH$_2$- COOCH$_3$), 1.71-1.23 (15H, aliphatic H + main chain), 0.86 (3H, O-R-CH$_3$).
IR (ATR): 2927, 2853 (C-H aliphatic), 1737 (COO-CH$_3$), 1644 (CO- NHR), 1497, 1238, 1173, 1035, 822 cm^{-1}.

Cleavage of the Ester Bond To Obtain LC Ionomer P2. A solution of 200 mg of the precursor of **P2** in 15 mL of DMF was heated to 40 °C under a nitrogen atmosphere. After that a solution of 1.1 g of potassium hydroxide in 5.5 mL of water was added to the reaction mixture with a syringe. The mixture was stirred for 5 h at 40 °C. As a white product had formed, the solvent was evaporated, and the residue was washed three times with 100 mL of water. The mixture was then centrifuged, and the solvent was decanted. The crude product

was added to the solution of K_2CO_3 (pH = 9) and then again centrifuged, and the solvent was decanted. After drying, 229 mg (9.6 mmol repeating units, 72 %) of a pink solid was obtained.

IR (ATR): 2928, 2856 (C-H aliphatic), 1642 (CO- NHR), 1564, 1497, 1397, 1239, 821 cm^{-1}.

P3 LC Ionomer. For the synthesis of **P3a** with 20 % of ionic amines or **P3b** with 50 % of ionic amines, 251.9 mg (1.487 mmol repeating units) of poly(N-acryloyloxysuccinimide) was dissolved in 15 mL of DMF and heated to 50 °C. Subsequently, a solution of 473.6 mg (1.191 mmol repeating units) of primary amine for **P3a** or 295.6 mg (0.744 mmol repeating units) of primary amine for **P3b** in 10 mL of DMF was added. The mixture was stirred for 5 h at 70 °C and then cooled to 50 °C. After that, a solution of 239 mg (0.912 mmol) of 4-aminobutyltriethylphosphonium chloride hydrochloride in 10 mL of methanol and 4 mL of triethylamine for **P3a** or 194 mg (0.744 mmol) of 4-aminobutyltriethylphosphonium chloride hydrochloride in 8 mL of methanol and 4 mL of triethylamine for **P3b** was added. The mixture was stirred for another 24 h at 50 °C. Afterward, the mixture was concentrated in a vacuum to 10 mL. The polymer was precipitated by pouring the solution into 100 mL of diethyl ether. After centrifugation, the solvent was decanted, and the product was washed several times with diethyl ether and dried. The reaction yielded **P3a** or **P3b**.

Polyelectrolytes. Branched poly(ethylenimine) (PEI) was purchased from Aldrich and used without further purification. The synthesis of poly(2-acryloylamino-2-methylpropyl sulfonate sodium salt) (PAMPS) and poly(choline methacrylate) (PCM) were already described elsewhere.[36]

Substrates for the Multilayer Build-up. The formation of multilayers was performed on a quartz glass or a silicon wafer used as substrates. Cleaning of these substrates was achieved using a classical procedure.[10] The substrates were immersed for 20 min in a 1:1 mixture of concentrated H_2SO_4 and a 30 % H_2O_2 ("piranha solution"; caution: piranha reacts violently with organic compounds and should not be stored in closed containers) and then extensively rinsed with ultrapure water (obtained by deionization and purification using the Milli-Q system from Millipore) at three times. And then the substrates were treated with a 1:1:5 mixture of 25 % aqueous NH_3, 30 % H_2O_2, and H_2O at 80 °C to functionalize and thoroughly rinsed with ultrapure Milli-Q water. After further washing, the substrates were used for multilayer adsorption.

Multilayer build-up. In the beginning, two double layers of poly(ethylene imine) (PEI) (from a solution of 2.5 mg/mL PEI in 1 N hydrochloric acid) and poly(2-acryloylamino-2-methylpropyl sulfonate sodium salt) (PAMPS) (from a solution of 3.5 mg/mL PAMPS in water) were adsorbed on the substrates as basis layers. At each time, the substrates were dipped into the solution for 20 min, and then the substrates were rinsed three times with plenty of Milli-Q water (each time for 1 min) between these two steps, as already described in the literature.[1] The initially deposited double basis layers are sufficient to start the multilayer deposition process; the surface coverage and charge density appear to be more uniform after a number of bilayers of highly charged polyelectrolytes have been deposited, thereby eliminating any effects that the substrate itself may have on the adsorption process. After fabrication of these basis layers, substrates were sequentially dipped in a cationic poly(choline methacrylate) (PCM) solution for 10 min (from a solution of 2.5 mg/mL PCM in water) rinsed three times by immersion in ultrapure water (1 min). And then dipped for 10 min in a polyanion solution and three times rinsing steps were performed. This deposition procedure was then cycled to obtain multilayers. The multilayers were dried under nitrogen gas purging at the end of their fabrication.

Identical procedure was adopted when the multilayers assembled by the spin-coating method. In this case, however, the polymer/solvent solution and aqueous solution of PCM were poured onto a substrate, and then the substrate was spun at a speed of 4000 rpm for 15 s. Subsequently, plenty of Milli-Q water was put on the substrate, and then the substrate was spun again at the same conditions. Before alternately depositing polymer **P2** and PCM onto the prepared substrate by the spin-coating method, PEI and PAMPS were also predeposited two times as basis layers alternately in cationic aqueous solution of PEI and then in anionic aqueous PAMPS like the solution-dipping method at same condition. The washing steps were repeated three times. At the end of every adsorption cycle, the multilayers were dried under nitrogen gas purging, and UV/VIS spectra were measured.

Instruments. ^{1}H and ^{13}C NMR spectra were mostly measured on a Bruker 200 MHz FT spectrometer. In some cases spectra were also measured on a Bruker 400 MHz FT spectrometer. The spectra were analyzed with the software Win-NMR 6.1. Infrared spectra were measured on a Bruker Vector 22 FT-IR spectrometer with a Harrick ATR unit. The analysis of the spectra was performed with the software OPUS 3.1. The phase transitions

temperatures of the polymers were investigated by differential scanning calorimetry (DSC) performed with a Perkin-Elmer DSC 7 at a scan rate of 10 °C min^{-1}. To determine the molecular weight of the polymers, gel permeation chromatography (GPC) was performed on a Jasco instrument and THF was used as mobile phase. The separation was done on a MZ-Gel SD plus precolumn (8 mm x 50 mm) and three MZ-Gel SD plus main columns (8 mm x 50 mm) produced by Mainz Analysentechnik. For each measurement 100 μL solution of the polymer in THF (2 mg/mL) was injected. The detection was performed with Jasco refractive index and UV detectors and a Viscotek light scattering detector. Polarizing microscopy investigations were performed with a Zeiss Jenapol SL 100 microscope. The samples were analyzed in a Linkam THMS 600 hot stage and tempered with a Linkam TMS 93-control module. X-ray measurements (LC phases) for bulk state were carried out on a Siemens D-500 diffractometer using Cu KR radiation λ = 1.54 Å) and a single crystal graphite monochromator. Additionally, X-ray reflectivity measurements for multilayers were done with the setup described in ref 19.

Samples were imaged at room temperature with a commercial AFM (Nanoscope IIIa, Digital Instruments, Santa Barbara, CA) employing Tapping Mode using rectangular silicon cantilevers (Nanosensors, 125 μm long, 30 μm wide, 4 μm thick) with an integrated tip, a nominal spring constant of 42 N m^{-1}, and a resonance frequency of 330 kHz. To control and enhance the range of the attractive interaction regime, the instrument was equipped with a special active feedback circuit, called Q-control (Nanoanalytics, Germany). The quality factor Q of this oscillating system is increased up to 1 order of magnitude. As a consequence, the sensitivity and lateral resolution are enhanced, allowing us to prevent the onset of intermittent repulsive contact and thereby to operate the AFM constantly in the attractive interaction regime.

SPR measurements were performed in the Kretschmann configuration against ethanol. Optical coupling was achieved with a LASFN 9 prism, n = 1.85 at λ = 632.8 nm and index matching fluid n = 1.70 between prism and the BK270 glass sildes. The plasmon was excited with P-polarized radiation using a He/Ne laser (632.6 nm, 5 mW). For SPR, glass slides (3.5 cm x 2.5 cm) were used, and glass slides were cleaned with aqueous $NH_3/H_2O_2/H_2O$ (1:1:5) for 10 min at 80 °C, washed with water and 2-propanol, and dried in a stream of nitrogen. These glass slides were coated with gold using a Balzer BAE 250 vacuum coating unit under pressure of less than 5 x 10^{-6} hPa, typically depositing 50 nm of gold after first depositing 2

nm of Cr. The slides were exposed to 3-mercaptopropionic acid solution (1 mmol) for 12 h and then deprotonated by using 1 mmol of aqueous NaOH solution.

UV/VIS measurements were performed on a Shimadzu UV- 2102 PC spectrometer. Angular dependent UV/VIS spectra were also examined by using the same spectrometer. A custom-built sample holder equipped with a rotation stage to which the quartz substrates were affixed was placed in the middle of the light path. Rotation of the sample holder resulted in illumination of the same area of the sample both in the parallel (0°, shear direction parallel to the electric field vector of the incident radiation) and perpendicular (90°, shear direction perpendicular to the electric field vector of the incident radiation) configurations. We performed the angular dependence of both types of samples for angles from -70° to +70°. The spectra were plotted as the absorbance at a given angle of the incident light beam; however, there is a tendency for the absorbance to increase with increase in the angle used. Above all, increasing absorption which is related to the increasing optical thickness has to be corrected by a correction factor d.

$$d = \cfrac{1}{\cos\left(\arcsin\left(\cfrac{\sin\Theta}{1.65}\right)\right)} \qquad \begin{cases} \Theta = \text{angle} \\ d = \text{correction factor} \end{cases}$$

To correct for the light polarized perpendicular to the plane defined in Figure 7a (paper plane), 50 % of the absorption at 0° was subtracted. This corresponds to 0.35005 for the spin-coated sample and to 0.01375 for the solution-dipped sample (two times this value plus the corrected absorption resulted in Figure 3.7(b),(c) representing therefore the real measured absorption). The angular dependent absorption minus the 50 % absorption at 0° was fitted with formula 1 from -50° to +50°. This yielded an $A^\perp$ of 0.011 44 and $A_{\parallel}$ of 0.02828 for the solution-dipped sample and $A^\perp$ of 0.3484 and $A_{\parallel}$ of 0.4253 for the spin-coated sample. These values were used for the estimate of the order parameter.

3.5. References

(1) Ferreirat, M.; Rubner, M. F. *Macromolecules* **1995**, 28, 7107.

(2) Park, S. Y.; Rubner, M. F.; Mayes, A. M. *Langmuir* **2002**, 18, 9600.

(3) Tovar, G.; Paul, S.; Knoll, W.; Prucker, O.; Rühe, *J. Supramol. Sci.* **1995**, 2, 89.

(4) Piscevic, D.; Knoll, W.; Tarlov, M. *J. Supramol. Sci.* **1995,** 2, 99.

(5) Katz, H. E.; Sheller, G.; Putvinski, T. M.; Shilling, M. L.; Wilson, W. L.; Chidsey, C. E. D. *Science* **1991**, 254, 1485

(6) (a) Vermeulen, L. A.; Snover, J. L.; Sapochak, L. S.; Thompson, M. E. *J. Am. Chem. Soc.* **1993**, 115, 11767. (b) Vermeulen, L. A.; Pattanayak, J.; Fisher, T.; Hansford, M.; Burgmeyer, S. *J. Mater. Res. Soc. Symp. Proc.* **1996**, 431, 271.

(7) Rubinstein, I.; Steinberg, S.; Tor, Y.; Shanzer, A.; Sagiv, *J. Nature (London)* **1988**, 332, 426.

(8) Li, D.-Q.; Ratner, M. A.; Marks, T. J.; Zhang, C. H.; Yang, J.; Wang, G. K. *J. Am. Chem. Soc.* **1990**, 112, 7389.

(9) Vermeulen, L. A.; Thompson, M. E. *Nature (London)* **1992**, 358, 656.

(10) Fou, A. C.; Onisuka, O.; Ferreira, M.; Rubner, M. F. *J. Appl. Phys.* **1996**, 79, 7501.

(11) Decher, G.; Hong, J. D.; Schmitt, J. *Thin Solid Films* **1992**, 210/211, 831.

(12) Dubas, S. T.; Schlenoff, J. B. *Macromolecules* **2001**, 34, 3736.

(13) Dubas, S. T.; Schlenoff, J. B. *Macromolecules* **1999**, 32, 8153.

(14) Schoeler, B.; Kumaraswamy, G.; Caruso, F. *Macromolecules* **2002**, 35, 889.

(15) Steitz, R.; Jaeger, W.; Klitzing, R. v. *Langmuir* **2001**, 17, 4471.

(16) Bertrand, P.; Jonas, A.; Laschewsky, A.; Legras, R. *Macromol. Rapid Commun.* **2000**, 21, 319.

(17) Bertrand, P.; Jonas, A.; Laschewsky, A.; Legras, R. *Macromol. Rapid Commun.* **2000**, 21, 319.

(18) Fischer, P.; Laschewsky, A.; Wischerhoff, E.; Arys, X.; Jonas, A.; Legras, R. *Macromol. Symp.* **1999**, 137, 1.

(19) (a) Arys, X.; Laschewsky, A.; Jonas, A. M. *Macromolecules* **2001**, 34, 3318. (b) Arys, X.; Fischer, P.; Jonas, A. M.; Koetse, M. M.; Laschewsky, A.; Legras, R.; Wischerhoff, E. *J. Am. Chem. Soc.* **2003**, 125, 1859. (c) Glinel, K.; Jonas, A. M.; Laschewsky, A.; Vuillaume, P. Y. Multilayer Thin Films. Sequential Assembly of Nanocomposite

Materials; Decher, G., Schlenoff, J. B., Eds.; Wiley-VCH: Weinheim, 2003; Chapter 7, pp 177.

(20) Kleinfeld, E. R.; Ferguson, G. S. *Science* **1994**, 265, 370.

(21) Kotov, N. A.; Haraszti, T.; Turi, L.; Zavala, G.; Geer, R. E.; Dékány, I.; Fendler, J. H. *J. Am. Chem. Soc.* **1997**, 119, 6821.

(22) Kim, H. N.; Keller, S. W.; Mallouk, T. E.; Schmitt, J.; Decher, G. *Chem. Mater.* **1997**, 9, 1414.

(23) Kotov, N. A.; Dékány, I.; Fendler, J. H. *Adv. Mater.* **1996**, 8, 637.

(24) Cochin, D.; Passmann, M.; Wilbert, G.; Zentel, R.; Wischerhoff, E.; Laschewsky, A. *Macromolecules* **1997**, 30, 4775.

(25) Passmann, M.; Wilbert, G.; Cochin, D.; Zentel, R. *Macromol. Chem. Phys*. **1998**, 199, 179.

(26) (a) Zentel, R.; Mruk, R.; Allard, D. *Polym. Mater. Sci. Eng*. **2004**, 90, 186. (b) Murk, R. *Ph.D. Thesis* Mainz, Germany, **2003**.

(27) Cho, J.; Char, K.; Hong, J. D.; Lee, K. B. *Adv. Mater*. **2001**, 13,14, 1076.

(28) Ferruti, P.; Bettelli, A.; Fere´, A. *Polymer* **1972**, 13, 462.

(29) Hausch, M.; Zentel, R.; Knoll, W. *Macromol. Chem. Phys*. **1999**, 200, 174.

(30) Théato, P.; Zentel, R.; Schwarz, S. *Macromol. Biosci*. **2002**, 2, 387.

(31) Hong, H.; Roland, S.; Kirstein, S.; Davidov, D. *Adv. Mater*. **1998**, 10, 1104.

(32) Dubas, S. T.; Schlenoff, J. B. *Macromolecules* **1999**, 32, 8153.

(33) Chiarelli, P. A.; Johal, M. S.; Casson, J. L.; Roberts, J. B.; Robinson, J. M.; Wang, H.-L. *Adv. Mater*. **2001**, 13, 1167.

(34) Chiarelli, P. A.; Johal, M. S.; Holmes, D. J.; Casson, J. L.; Robinson, J. M.; Wang, H.-L. *Langmuir* **2002**, 18, 168.

(35) Advincula, R.; Aust, E.; Meyer, W.; Knoll, W. *Langmuir* **1996**, 12, 3536.

(36) Passmann, M.; Zentel, R. *Macromol. Chem. Phys*. **2002**, 203, 363.

(37) Mruk, R.; Prehl, S.; Zentel, R. *Macromol. Chem. Phys*. **2004**, 205, 2169.

(38) Brodowsky, H. M.; Boehnke, U.-C.; Kremer, F.; Gebhard, E.; Zentel, R. *Langmuir* **1997**, 13, 5378.

(39) Vix, A.; Stocker, W.; Stamm, M.; Wilbert, G.; Zentel, R.; Rabe, J. *Macromolecules* **1998**, 31, 9154.

(40) Gebhard, E.; Zentel, R. *Liq. Cryst*. **1999**, 26, 299.

(41) *Textures of Liquid Crystals*, Dierking, I; Wiley-VCH: Weinheim, **2003**.

(42) *Smectic Liquid Crystals, Textures and Structures*; Gray, G. W., Goodby, J. W. G., Eds.; Leonard Hill: Glasgow, **1984**.

(43) *Handbook of Liquid Crystals*; Demus, D., Goodby, J., Gray, G. W., Spiess, H.-W., Vill, V., Eds.; Wiley-VCH: Weinheim, **1998**.

(44) Pohl, L. *In Liquid Crystals*; Stegemeyer, H., Ed.; Topics in Physical Chemistry; Steinkopf: Darmstadt, **1994**.

4. Multilayer Thin Films by Layer-by-Layer Assembly of Hole and Electron Transport Polyelectrolytes: Their Optical and Electrochemical Properties.*

4.1. Introduction

Organic semiconductors and conjugated polymers are currently of wide interest for applications in electronic and optoelectronic devices including light-emitting diodes (LEDs),[1-5] thin film transistors,[6-10] photovoltaic cells[11-14] and electrochromic devices.[15,16] The enormous majority of synthetic effort and structure property studies in these fields have been dedicated to organic and polymeric semiconductors having p-type (electron donor, hole transport)[17,18] and n-type (electron acceptor, electron transport)[19-21] properties. In detail, triarylamine has been widely used as the hole-transporting materials (stable radical cations),[22,23] while oxadiazole, thiadiazole and triazine have been used as the electron-transporting (stable radical anions) or hole-blocking materials in the organic LEDs.[24-26] However, surprisingly, only a limited number of hole- and electron-transporting conjugated polymers with ionic groups (polyelectrolytes) have been explored.[27] Well known hole- and electron-transporting materials with free ionic groups are not applicable for the use in electronic devices, as the ionic conductivity would lead to a short circuit in the device.[32] This problem can be solved, in principle, by the formation of polyelectrolyte complexes of the ionic hole- or electron-transporting polymer and an oppositely charged polymer. Moreover, the charged polyelectrolytes are suitable for deposition by the layer-by-layer (LBL) method from dilute polymer solutions. Since the first report of Decher and coworkers in the early 1990s, there have been numerous reports on the LBL deposition based on the electrostatic attraction between polycations and polyanions.[28(a)-(c)] The LBL technique can form a variety of ultra-thin interfacial layers and create films comprised of semi-interpenetrated bilayers of polycations and polyanions. The film thickness can be easily controlled at the molecular level and multilayer architecture does indeed make it possible to realize significant improvements in the device performance.[29] More recently, water/alcohol soluble conjugated polyelectrolytes for the LBL assembly have been strongly favored, because multilayer devices are difficult to produce from various organic polymer solutions. As the layers are typically deposited by spin-coating it is rarely possible to choose a solvent that will dissolve the material being

deposited and yet will not dissolve the previous deposited layer. At that point, water/alcohol soluble materials are perfect candidates to deposit after previously deposited layer from normal organic solvents for example, "toluene or chloroform."

In this paper, we report the synthesis of a series of water/alcohol soluble p-type and n-type semiconducting polyelectrolytes with triarylamine, oxadiazole, thiadiazole, and triazine moieties; their multilayer build-up, optical and electrochemical performances are investigated by UV/VIS spectroscopy, photoluminescence (PL) spectroscopy and cyclic voltammetry (CV). The synthetic scheme and chemical structures of the p-type and n-type semiconducting polyelectrolytes are shown below.

Scheme 4.1. Synthetic route to the p-type and n-type semiconducting polyelectrolytes **P1-P8**.
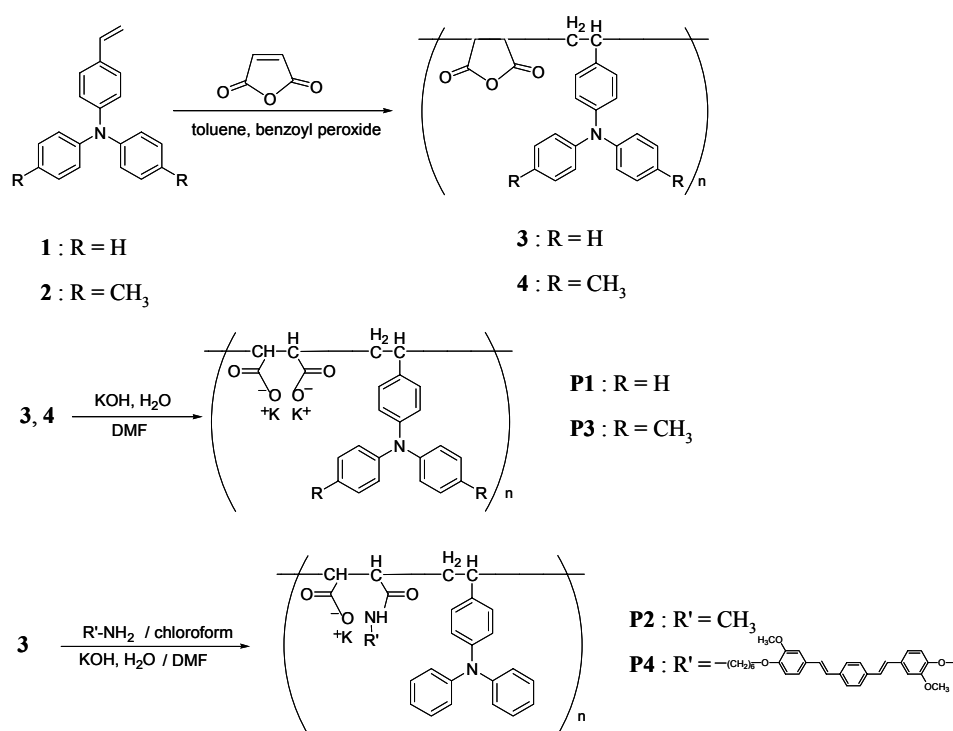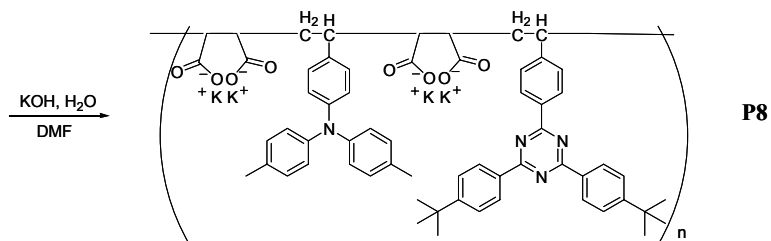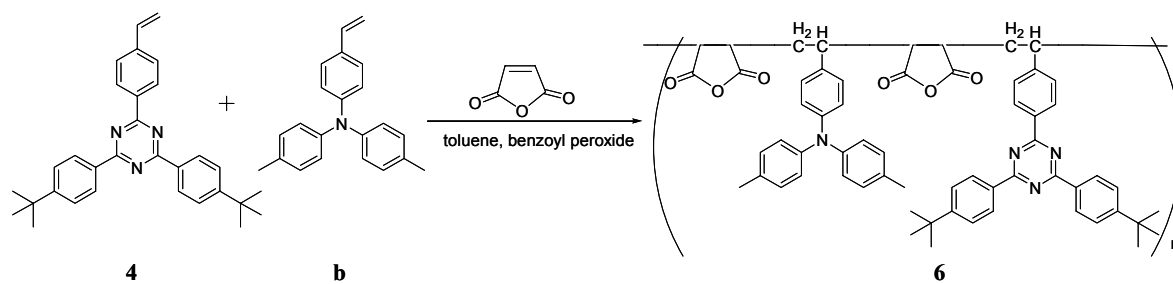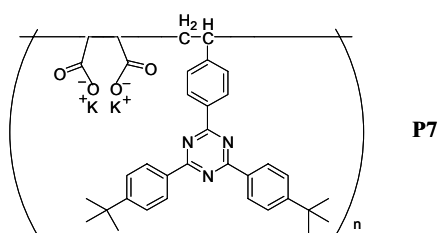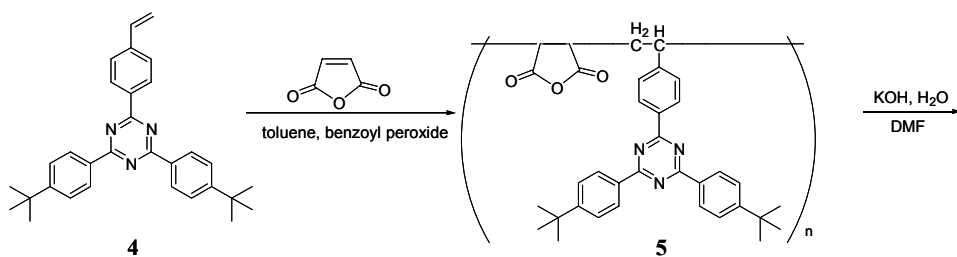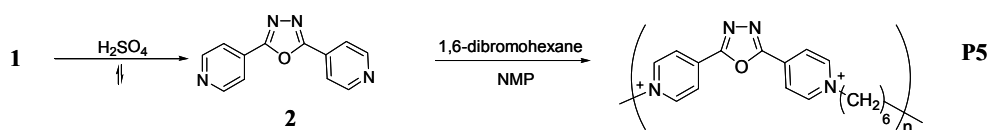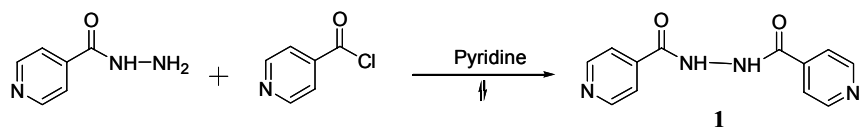
4.2. Results and discussion

Synthesis and characterization. The p-type and n-type semiconducting polyelectrolytes with triarylamine, oxadiazole, thiadiazole, and triazine functionalities were synthesized using the route illustrated in Scheme 4.1. The synthesis of the triarylamine polymers **P1-P4** started with the copolymerization of maleic anhydride and triarylamine monomers **a** and **b**[44] by radical polymerization. To determine the molecular weight, the resulting alternating copolymers **c** and **d** were analyzed by GPC with THF as eluent. (See experimental section) The synthesized alternating copolymers **c** and **d** can be subsequently treated with an amine solution (**P2**, **P4)** or with potassium hydroxide (**P1**, **P3)**. After the reaction, ring opening of anhydride and formation of the amide bond were checked by ^{1}H NMR and FT-IR spectroscopy. ^{1}H NMR proves that all functional groups are present: bisstilbene (7.78~6.70 ppm in CD_2Cl_2), triarylamine (6.89~6.97 ppm in CD_2Cl_2), as well as amide structure (1.82~1.02 ppm in CD_2Cl_2). From the FT-IR analysis, we found a sharp carboxylate peak for **P1** and **P3** at about 1586 cm^{-1} and an amide peak for **P2** and **P4** at about 1640 cm^{-1}.

Due to the electron-donating nature of the nitrogen atom, triarylamine polymers act as hole-transporting materials in various applications like xerography, light emitting diodes, solar cells, photorefractive systems, etc.[31] Two basic properties of the triarylamine unit are the easy oxidizability of the nitrogen center and its ability to transport positive charges via the radical cation species. Under the influence of an electric field, positive charge is transported by a hopping mechanism and drift mobility of holes can be up to 10^{-3} cm^2/(V•s).[31] In addition, **P3** consisting of triarylamine and bisstilbene moieties acts not only as hole-transporting material, but also as emitting material. Such mixed material, comprised of hole- and electron-transporting or hole-transporting and emitting materials can be used as a efficient single-layer device.[33]

The n-type semiconducting polyelectrolytes with oxadiazole and thiadiazole functionalities were synthesized by polycondensation. In general, polymers containing oxadiazole and thiadiazole derivatives either in the main chains or in the side chains have been widely used as electron-transporting/hole blocking materials in organic LEDs.[34-39] However, the electron deficiency in polymers was not high enough to obtain compounds with a reduction potential

less negative than -0.8 V, which means that oxygen is more easily reduced. High electron deficiency can be achieved by using additional electron-withdrawing groups like pyridines instead of phenyl groups. In addition, a further improvement can be obtained by quarternization of these pyridines by alkyl halides. Hünig et al. showed that the tripyridyltriazine compound, in which all three pyridine units are quarternized by methyl iodide, shows a first reduction potential of -0.28 V.[40] Our approach to a polymeric compound with comparable electronic properties to Hünig's system was the use of dihalogen alkanes instead of monohalogen alkanes for the quarternization of pyridine-substituted **P5-P6** with oxadiazole and thiadiazole derivatives. For the synthesis of **P5** and **P6**, compounds **2** and **3** were stirred with 1,6-dibromohexane in N-methylbutylactam (NMP) at 60 °C for 10 days yielding water soluble polymers. ^{1}H NMR spectra of **P5-P6** showed the quarternized pyridine groups of the oxathiazole and thiadiazole by alkylation, which gives cationic polyelectrolytes **P5-P6**.

Triazines have been studied also as electron transporting materials, since the triazine core has strong electron-accepting characteristics.[25] We had synthesized triazine polymers, which were substituted with additional electron-withdrawing groups like pyridine.[32] The synthesized branched triazine polymer has shown four reduction steps with the first step at a very low potential (-0.39 V) while the linear triazine polymer showed only one reduction step at -0.48 V. However, only the branched polymer was soluble in water, whereas the less polar linear polymer was only slightly soluble in water. Therefore, to increase the solubility in water or alcohol, we have introduced separated anionic charged parts to the triazine polymer. The polymers with triazine functional units were synthesized with maleic anhydride by a polymer analogous reaction like triarylamine polymers **P1-P4** and the resulting alternating copolymer **5** was characterized by ^{1}H NMR, FT-IR spectroscopy and GPC to examine the polymeric properties. The copolymer **5** was subsequently treated with potassium hydroxide and **P7** was obtained. The successful ring opening of the anhydride was checked by FT-IR spectroscopy and ^{1}H NMR.

Conjugated polymers with donor-acceptor architecture are currently of interest to balance electron or hole conductivity affinities. We have synthesized polymer **P8** composed of triarylamine and triazine derivatives. For the synthesis of **P8**, two equivalents of maleic

anhydride and a 1:1 molar ratio of triarylamine and triazine monomers were reacted. The 1:1 stoichiometry of monomers to maleic anhydride was proven by ^{1}H NMR. Finally the copolymer **6** was treated with potassium hydroxide solution to get the anionic charge.

Optical and Elctrochemical Properties. The optical properties of the synthesized polymers were investigated by UV/VIS and PL spectroscopy. Figure 4.1(a) shows UV/VIS spectra of polymers **P1**–**P8**. The maximums of the π-π* absorbance of the conjugated triarylamine polymers **P1**, **P2** and **P4** are located at 299~301 nm. **P3** shows two UV/VIS absorption peaks at 305 nm and 374 nm which are assigned to triarylamine and bisstilbene moieties. The maximums of the π-π* absorbance of polymers **P5-P6** with oxadiazole and thiadiazole, and polymer **P7-P8** with triazine and triarylamine are found identically at 287~310 nm. For the solid state behavior of the polymers, 12 thin bilayer films of **P1-P8** were assembled on quartz substrate by LBL solution-dipping and spin-coating methods (1mg/mL in THF:H_2O = 5:1) and measured also by UV/VIS spectroscopy. Because of the formation of intermolecular excimers originating from interchain interaction in the film state, slightly bathochromic shifts occurred. All results are summarized in Table 4.1. Also, PL spectroscopy was examined for all polymers (see Table 4.1). **P3** consisting of triarylamine and bisstilbene moieties at the same polymer shows very strong blue emission in the solid state at 448 nm. Therefore, synthesized **P3** containing both hole-transporting and blue light emitting moieties can be a promising candidate in single-layer OLEDs.
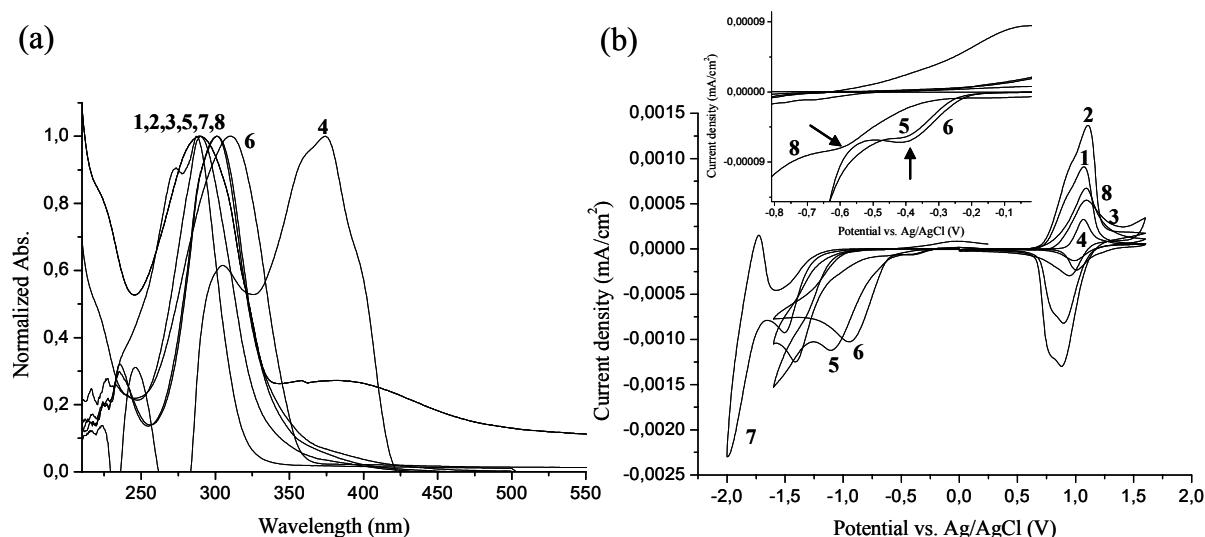
(a)

(b)

Figure 4.1. (a) UV/VIS spectra of triarylamine, oxadiazole, thiadiazole, and triazine polymers **P1-P8** in solution of THF: H_2O = 5:1 mixture solvents (b) Cyclic Voltammograms of multilayer films from **P1-P8** at a scan rate of 20 mV/s. (onset: reduction behaviors of **P5-P8**, in detail procedure of the multilayer build-up will discuss later).

Following the optical measurements, the electrochemical properties of the polymers were evaluated by CV. All CV data were obtained using a three-electrode cell in an electrolyte of 0.1 M tetrabutylammonium tetrafluoroborate (TBABF$_4$) in acetonitrile using ferrocene as the internal standard. For these investigations, multilayer films of **P1-P8** were prepared on ITO-coated glass substrates alternatively from the polymer solution in THF:H_2O = 5:1 mixture solvents. All films were examined cathodically or anodically, as seen in Figure 4.1(b). The scan for cyclic voltammograms of **P1-P4** was made anodically, proceeding from 0 V to +1.6 V and that of **P5-P7** was made cathodically, from 0 V to -1.6 or -2.0 V. For the **P8**, the film was scanned from +1.6 V to -1.6 V thoroughly. Upon oxidation of the films, oxidation peaks of **P1-P4** appear at 0.80 ~ 1.09 V, which are characteristics for triarylamine functional moieties in polymers. For **P5-P8**, as the potential becomes cathodic, reduction peaks appear corresponding to the reduction of the oxadiazole, thiadiazole, and triazine polymers. The **P5** and **P6** polymers, consisting of quaternized pyridine structures, have reduction peaks at about -0.39 V, which is well below -0.8 V (oxygen). The **P7** possesses a more negative reduction potential at -1.48 V. Interestingly, **P8**, which is combined with both triarylamine and triazine

functionalities, shows a less negative reduction potential at -0.58 V compared to that of **P7** at -1.48 V, although they have the same triazine moiety.

Based on the optical and electrochemical data, the energy levels of HOMO (highest occupied molecular orbital) and LUMO (lowest unoccupied molecular orbital) can be calculated (see Table 4.1). Due to the reduction potential, the **P7** has relatively high LUMO levels as electron-transporting materials. Furthermore, the **P8** shows a different behavior of energy band gap between the HOMO and LUMO levels. Band gap calculated from the onset of the UV/VIS absorption spectra shows much larger value (2.91 eV) than the band gap from the oxidation/reduction potentials of CV data (1.09 eV).

Table 4.1. Optical and electrochemical properties and energy levels of **P1-P8**.

| Polymers	UV/vis λ_{max} solution (nm)	UV/vis λ_{max} film (nm)	$E_g{}^a$ (eV)	PL λ_{max} solution (nm)	PL λ_{max} film (nm)	E_{ox} oneset (V)	E_{ox} (V)	E_{red} oneset (V)	E_{red} (V)	HOMO[b] (eV)	LUMO[c] (eV)
P1	299	308	3.04	455	462	0.71	0.87	x	x	5.11	2.07
P2	301	305	3.03	460	460	0.65	0.85	x	x	5.05	2.02
P3	305/374	307/362	2.96	432/448	436/459	0.83	1.09	x	x	5.23	2.27
P4	301	302	3.36	468	477	0.61	0.80	x	x	5.01	1.65
P5	293	292	3.65	379	387	x	x	-0.25	-0.38	7.80	4.15
P6	310	312	3.44	380	391	x	x	-0.22	-0.39	7.62	4.18
P7	287	292	3.80	444	494	x	x	-1.12	-1.48	7.08	3.28
P8	290	293	2.91	509	516	0.74	1.31	-0.35	-0.58	5.14	4.05

[a] Band gaps were calculated from the onset of the UV/VIS absorption spectra.

[b] HOMO levels were converted from the measured oxidation potentials assuming the absolute energy level of ferrocene to be -4.8 eV.[32]

[c] LUMO levels were estimated from the HOMO levels and energy gaps.

Optical and electrochemical properties and each of the energy levels are listed in Table 4.1. According to the calculation, **P1-P4** possess low enough HOMO levels around at -5.01~5.23 eV compared to the energy level of the ITO anode at -4.8 eV. It indicats that holes generated

from ITO anode can be effectively transported to the **P1-P4** layers in devices. Electron deficient polymers **P5-P7** possess LUMO levels around -3.28~4.18 eV, suggesting that they are quite promising as electron-transporting (n-type) materials. **P8** shows identical HOMO and LUMO levels of triarylamine and triazine functionalities. The electrochemically determined band diagrams of **P1-P8** are overlapped portions of the corresponding composing model compounds on polymer LEDs and they are collected in Figure 4.2.
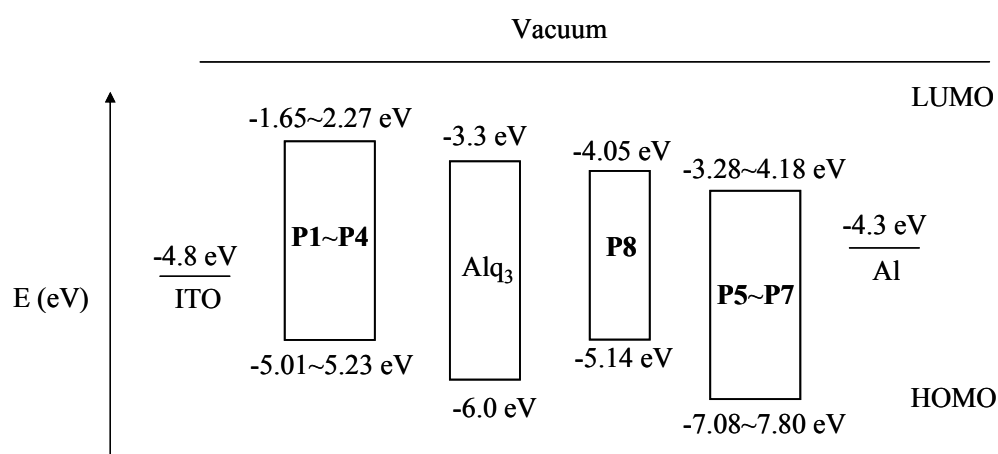
Figure 4.2. Energy band diagram of **P1-P8**.

Solubility of the Polymers. There is substantial and growing interest in using water/alcohol soluble conjugated polymers for chemical and biological applications. Using water or alcohol as a solvent has several benefits; it is an environmental friendly and low-cost solvent that allows safe processing. As summarized in Table 4.2, we have studied the solubility for the polymers **P1-P8** using water, THF/H_2O=5:1 mixture solvents, methanol, and ethanol. The anionic and cationic polymers are relatively soluble in water and alcohol, which means they are perfect candidates to build a multilayer structure after a previously deposited layer from normal organic solvents in a device. Water/alcohol soluble polymers are less sensitive to moisture and oxygen in the air[46] and especially, water-soluble conjugated polyelectrolytes can be used as highly sensitive materials in biosensors for aqueous environments in a living body.[30]

Table 4.2. Solubility of the **P1-P8** in water, THF: H_2O=5:1 mixture solvents, methanol, and ethanol.

Comp.	Type	H_2O	H_2O+THF (1:5)	ethanol	methanol
P1	**HTL**	+ +	+ + +	+ +	+ + +
P2	**HTL**	+ +	+ + +	+ +	+ +
P3	**HTL+EML**	+ +	+ + +	+ +	+ +
P4	**HTL**	+ +	+ + +	+ + +	+ + +
P5	**ETL**	+ + +	+ + +	+ + +	+ + +
P6	**ETL**	+ + +	+ + +	+ + +	+ + +
P7	**ETL**	+	+ + +	+ +	+ +
P8	**HTL+ETL**	+ +	+ + +	+ +	+ +

+ + + = very good soluble

+ + = good soluble

+ = slightly soluble

Multilayer build-up. The multilayer build-up of the synthesized **P1-P8** polymers can be done by both the solution-dipping and the spin-coating methods. Both methods lead to a regular multilayer build-up. The spin-coating method has proved, however, to be more advantageous as it can be done faster (multilayer film with 12 bilayers consumes 24 min). In addition, it needs less number of bilayers to achieve the desired film thickness, as the thickness per bilayer is increased.[43] In the beginning, two double layers of poly(ethylene imine) (PEI) and poly(2-acryloylamino-2- methylpropyl sulfonate sodium salt) (PAMPS) were adsorbed on the substrate as basis layers. After fabrication of these basis layers, substrates were sequentially deposited with a cationic poly(choline methacrylate) (PCM) solution and anionicic **P1-P4** and **P7-P8** polymer solutions. For the multilayer build-up of the cationic **P5-P6** polymers, an anionic PAMPS solution was used as oppositely charged polymer solution. The multilayer build-up was investigated by UV/VIS absorption spectroscopy as shown for the **P1**/PCM film and the **P5**/**P8** film in Figure 4.3. The **P1**/PCM film in Figure 4.3(a) showed the increase of the maximum π-π* absorbance of the spin-coated conjugated triarylamine at 308 nm. The deposition process is linear, indicating that the amount of material deposited per bilayer is completely reproducible from layer to layer. Thus it is possible to prepare multilayers, which grow constantly in thickness according to the number of bilayers. Five bilayers have thereby usually a thickness between 100 nm and 130 nm. (10 mg/mL concentration). The film of the **P5**/**P8** composition has three different

functionalities such as oxadiazole, triarylamine, and triazine. Due to the similar UV/VIS absorption ranges, the multilayer film shows broad spectra. Compared to the multilayer build-up from **P1**/PCM film, the build-up of the **P5**/**P8** film shows relatively small optical increase. It might be interpreted that the **P5**, which has cationic charges on the quarternized pyridine rings, has rather low ionic strength. Because the amount and conformation of adsorbed chains depend dramatically on processing parameters, particularly ionic strength and pH of the deposition solution, as well as the charge densities of both polyelectrolytes.[45]
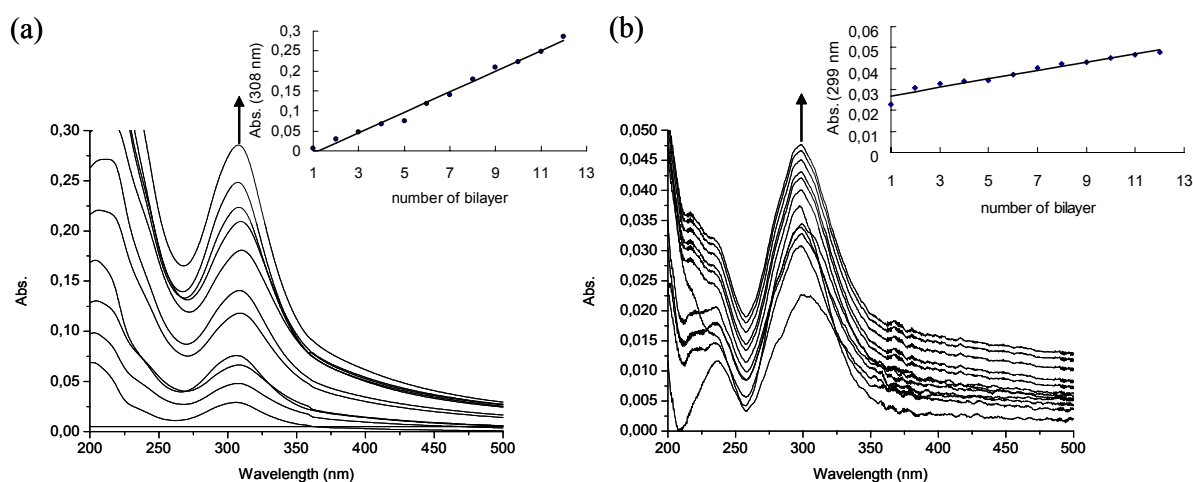
Figure 4.3. (a) Multilayer build-up from **P1**/PCM film (Inset: The growth of the multilayer films assembled by the spin-coating method at 308 nm). (b) Multilayer build-up from **P5**/**P8** film (Inset: The growth of the multilayer films assembled by the spin-coating method at 299 nm)

The multilayer build-up was also performed on ITO-coated glass substrate alternatively in the polyanion and polycation solutions. Monitoring the redox reaction of the **P1**/PCM film by CV as a function of film thickness for up to 10 bilayers reveals that the electroactivity of **P1** increases linearly with the number of bilayer, as seen in Figure 4.4. The films exhibit a redox response despite the insulating nature of the interstitial PCM layer. This suggests the presence of an interpenetrating polymer network as opposed to discrete bilayers within the film.
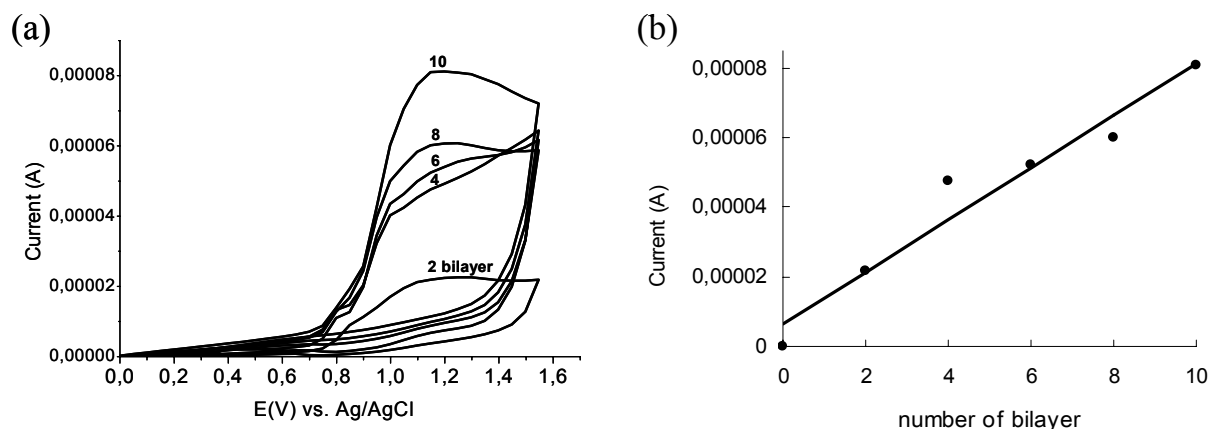
Figure 4.4. Multilayer build-up from **P1**/PCM. (a) Cyclic Voltammograms of sequential bilayer deposition, from 2-10 bilayer, at a scan rate of 20 mV/s, between 0 V and +1.6 V. (b) The peak current vs. the number of bilayer deposited on ITO-coated glass substrate.

4.3. Conclusion

The newly synthesized ionic polymers **P1** –**P8** with electron- or hole-transporting properties can be used well for a multilayer build-up by the LBL method, allowing a thickness control in the nanometer range. In this way, also a superstructure from electron- or hole-conducting moieties can be achieved, as it is necessary for 2 or 3 layer devices. As they are soluble in aqueous solutions and alcohols, they can also be useful to deposit a second organic layer (simple spin-coating) on top of a first layer, previously spin-coated from organic solvents. Therefore, the superstructure necessary for 2 or 3 layer devices is accessible. Since their electronic properties are well optimized (Figure 4.2), they have the appropriate properties for the preparation of complex OLEDs. Concerning the concept of "Green Chemistry", these polymers are favorable, because, using water or alcohol as a solvent has several benefits; it is an environmentally friendly, a safe processing, and less sensitive to moisture and oxygen in the air. Consequently, future direction of this work will be the fabrication of the thin LBL multilayer films at a nano-scale thickness with water/alcohol soluble conducting polymers, which may have applications in photodetectors, LEDs, displays and sensors, as well as in solar cells.

4.4. Experimental

^{1}H NMR spectra were measured on a Bruker 300 MHz FT spectrometer. FT-IR spectra were measured on a Bruker Vector 22 FT-IR spectrometer with a Harrick ATR unit. Gel permeation chromatography (GPC) at RT was used to determine the molecular weight with THF as eluent. For this purpose combination of a Jasco PU-1580 pump, Autosampler AS 1555, UV-detector UV 1575 and RI-detector RI 1530 were used (Wyatt light scattering, MZ-Gel SDplus10^2, 10^4 Å and 10^6 Å). To evaluate the data, universal calibration based on polystyrene standards was used. For water based GPC, only one RI-detector RI 1530 was used and pore sizes were 40, 10^2 Å and 10^3 Å. The UV/VIS absorption spectra were taken with a Shimadzu UV- 2102 PC spectrometer and photoluminescence (PL) spectra were taken with a Fluoromax-II fluorometer (ISA). All electrochemical tests were performed using an Autolab PGSTAT30 (Eco Chemie) Potentiostat/Galvanostat. Pt-wire and Ag/AgCl were used as the counter and reference electrodes, respectively. The fabricated polymer film on ITO-coated glass was used as the working electrode and 0.1 M tetrabutylammonium tetrafluoroborate (TBABF$_4$) in acetonitrile was used as the electrolyte. For spin-coating; a Convac ST146 spin-coater was used.

Preparation of triarylamine polyelectrolytes P1-P4

Preparation of alternating copolymer c, d

1:1 molar ratio of monomer **a** or **b**,[44] and maleic anhydride were dissolved in toluene and a catalytic amount of benzoyl peroxide was added to a solution mixture. The flask was swirled until most of the solid materials have dissolved and then degassed three times with nitrogen. The reaction mixture was refluxed over night for 24 h and the color changed from yellow to pink. After 24 h, the reaction mixture was cooled down to room temperature to end the reaction. The polymer was precipitated by pouring the solution into n-hexane, after centrifugation, the solvent was decanted. The product was washed three times with n-hexane and dried in a vacuum oven. The reaction yielded alternating copolymers **c** or **d**. 1:1 stoichiometry of monomer to maleic anhydride was proved by ^{1}H NMR.

copolymer c: ^{1}H NMR (CD$_2$Cl$_2$, 300 MHz): δ = 6.97 (14H, arom H), 1.66 (5H, main chain)

IR (ATR): 1777 (CO-O-CO) cm^{-1}

Mn : 98720 g/mol , Mw : 150900 g/mol, PDI (Mw/Mn) : 1.53

copolymer d: ^{1}H NMR (CD$_2$Cl$_2$, 300 MHz): δ = 6.89 (12H, arom H), 2.41~1.81 (5H, main chain),1.66 (5H, main chain)

IR (ATR): 1779 (CO-O-CO) cm^{-1}

Mn : 7442 g/mol , Mw : 10180 g/mol, PDI (Mw/Mn) : 1.37

Preparation of P1, P4

A solution of 200 mg of copolymer **c** or **d** in 10 mL of DMF was heated to 40 °C for 1 h. And then a solution of 5 g of potassium hydroxide in 15 mL of water was added to the reaction mixture with a syringe. The mixture was stirred for 5 h at 50 °C. As a yellow product had formed, the solid was suction filtered over a frit and washed three times with 100 mL of water. The product was dried in a vacuum oven. After drying, **P1** or **P4** was obtained as yellow solid.

P1: IR (ATR): 1586 (CO) cm^{-1}

P4: IR (ATR): 1579 (CO) cm^{-1}

Preparation of P2, P3

For the synthesis of **P2** or **P3**, 100 mg of copolymer **c** was dissolved in 10 mL of chloroform and stirred for 30 min. Subsequently, 1 molar ratio of alkyl amine solution in 5 mL of DMF was added. The mixture was stirred for 5 h and then a reaction mixture was concentrated at the rotovap. A reaction mixture was dissolved in 10 mL of DMF and stirred over night for 24 h. After that a solution of 3 g of potassium hydroxide in 5 mL of water was added to the reaction mixture with a syringe. The mixture was stirred for 5 h at 50 °C. As a dark yellow product had formed, the solid was suction filtered over a frit and washed three times with 100 mL of water. The product was dried in a vacuum oven. After drying, **P2** or **P3** was obtained as yellow solid.

P2 (before KOH addition): ^{1}H NMR (CD$_2$Cl$_2$, 300 MHz): δ = 6.93 (14H, arom H), 2.47 (5H, main chain), 1.82 (3H, NH-CH$_3$)

P3 (before KOH addition): ^{1}H NMR (CD$_2$Cl$_2$, 300 MHz): δ = 7.78 (4H, arom H of bisstilbene, =CH$_2$-C$_6$H$_4$-CH$_2$=), 7.31 (6H, arom H of bisstilbene, O-C$_6$H$_3$-OCH$_3$-), 6.95 (4H, double bond H of bisstilbene, -CH=CH-C$_6$H$_4$), 6.70 (14H, arom H of triarylamine), 4.16 (1H, O-CH-CH$_3$ of bisstilbene), 3.62 (6H, O-C$_6$H$_3$-OCH$_3$-), 3.29 (5H, main chain), 1.44 (3H, O-CH-CH$_3$ of bisstilbene), 1.17~1.02 (22H, N-(CH$_2$)$_6$ + O-CH-CH$_2$- of bisstilbene), 0.62 (3H, O-CH-CH$_2$-CH$_3$ of bisstilbene)

P2: IR (ATR): 1641 cm-1 (amide bond), 1585 (CO) cm^{-1}

P3: IR (ATR): 1641 cm-1 (amide bond), 1590 (CO) cm^{-1}

Preparation of oxadiazole and thiadiazole polyelectrolytes P5-P6

Isonicotinic acid N'-(pyridine-4-carbonyl)-hydrazide (1)

100 mg (0.729 mmol) of isonicotinic acid hydrazide and 156 mg (0.875 mmol) of isonicotinoyl chloride were dissolved in 50 mL of dry pyridine. The reaction mixture was refluxed at 130 °C over night for 24 h. As a pale-yellow product had formed, the solid was suction filtered over a frit and washed five times with 200 mL of water. The product was dried in a vacuum oven. After drying, white solid isonicotinic acid N'-(pyridine-4-carbonyl)-hydrazide (**1**) was obtained. (60.13 %)

^{1}H NMR (DMSO, 300 MHz): δ = 10.06 (2H, NH), 8.80 (4H, CO-C-CH$_2$), 7.82 (4H, N-CH$_2$)

2,5-di(4-pyridyl)-1,3,4-oxadiazole (2)

700 mg (2.889 mmol) of isonicotinic acid N'-(pyridine-4-carbonyl)-hydrazide (**1**) was dissolved very slowly in 5 mL of H$_2$SO$_4$ and stirred for 20 min with ice bath. The resulting mixture was kept under reflux condition at 100 °C for 1 h and then cooled down with 100 mL

of ice water. After cooling to room temperature, the solution was neutralized with the ammonia solution (pH = 9) and precipitated the crude product. Afterwards, this material was filtered, dried and recrystallized from methanol; the colorless needles were obtained. (40.47 %)

^{1}H NMR (DMSO, 300 MHz): δ = 8.84 (4H, aroma, N-CH$_2$), 7.97 (4H, CN-C-CH$_2$)

2,5-di(4-pyridyl)-1,3,4-thiadiazole (3)

100 mg (0.412 mmol) of isonicotinic acid N'-(pyridine-4-carbonyl)-hydrazide (**1**) and 199 mg (0.494 mmol) of Lawesson's reagent were dissolved in 10 mL of anhydrous toluene and the resulting mixture was kept under reflux condition at 110 °C over nigh for 24 h. After cooling to room temperature, the mixture was concentrated in vacuum to 3 mL and poured water to precipitate the crude product. Afterwards, this material was filtered, dried and recrystallized from ethanol; the pale yellow needles were obtained. (60.56 %)

^{1}H NMR (DMSO, 300 MHz): δ = 8.82 (4H, aroma, N-CH$_2$), 8.01 (4H, aroma, CN-C-CH$_2$)

Polycondensation to obtain P5-P6

1 g (4.46 mmol or 4.16 mmol) of 2,5-di(4-pyridyl)-1,3,4-oxadiazole (**2**) or 2,5-di(4-pyridyl)-1,3,4-thiadiazole (**3**) was dissolved 30 mL of N-methylbutylactam (NMP) and stirred for 1 h at room temperature. After that, 0.5 mL (5.21 mmol) of 1,6-dibromohexane was added to the reaction mixture with a syringe. The resulting mixture was heated to 60 °C under nitrogen atmosphere for 10 days. As a yellow product had formed, the solution was concentrated in vacuum to 5 mL and the polymer was precipitated by pouring the solution into 100 mL diethyl ether. After centrifugation, the solvent was decanted. The product was washed three times with diethyl ether and dried. The reaction yielded **P5-P6** as pale-yellow colored solids.

P5: ^{1}H NMR (DMSO, 300 MHz): δ = 9.54~8.52 (8H, arom. H), 4.73 (4H, N-CH$_2$), 2.00 (4H, N-CH$_2$-CH$_2$), 1.43 (4H, N-CH$_2$-CH$_2$-CH$_2$)

Water based GPC: Mw: 4282500 g/mol

P6; ^{1}H NMR (DMSO, 300 MHz): δ = 9.41~8.08 (8H, arom. H), 4.73 (4H, N-CH$_2$), 2.00 (4H, N-CH$_2$-CH$_2$), 1.43 (4H, N-CH$_2$-CH$_2$-CH$_2$)

Water based GPC: Mw: 4902150 g/mol

Preparation of triazine polyelectrolytes P7

The monomer **4**, preparing according to ref. 44 can be polymerized by radical polymerization with maleic anhydride. 1:1 molar ratio of monomer **4** and maleic anhydride were dissolved in toluene and catalytic amount of benzoyl peroxide was added to solution mixture. The flask was swirled until most of the solid materials have dissolved and then degassed three times with nitrogen. The reaction mixture was refluxed over night for 24 h and the color changed from white to yellow. After 24 h, to end the reaction, the reaction mixture was cooled down to room temperature. The polymer was precipitated by pouring the solution into n-hexane. After centrifugation, the solvent was decanted, and the product was washed three times with n-hexane and dried. The reaction yielded alternating copolymer **5** and the 1:1 stoichiometry of monomer to maleic anhydride was proved by ^{1}H NMR.

^{1}H NMR (CD$_2$Cl$_2$, 300 MHz): δ = 8.39 (6H, arom H), 7.32 (6H, aroma H), 1.66 (5H, main chain + tertiary butyl)

IR (ATR): 1780 (CO-O-CO) cm^{-1}

Mn: 195400 g/mol, Mw: 232400 g/mol, PDI (Mw/Mn): 1.52

A solution of 400 mg of copolymer **5** in 15 mL of DMF was heated to 40 °C for 1 h. After that a solution of 5 g of potassium hydroxide in 10 mL of water was added to the reaction mixture with a syringe. The mixture was stirred for 5 h at 50 °C. As a yellow product had formed, the solid was suction filtered over a frit and washed three times with 100 mL of water. The product was dried in a vacuum oven. After drying, white solid **P7** was obtained.

IR (ATR): 1578 (CO) cm^{-1}

Preparation of triazine and triarylamine polyelectrolytes P8

The monomers **4** and **b**, whose synthesis is described elsewhere[44] can be polymerized by radical polymerization with maleic anhydride. 1:1 molar ratio of monomers **4** and **b** were dissolved in toluene and then subsequently 2 equivalent maleic anhydride were added. Catalytic amount of benzoyl peroxide was added to solution mixture. The flask was swirled until most of the solid materials have dissolved and then degassed three times with nitrogen. The reaction mixture was refluxed over night for 24 h and the color changed from yellow to pink. After 24 h, to end the reaction, the reaction mixture was cooled down to room temperature. The polymer was precipitated by pouring the solution into n-hexane. After centrifugation, the solvent was decanted, and the product was washed three times with n-hexane and dried. The reaction yielded alternating copolymer **6**. 1:1 stoichiometry of monomers **4** or **b** to maleic anhydride was proved by ^{1}H NMR.

^{1}H NMR (CD$_2$Cl$_2$, 300 MHz): δ = 8.68~6.82 (24H, arom H of triarylamine and triazine), 2.21 (10H, main chain H), 1.41 (5H, methyl + tertiary butyl)

IR (ATR): 1780 (CO-O-CO) cm^{-1}

Mn: 22260 g/mol, Mw: 27690 g/mol, PDI (Mw/Mn): 1.24

A solution of 400 mg of copolymer **6** in 15 mL of DMF was heated to 40 °C for 1 h. After that a solution of 10 g of potassium hydroxide in 20 mL of water was added to the reaction mixture with a syringe. The mixture was stirred for 5 h at 50 °C. As a pale-yellow product had formed, the solid was suction filtered over a frit and washed three times with 200 mL of water. The product was dried in a vacuum oven. After drying, white solid **P8** was obtained.

IR (ATR): 1577 (CO) cm^{-1}

Multilayer build-up. PEI was purchased from Aldrich and used without further purification. The synthesis of PAMPS and PCM were already described elsewhere.[45] The formation of multilayers was performed on a quartz glass used as substrate. Cleaning of this substrate was achieved using a classical procedure. The substrates were immersed for 20 min in a 1:1 mixture of concentrated H$_2$SO$_4$ and a 30 % H$_2$O$_2$ ("piranha solution"; caution: piranha reacts violently with organic compounds and should not be stored in closed containers) and then

extensively rinsed with ultra-pure water (obtained by deionization and purification using the Milli-Q system from Millipore) at three times. And then the substrates were treated with a 1:1:5 mixtures of 25 % aqueous NH_3, 30 % H_2O_2, and H_2O at 80 °C to functionalize and thoroughly rinsed with ultrapure Milli-Q water. After further washing, the substrates were used for multilayer adsorption. In the beginning, two double layers of PEI (from a solution of 2.5 mg/mL PEI in 1 N hydrochloric acid) and PAMPS (from a solution of 3.5 mg/mL PAMPS in water) were adsorbed on the substrates as basis layers.

At each time, the substrates were dipped into the solution for 20 min, and then the substrates were rinsed three times with plenty of Milli-Q water (each time for 1 min). After fabrication of these basis layers, substrate was sequentially dipped in a polycationic solution (for example, PCM, from a solution of 2.5 mg/mL PCM in water) for 10 min and rinsed three times by immersion in ultrapure water (1 min). And then dipped for 10 min in a polyanion solution (for example, **P1**, from a solution of 1 mg/mL in THF: H_2O = 5:1 mixture solution) and three times rinsing steps were performed. This deposition procedure was then cycled to obtain desired number of bilayers. The multilayers were dried under nitrogen gas purging at the end of their fabrication and UV/VIS spectra were measured. Identical procedure was adopted when the multilayers assembled by the spin-coating method. In this case, however, the polymer/solvent solution was poured onto a substrate, and then the substrate was spun at a speed of 4000 rpm for 15 s. Subsequently, plenty of Milli-Q water was put on the substrate, and then the substrate was spun again at the same conditions. Before alternately depositing cationic and anionic polymer solutions, PEI and PAMPS were also predeposited two times as basis layers alternately in cationic aqueous solution of PEI and then in anionic aqueous PAMPS like the solution-dipping method at same conditions. The washing steps were repeated three times. At the end of every adsorption cycle, the multilayers were dried under nitrogen gas purging and UV/VIS spectra were measured.

The formation of multilayer was also performed on a transparent Indium tin oxide (ITO)-coated glass substrate. Cleaning of the substrate was achieved using an ultrasonicator bath in acetone, ethanol and then deionized water for 20 min. After drying, substates were treated by UV ozone ambient condition for 2 min, prior to use (UVO cleaner, UVO-42). Thin LBL

multilayer assembly was followed as stated and for this measurement, the multilayer build-up was done without the basis layers.

4.5. References

(1) Tang, C. W.; Van Slyke, S. A. *Appl. Phys. Lett*. **1987**, 51, 913.

(2) Kolosov, S.; Adamovich, V.; Djurovich, P.; Thompson, M. E.; Adachi, C. *J. Am. Chem. Soc*. **2002**, 124, 9945.

(3) Baldo, M. A.; O'Brien, D. F.; You, Y.; Shoustikov, A.; Sibley, S.; Thompson, M. E.; Forrest, S.R. *Nature* **1998**, 395, 151.

(4) Shirota, Y.; Kinoshita, M.; Noda, T.; Okumoto, K.; Ohara, T. *J. Am. Chem. Soc*. **2000**, 122, 1102.

(5) Mitschke, U.; Bauerle, P. *J. Mater. Chem*. **2000**, 10, 1471.

(6) Katz, H. E.; Bao, Z. *J. Phys. Chem. B*. **2000**, 104, 671.

(7) Katz, H. E.; Bao, Z.; Gilat, S. L. *Acc. Chem. Res.* **2001**, 14, 359.

(8) Dimitrakopoulos, C. D.; Malenfant, P. R. L. *Adv. Mater*. **2002**, 14, 99.

(9) Horowitz, G. *Adv. Mater*. **1998**, 10, 365.

(10) Sirringhaus,H.; Tessler, N.; Friend, R. H. *Science* **1998**, 280, 1741.

(11) Brabec, C. J.; Sariciftci, N. S.; Hummelen, J. C. *Adv. Funct. Mater*. **2001**, 11, 15.

(12) Yu, G.; Gao, J.; Hummelen, J. C.; Wudl, F.; Heeger, A. J. *Science* **1995**, 267, 1969.

(13) Antoniadis, H.; Hsieh, B. R.; Abkowitz, M. A.; Jenekhe, S. A.; Stolka, M. *Synth. Met.* **1994**, 62, 265.

(14) Jenekhe, S. A.; Yi, S. *Appl. Phys. Lett*. **2000**, 77, 2635.

(15) Sapp, S. A.; Sotzing, G. A.; Reynolds, J. R. *Chem. Mater*. **1998**, 10, 2101.

(16) Kumar, A.; Welsh, D. M.; Morvant, M. C.; Piroux, F.; Abboud, K. A.; Reynolds, J. R. *Chem. Mater*. **1998**, 10, 896.

(17) Mitschke, U.; Bauerle, P. *J. Mater. Chem*. **2000**, 10, 1471.

(18) Kraft, A.; Grimsdale, A. C.; Holmes, A. B. *Angew. Chem. Int. Ed*. **1998**, 37, 402.

(19) Strukelj, M.; Papadimitrakopoulos, F.; Miller, T. M.; Rothberg, L. J. *Science* **1995**, 67, 1969.

(20) Dimitrakopoulos, C. D.; Malenfant, P. R. L. *Adv. Mater*. **2002**, 14, 99.

(21) Babel, A.; Jenekhe, S. A. *Adv. Mater*. **2002**, 14, 371.

(22) Adachi C, Tsutsui T, Saito S, *Appl. Phys. Lett*. **1989**, 55, 1489

(23) Adachi C, Tokito S, Tsutsui T, Saito S. *Jpn. J. Appl. Phys*. **1988**, 27, L269

(24) Kraft A. *Chem. Commun*. **1996**, 1, 77

(25) Fink R, Frenz C, Thelakkat M, Schimidt HW. *Macromolecules* **1997**, 30, 8177

(26) Strukelj M. J. *Science* **1995**, 267, 1969.

(27) F. Huang, H. Wu, D. Wang, W. Yang, Y. Cao, *Chem. Mater*. **200**4, 16, 708.

(28) (a) Decher, G.; Hong, J. D.; Schmitt, J. *Thin Solid Films* **1992**, 210/ 211, 831. (b) Ferreirat, M.; Rubner, M. F. *Macromolecules* **1995**, 28, 7107. (c) Park, S. Y.; Rubner, M. F.; Mayes, A. M. *Langmuir* **2002**, 18, 9600.

(29) A. Berlin, G Zotti, *Macromol. Rapid Commun*. **2000**, 21, 301.

(30) X. Song, H. Wang, Shi. I, J. Park, W. J, B. I. Swanson, *Chem. Mater*. **2002**, 14, 2342.

(31) M, Thelakkat. *Macomol. Mater. Eng*. **2002**, 287, 442.

(32) R. Mruk, S. Prehl, R Zentel, *Macromol. Rapid Commun*. **2003**, 24, 1014.

(33) X. Jiang, R. A. Register, *Chem. Mater*. **2000**, 12, 2542.

(34) C. F. Shu, R. Dodda, F. I Wu, M. S. Liu, A. K. Y. Jen, *Macromolecules* **2003**, 36, 6698.

(35) Meier, M.; Buchwald, E.; Karg, S.; Pösch, P.; Greczmiel, M.; Strohriegel, P.; Riess, W. *Synth. Met*. **1996**, 76, 95.

(36) Pei, Q.; Yang, Y. *Chem. Mater*. **1995**, 7, 1568.

(37) E. Buchwald, M. Meier, S. Karg, P. Posch, H. W Schmidt, P. Strohriegl, W. Riess, M. Schwoerer. *Adv. Mater*. **1995**, 7, 839.

(38) Schulz, B.; Kaminorz, Y.; Brehmer, L. *Synth. Met*. **1997**, 84. 449.

(39) Gruner, J.; Friend, R. H.; Huber, J.; Scherf, U. *Chem. Phys. Lett*. **1996**, 251, 204.

(40) W.K. Gries, E. Günther, S.Hünig, Liebigs *Ann. Chem*. **1991**. 1021, 1028.

(41) Lee, D. W.; Kwon, K.-Y.; Jin, J.-I.; Park, Y.; Kim, Y.-R.; Hwang, I.-W. *Chem. Mater*. **2001**, 13, 565.

(42) Braun, D.; Heeger, A. *J. Appl. Phys. Lett.* **1982**, 58, 991.

(43) J. Cho, K. Char, J. D Hong, K.B. Lee. *Adv. Mater*. **2001**, 13, 1076.

(44) M. Behl, E. Hattemer, M. Brehmer, R. Zentel. *Macromol. Chem. Phys*. **2002**, 203, 503.

(45) K. Choi, R. Mruk, A. Moussa, A. M. Jonas, R. Zentel. *Macromolecules* **2005**, 38, 9124.

(46) Q. Qiao, J. T. McLeskey, *Appl. Phys. Lett*. **2005**, 86, 153501.

5. High Contrast Ratio and Rapid Switching Organic Polymeric Electrochromic Thin Films Based on Triarylamine derivatives from Layer-by-Layer-Assembly.*
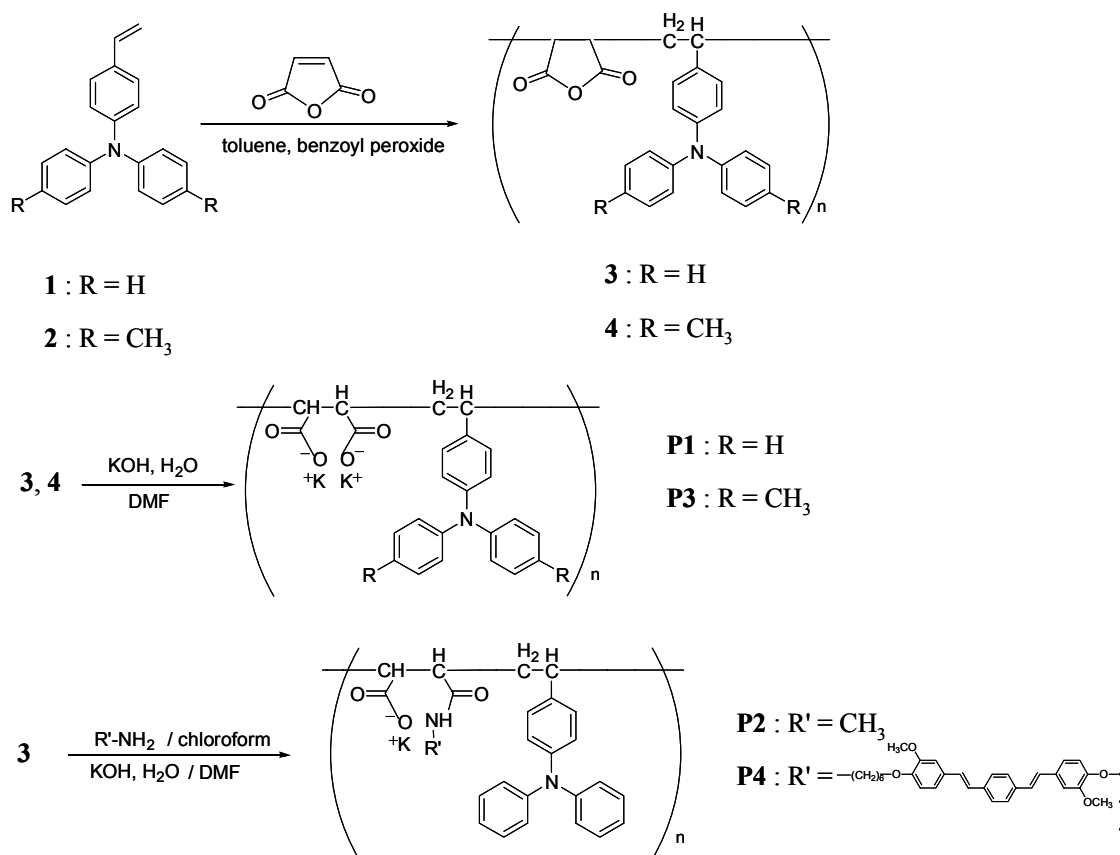
5.1. Introduction

Organic semiconductors and conjugated polymers are currently of wide interest for applications in electronic and optoelectronic devices including light-emitting diodes,[1] thin film transistors,[2] and photovoltaic cells.[3] However, these systems often require expensive and specifically designed organic or polymeric systems to achieve good performance and stability. The desire for cheap and simple displays with reasonable contrast in multiple colors has lead to investigation of electrochromic device, which can provide reasonable contrast without angle dependence, backlights or extensive synthetic efforts.[4] Most of the studies have utilized inorganic or low-molecular weight organic materials for electrochromism, however, more recently thin conducting polymer films have also received attention. Conducting polymers have several advantages. Such as outstanding coloration efficiency, long lifetime, faster switching time,[5] multiple colors with the same material while switching between their different redox states,[6] and fine-tuning of the band gap (and the color) through chemical structure modification.[7]

Concerning the making of electrochromic films, mostly conventional electropolymerization or spin-casting of soluble derivatives have been used. An interesting alternative layer-by-layer (LBL) method developed by Decher and co-workers.[8] It is an effective and convenient method for ultra thin film assembly, based on alternatively electrostatic adsorption of oppositely charged species from dilute solutions (solution-dipping variant). The process is simple, inexpensive and allows the incorporation of many different functional materials within a single film without the phase separation. Moreover, typical LBL films consist of highly interpenetrated polymer layers that are regarded as homogeneous composite films and this technique can create high-quality electrochromic thin films. This also reduces the problem of pin-hols, which easily occur during the one step spin-coating of the bulk polymer. For the fabrication of thin electrchromic films, the spin-coating variant of the LBL method looks even more promising as it works faster and the films are smoother.[9] The biggest advantage of this technique is the fact that the film thickness can be easily controlled in the

nano-scale range. So far, electrochromism has been explored on thin films of classical conductive redox-active polymers, like PEDOT:SPS/PXV, polyaniline/Prussian blue nanocomposite and PEDOT-S/PAH prepared via the solution-dipping variant of the LBL technique.[10] However, fast switching time well below 1 s in combination with high contrast ratio (>50 %) has been difficult to achieve and the typical switching time for electrochromic polymer films is 1-2 s.[10,11] The use of electroactive multilayers with high carrier mobility like triarylamines and their dimers[12] in nano-scale thin film geometry may be a concept to improve switching time.

In this paper, we present electroactive organic polymeric thin films prepared by LBL method, in which the polyanion species are incorporated in triarylamine polymers. The electroactive **P1–P4**, triarylamine polymers are newly synthesized and they are anodically coloring electrochromic species within the LBL film. Because of the dimer formation of triarylamine, anodically colored thin films are chemically and mechanically stable. In addition, it is possible to achieve high contrast ratio and a fast switching time. A series of electroactive polymer thin films are used as simple electrochromic cells; their multilayer build-up, electrochemical, and electrochromic characteristics are investigated by UV/VIS spectroscopy and cyclic voltammetry (CV). The synthetic scheme and chemical structures of these four electrochromic polymers are shown below (see supporting information).

Scheme 5.1. Synthetic route to the electrochromic Polyanions **P1-P4**.

1 : R = H

2 : R = CH₃

3 : R = H

4 : R = CH₃

3, 4 — KOH, H₂O / DMF →

P1 : R = H

P3 : R = CH₃

3 — R'-NH₂ / chloroform ; KOH, H₂O / DMF →

P2 : R' = CH₃

P4 : R' = —(CH₂)₆—O—...

5.2. Results and discussion

Polymers **P1-P4** were synthesized using the route illustrated in Scheme 5.1. The monomers **1** and **2**, whose synthesis is described elsewhere[13] can be polymerized by radical polymerization with maleic anhydride. The synthesized alternating copolymer **3** and **4** were subsequently treated with amine solution and potassium hydroxide (**P2**, **P4**) or only with potassium hydroxide (**P1**, **P3**). The charged polymers are suitable for deposition by LBL multilayer deposition from a solution using the spin coating technique.

As an electrochromic functional moiety, triarylamine has unique properties. Two basic properties of the triarylamine unit are the easy oxidizability of the nitrogen center and its ability to transport positive charges via the radical cation species. Under the influence of an electric field, positive charge is transported by a hopping mechanism and drift mobility of

holes is up to 10^{-3} cm^2/(V•s).[12] Unsubstituted triarylamine undergoes dimerization to tetraarylbenzidine, generally called triaryldiamine, after the formation of the primary monocation radical. This is accompanied by the loss of two protons per dimer and the dimer is more easily oxidized than triarylamine. In addition, this dimer forms a more stable radical cation or dication and shows further increased charge carrier mobility.[12] A proof for the formation of the dimer can be observed clearly through the additional oxidation peak of the **P1** or **P2** monolayer films, as seen in Figure 5.1(a). The **P1** monolayer films were simply deposited on a Pt-working electrode. Cyclic voltammograms show a clear peak of the monomer at about 855 mV, while the dimer formed during the first oxidation cycle undergoes reversible oxidation at a lower potential of about 685 mV. However, bulky triarylamines, p-substituted derivatives of triarylamine and its higher homologues do not exhibit this dimerization.[12] Therefore, monolayer films from the p-substituted polymer, **P3** or polymer, **P4** with bulky amine substituents do not show the additional oxidation peak originated from the formation of the dimer, as seen in Figure 5.1(b). In addition, monolayers of **P3** and **P4** are unstable under the applied potential and start to dissolve from the electrode.
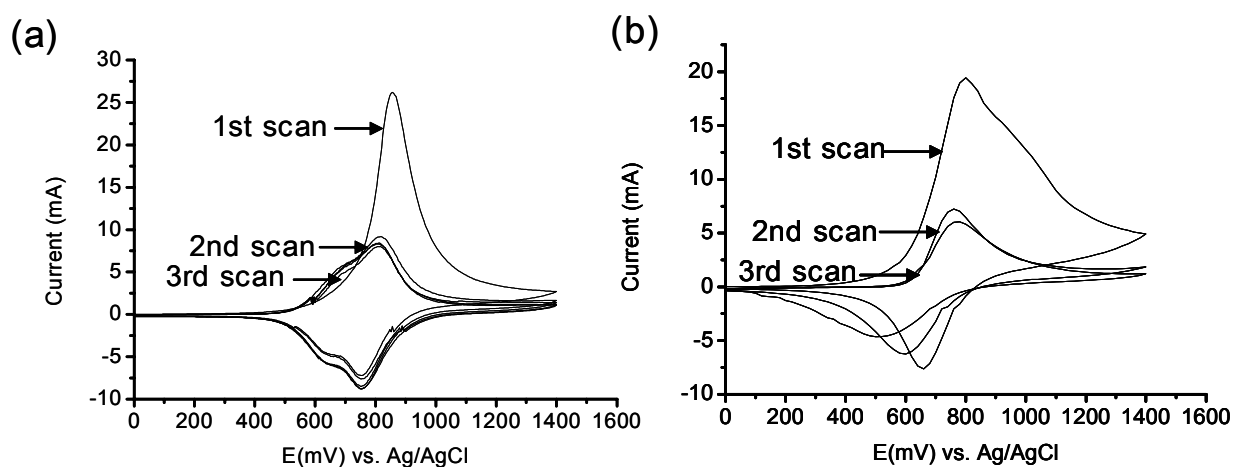
Figure 5.1. Cyclic voltammograms of triarylamine polymers measured on Pt-working electrode (with 0.1 M TBABF$_4$) at 20 mV/s. (a) Unsubstituted triarylamine polymer, **P1**. (b) p-substituted triarylamine polymer, **P3**.

The multilayer build-up from anionic **P1-P4** polymers solution and cationic poly(choline methacrylate) (PCM) solution was done by the solution-dipping and the spin-coating methods.[14] Both methods lead to a regular multilayer build-up. The spin-coating method

proved, however, to be advantageous, as it can be done faster (multilayer film with 12 bilayers in 24 min). In addition, it needs a fewer number of bilayers to achieve the desired film thickness, as the thickness per bilayer is increased.[9] The multilayer build-up was investigated by UV/VIS spectroscopy as shown for the **P1**/PCM film in Figure 5.2(a) using quartz as a substrate. It shows the increase of the maximum of the π-π* absorbance at 308 nm of the spin-coated conjugated triarylamine film. The deposition process is linear, indicating that the amount of material deposited per bilayer is completely reproducible from layer to layer. Moreover, it is possible to prepare multilayers, which grow constantly in thickness according to the number of bilayers. Five bilayers film has thereby usually a thickness between 100 nm and 130 nm (10 mg/mL concentration), which is not typical for spin-coated LBL-layers from less polar polyanions.[14] The multilayer build-up was also performed on ITO-coated glass substrate with the polyanion and polycation solutions alternatively. Monitoring the redox reaction of the **P1**/PCM film by cyclic voltammetry as a function of film thickness for up to 10 bilayers reveals the electroactivity of the **P1**, as seen in Figure 5.2(b). The films exhibited a redox response despite the insulating nature of the interstitial PCM layer. This supports models suggesting the presence of an interpenetrating polymer network as opposed to discrete bilayers within the film.
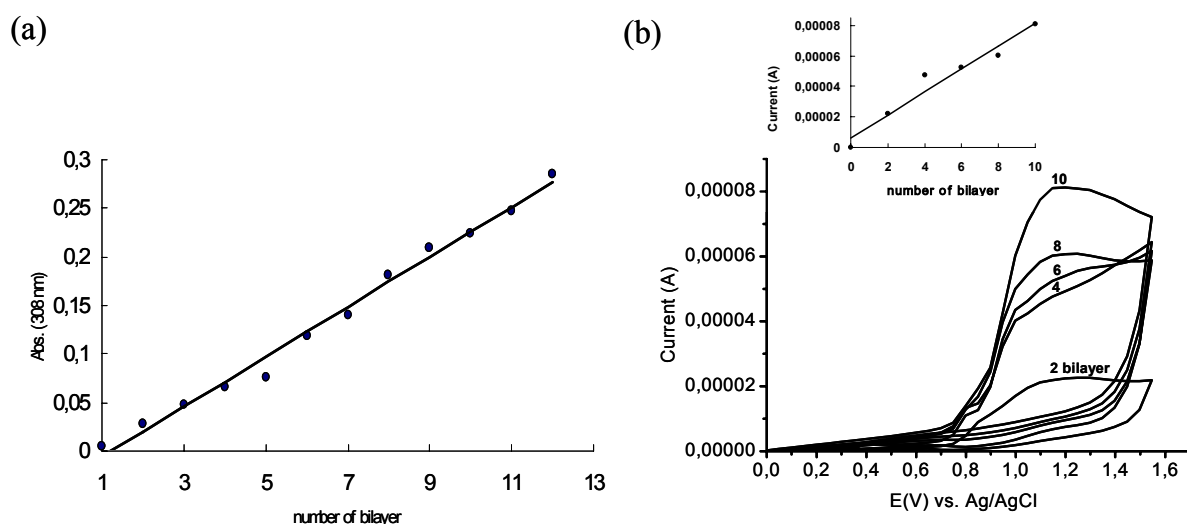
Figure 5.2. Multilayer build-up from a **P1**/PCM film. (a) The growth of the multilayer films assembled by the spin-coating method at 308 nm. (b) Cyclic voltammograms of sequential bilayer deposition, from 2-10 bilayers, at a scan rate of 20 mV/s, between 0 V and +1.6 V (Inset: The peak current vs. the number of bilayer deposited on ITO-coated glass).

Following the electrochemical tests, the optical properties of the electrochromic films were evaluated by using spectroelectrochemistry. For these investigations, 5 bilayer **P1-P4**/PCM films were assembled on an ITO-coated glass substrate, as described earlier.[14] These transparent working electrodes were inserted into a electrochemical cuvette cell. The result of the **P2**/PCM film is presented in Figure 5.3 as a series of UV/VIS absorbance curves correlated to film potentials. The potential range and other electrochemical experimental conditions were identical to those used for CV measurements. The scan for spectroelectrochemistry was made anodical, proceeding from 0 V to +2.0 V. Upon oxidation of the **P2**/PCM film, a second band appears at 350 nm besides a band at 303 nm, which is characteristic for triarylamine. We attribute this band to the dimerization of triarylamine, after the formation of an unstable monocation radical. Due to the more extended π-conjugation, the absorption band of the triaryldiamine appears in the lower energy region.[15] From its intensity, a dimerzation can be analyzed quatitatively. As the potentials became more positive, the absorption bands of the triarylamine and triaryldiamine decreased gradually, with the formation of two new bands at 480 nm and 710 nm. The lower energy intra-band transitions are assigned to charged species such as cation and dication radicals, which exhibit strong absorption in the near-infrared region. Consequently, the spectroelectrochemical studides confirm the findings using cyclic voltammetry regarding the dimer formation and proves the formation of highly colored radical cations and dications.
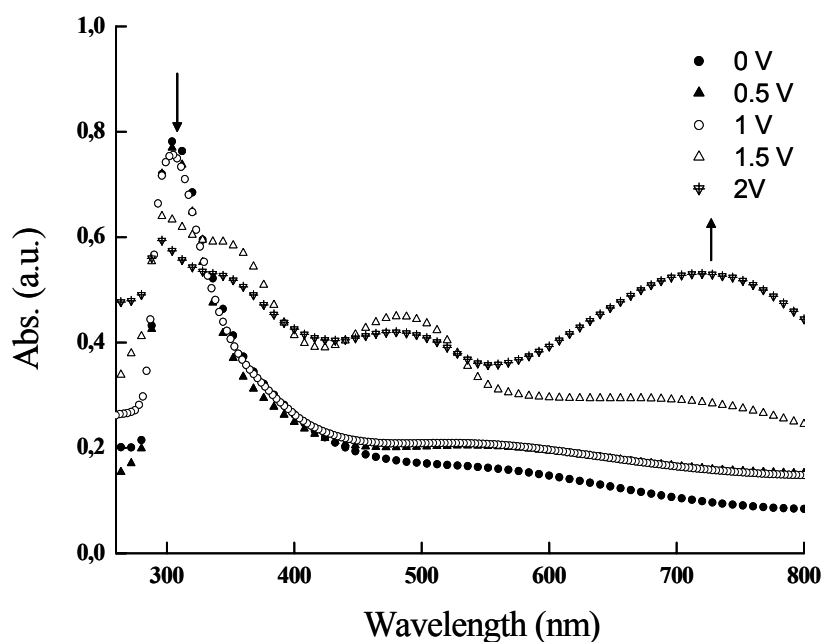
Figure 5.3. Spectroelectrochemistry of **P2**/PCM film on ITO-coated glass substrate at applied potential levels: between at neutral (0 V) and oxidized state (+2.0 V) states.

For the electrochromic studies, the potential of multilayer films on ITO coated glass was cycled between the neutral (0 V) and the oxidized (+1.6 V) states. While the films were switched, the percentage transmittance (at 633 nm) was simultaneously monitored. As a reference, the transmittance of the ITO/glass with the electrolyte and the cell window was assumed to be 100 %. Figure 5.4(a) shows the in situ transmittance of **P2**/PCM film during continuous cycling test of applied potential. **P1**/PCM and **P2**/PCM films showed a stable pulse potential cycling performances and similar high transmittance differences (ΔT %) of 45.83 % and 50.01 % at 633 nm. In contrast, **P4**/PCM film showed poor pulse potential cycling performance (ΔT % = 26.1 %), whereas polymer film of **P3**/PCM film did immediately disintegrate after switching under the applied potential. The result for **P3**/PCM film can be explained by the fact that it consists of p-substituted triarylamine polymers. Due to the lack of dimerization, it does not form stable thin films after oxidation (the positive charges of the radical cation compensate the negative charges of the carboxylate groups). As a result, the formation of the dimer via the radical cation species could be the key factor to achieve stable and high contrast ratio electrochromic films, both with respect to mechanical stability (no dissolution due to the crosslinking) and chemical stability (more stable radical cations of the dimer). For the **P4**/PCM film, dimerization is also limited (it was not observed in the CV measurements), but generally possible. Here the bulky bisstilbene side-group may hinder the hopping process of the charge carriers, because they have a larger band gap than the triarylamine monomers. The most important figure of merit for electrochromic materials is the contrast between oxidation and reduction. **P1**/PCM and **P2**/PCM films showed that the high (>50 %) electrochromic contrast (ΔT %) values are attainable using 5 bilayers with thin polymer films in nano-scale. Therefore, these results demonstrate that dimerizable **P1** and **P2** are the proper candidates as electrochromic materials to make efficient electrochromic devices. Although these contrast values are already quite high, it is clear that an even greater maximum contrast might be achievable in a film of 10 or 15 bilayers.

In addition, the switching time of electrochromic films may limit their applications. For the switching time between all samples, the normalized transmittance was introduced as measured previously.[16] Figure 5.4(b) shows the normalized transmittance during the coloring/bleaching processes of **P2**/PCM film. The switching time was calculated on the level of a 90 % transmittance change. Switching time is based on the charge response of the film. **P1**/PCM and **P2**/PCM films showed very rapid switching times on the order of 0.30-0.55 s,

which is faster than the typical switching time of 1-2 s for electrochromic polymer films.[10] This is a result of both the high charge carrier mobility[12] and the thin nano-scale film structure.
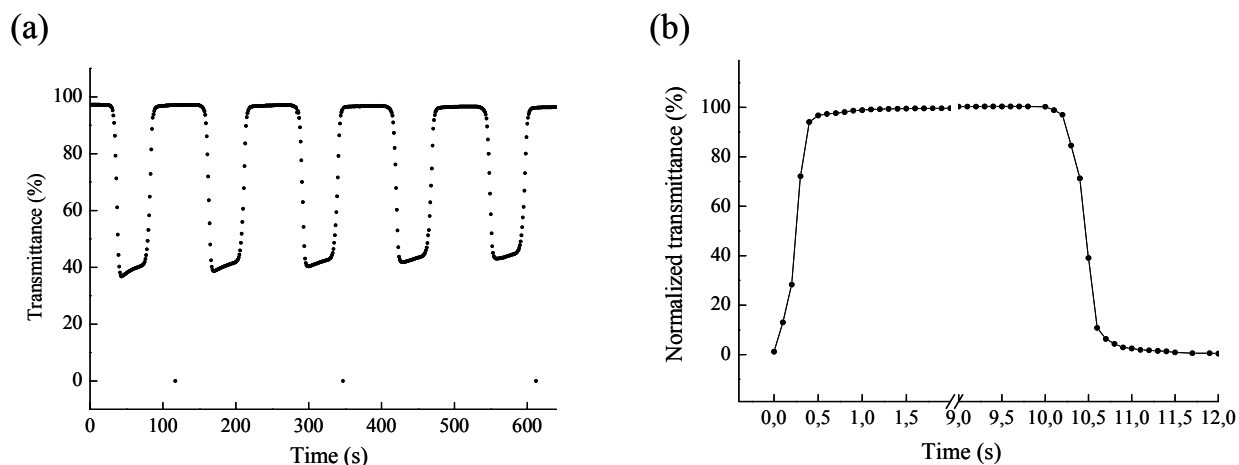
Figure 5.4. (a) In situ transmittance curves during the continuous cycling test of applied potential of **P2**/PCM film. (b) Normalized transmittance curve during the first pulse potential cycling. (films were cycled between 0 V and +1.6 V and the percentage transmittances were measured at 633 nm)

In order to quantitatively determine the electrochromic properties of **P1**/PCM and **P2**/PCM films, the transmittance difference (ΔT %) during the coloring/bleaching processes, coloration efficiency (CE), and response time were calculated as shown in Table 5.1. Coloration efficiencies have been used extensively in electrochromic materials to compare devices containing different types of materials. The CE is obtained by determining the injected/ejected charge as a function of electrode area (Q_d) and the change in optical density $\Delta OD(\lambda)$ when switching an electrochromic device from one state to another, and is given by Equation, where $\Delta OD(\lambda) = \log[T_b(\lambda)/ T_c(\lambda)]$.[17]

$$CE(\lambda) = \Delta OD(\lambda) /Q_d$$

Table 5.1. Switching time, contrast ratio and coloration efficiency of the **P1**/PCM and **P2**/PCM films.

Polymer film	Color time (s)	Bleach time (s)	$\Delta T\%$ (λ=633 nm)	CE (cm^2/C) (λ=633 nm)
P1	0.35	0.30	45.83	58.2
P2	0.55	0.35	50.01	67.1

CE values were calculated for the **P1**/PCM and **P2**/PCM films and the average CE value of two samples showed approximately 63 cm^2/C. This value is already good enough for an electrochromic films, however, the performance would increase further if a solid electrolyte is used as in commercial electrochromic devices. The stability of the electrochromic films was tested by performing continuous 500 cycle numbers in the same experimental setup under the same conditions as described above. After 500 potential cycles, **P1**/PCM film had degraded slightly whereas the **P2**/PCM film did not change (it is able to retain approximately 93 % of its optical response after 500 cycles). This gives an indication of the relatively high environmental and redox stability of the **P2**/PCM film compared to the **P1**/PCM film. It can be explained by the fact that **P1**/PCM film showed 24 % of conversion from triarylamine monomer to dimer based on the quatitative analysis of the UV/VIS spectra. Interestingly, **P2**/PCM film showed 63 % of conversion, suggesting that relatively high amount of dimer can be the origin of the stable film.

5.3. Conclusion

In summary, we present thin organic electrochromic films from newly synthesized anionic triarylamine polymers. As electrochromic functional moiety, triarylamine has unique properties, under the influence of an electric field. The thin polymer films were fabricated using LBL assembly, which is the ideal processing technique to prepare electroactive polymer thin film composites with fine control over morphology and composition. Due to the dimerization of the triaylamine in multilayers of **P1** and **P2**, fabricated thin films were electrochemically and mechanically stabilized. Electrochemical and electrochromic

characterizations of assembled films revealed that the newly synthesized polymers give rise to high contrast ratio and fast switching electrochromic films. This is a result of the thin nano-scale film formed by the spin-coating variant of the LBL technique in combination with the high charge carrier mobility of triarylamine dimers.

Future direction of this work involves enhancing the electrochromic properties by the fabrication and optimization of efficient electrochromic device. Development in this area will be accelerated with the solid polymeric electrolytes for the solid state electrochromic films[18] and "dual elecrochrome" without an inert polymer using LBL multilayer build-up method. Because, an inert (not electroactive) polymer is employed so far as the counter-polyion in the LBL films, the inclusion of inert material reduces the performance. Therefore, the synthesis of the oppositely charged polymers is requirred and they could be used as polycations and polyanions.

5.4. Experimental

General Experiments: All reagents were used without further purification. ^{1}H NMR spectra were measured on a Bruker 300 MHz FT spectrometer and the spectra were analyzed with the software Win-NMR 6.1. UV/VIS absorption spectra were taken with a Shimadzu UV-2102 PC spectrometer. FT-IR spectra were measured on a Bruker Vector 22 FT-IR spectrometer with a Harrick ATR unit and the analysis of the spectra was performed with the software OPUS 3.1. To determine the molecular weight of the polymers, gel permeation chromatography (GPC) was performed on a Jasco instrument and THF was used as mobile phase. The separation was done on a MZ-Gel SD plus precolumn (8 mm x 50 mm) and three MZ-Gel SD plus main columns (8 mm x 50 mm) produced by Mainz Analysentechnik. For each measurement 100 μL solution of the polymer in THF (2 mg/mL) was injected. The detection was performed with Jasco refractive index and UV detectors and a Viscotek light scattering detector.

Triarylamine Polymer synthesis

Preparation of alternating copolymer 3, 4: 1:1 molar ratio of monomer **1** or **2**, and maleic anhydride were solved in toluene and catalytic amount of benzoyl peroxide was added to solution mixture. The flask swirled until most of the solid materials has dissolved and then degassed three times with nitrogen. The reaction mixture is refluxed over night and the color changed from yellow to pink. After 24 h, to end the reaction, the reaction mixture was cooled down. The polymer was precipitated by pouring the solution into n-hexane. After centrifugation, the solvent was decanted, and the product was washed several times with n-hexane and dried. The reaction yielded alternating copolymer **3** or **4**. 1:1 stoichiometry of monomer to maleic anhydride was proved by ^{1}H NMR.

^{1}H NMR (CD2Cl2, 300 MHz): 6.97 (14H, aroma H), 1.66 (5H, main chain)
IR (ATR): 1777 (CO-O-CO) cm^{-1}
Mn: 98720 g/mol, Mw: 150900 g/mol, PDI (Mw/Mn): 1.53

Preparation of P1, P3: A solution of 200 mg of copolymer **3** or **4** in 15 mL of DMF was heated to 40 °C for 1 h. After that a solution of 5 g of potassium hydroxide in 10 mL of water was added to the reaction mixture with a syringe. The mixture was stirred for 5 h at 50 °C. As a yellow product had formed, the solid was suction filtered over a frit and washed three times with 100 mL of water. The product was dried in a vacuum oven. After drying, yellow solid **P1** or **P3** was obtained.

IR (ATR): 1586 (CO) cm^{-1}

Preparation of P2, P4: For the synthesis of **P2** or **P4**, 100 mg (0.269 mmol repeating units) of copolymer **3** was dissolved in 10 mL of chlroform and stirred for 30 min. Subsequently, 1 molar ratio of alkyl amine solution in 5 mL of DMF was added. The mixture was stirred for 5 h and then a reaction mixture was concentrated at the rotovap. A reaction mixture was dissolved in 10 mL of DMF and stirred over night. After that a solution of 3 g of potassium hydroxide in 5 mL of water was added to the reaction mixture with a syringe. The mixture was stirred for 5 h at 50 °C. As a dark yellow product had formed, the solid was suction filtered over a frit and washed three times with 100 mL of water. The product was dried in a vacuum oven. After drying, yellow solid **P2** or **P4** was obtained.

IR (ATR): 1641 (CO-NHR), 1585 (CO) cm^{-1}

Multilayer thin film build-up. The formation of multilayer was performed on a quartz glass and a transparent Indium tin oxide (ITO)-coated glass substrate for optical and electrochemical measurements. The quartz substrates used for optical measurements were immersed for 20 min in a 1:1 mixture of concentrated H_2SO_4 and a 30 % H_2O_2 ("piranha solution"; caution: piranha reacts violently with organic compounds and should not be stored in closed containers) and then extensively rinsed with ultra-pure water (obtained by deionization and purification using the Milli-Q system from Millipore) at three times. And then the substrates were treated with a 1:1:5 mixtures of 25 % aqueous NH_3, 30 % H_2O_2, and H_2O at 80 °C to functionalize and thoroughly rinsed with ultra-pure Milli-Q water. After further washing, the substrates were used for multilayer adsorption.

The synthesis of poly(choline methacrylate) (PCM) (from a solution of 2.5 mg/mL PCM in water) used as a polycation was done according to ref 14. In the beginning, two double layers of poly(ethylene imine) (PEI) (from a solution of 2.5 mg/mL PEI in 1 N hydrochloric acid) and poly(2-acryloylamino-2-methylpropyl sulfonate sodium salt) (PAMPS) (from a solution of 3.5 mg/mL PAMPS in water) were adsorbed on the substrates as basis layers. The aqueous solutions of PEI and PAMPS were poured onto a substrate, and then the substrate was spun at a speed of 4000 revolutions per minute (rpm) for 15 s. Subsequently, plenty of Milli Q water was put on the substrate and then the substrate was spun again at same condition. The washing steps were repeated three times. The initially deposited double basis layers are sufficient to start the multilayer deposition process, the surface coverage and charge density appear to be more uniform after a number of bilayers of highly charged polyelectrolytes have been deposited, thereby eliminating any effects that the substrate itself may have on the adsorption process. After fabrication of these basis layers, substrates were sequentially spin coated in a cationic poly(choline methacrylate) (PCM) solution (from a solution of 2.5 mg/ml PCM in water) and **P1-P4** solution (from a solution of 10 mg/mL in THF:H_2O=5:1 mixture solvents) at same condition like basis layers and then rinsed three times with ultra-pure water. This deposition procedure was then cycled to obtain multilayer. At the end of every adsorption cycle, the multilayer was dried under nitrogen gas purging and UV/VIS spectra were measured.

A transparent Indium tin oxide (ITO)-coated glass substrate was used for optical electrochemical measurements. Identical procedure was adopted like the multilayers assembled onto the quartz substrates at same condition. In this case, however, pre-deposited PEI and PAMPS basis layers were omitted to eliminate the insulating nature of two basis materials. At the end of every adsorption cycle, the multilayers were dried under nitrogen gas purging and CV spectra were measured. Cleaning of the substrates was achieved using an ultra-sonicator bath in acetone, ethanol and then deionized water for 20 min. After drying, substrates were treated by UV ozone ambient condition for 2 min, prior to use. (UVO cleaner, UVO-42) For spin-coating, a Convac ST146 spin-coater was used. Film thickness was determined using an Alpha-step 500. (KLA-TENCOR, Nanospec AFT/200) All electrochemical potential cycling tests were performed using an Autolab PGSTAT30 (Eco Chemie) Potentiostat/Galvanostat. Pt-wire and Ag/AgCl were used as the counter and reference electrodes, respectively. Polymer films coated on ITO-coated glass were used as the working electrodes and 0.1 M tetrabutylammonium tetrafluoroborate (TBABF$_4$) in acetonitrile was used as the electrolyte. Continuous potential cycling (or linear-sweep potential cycling) was carried out for up to 20 cycles in the range of 0 V to +1.6 V at a scan rate of 10 mV/s. The electrochromic response time was then tested by applying a pulse potential wave between 0 V and +1.6 V with a duration time of 10 s, referred to as pulse potential cycling. The transmittance (633 nm, 10 mW) was simultaneously measured in situ during all experiments. The transmittance of the ITO/glass with the electrolyte and the cell window was assumed to be 100 %.

5.5. References

(1) (a) Tang, C. W.; Van Slyke, S. A. *Appl. Phys. Lett.* **1987**, 51, 913. (b) Kolosov, S.; Adamovich, V.; Djurovich, P.; Thompson, M. E.; Adachi, C. *J. Am. Chem. Soc.* **2002**, 124, 9945. (c) Baldo, M. A.; O'Brien, D. F.; You, Y.; Shoustikov, A.; Sibley, S.; Thompson, M. E.; Forrest, S.R. *Nature.* **1998**, 395, 151. (d) Shirota, Y.; Kinoshita, M.; Noda, T.; Okumoto, K.; Ohara, T. *J. Am. Chem. Soc.* **2000**, 122, 11021. (e) Mitschke, U.; Bauerle, P. *J. Mater. Chem.* **2000**, 10, 1471.

(2) (a) Katz, H. E.; Bao, Z. *J. Phys. Chem. B.* **2000**, 104, 671. (b) Katz, H. E.; Bao, Z.; Gilat, S. L. *Acc. Chem. Res.* **2001**, 14, 359. (c) Dimitrakopoulos, C. D.; Malenfant, P. R. L. *Adv.*

Mater. **2002**, 14, 99. (d) Horowitz, G. *Adv. Mater*. **1998**, 10, 365. (e) Sirringhaus,H.; Tessler, N.; Friend, R. H. *Science*. **1998**, 280, 1741.

(3) (a) Brabec, C. J.; Sariciftci, N. S.; Hummelen, J. C. *Adv. Funct. Mater*. **2001**, 11, 15. (b) Yu, G.; Gao, J.; Hummelen, J. C.; Wudl, F.; Heeger, A. J. *Science*. **1995**, 267, 1969. (c) Antoniadis, H.; Hsieh, B. R.; Abkowitz, M. A.; Jenekhe, S. A.; Stolka, M. *Synth. Met*. **1994**, 62, 265. (d) Jenekhe, S. A.; Yi, S. *Appl. Phys. Lett*. **2000**, 77, 2635.

(4) (a) C. W. Tang, S. A. VanSlyke, *Appl. Phys. Lett.* **1987**, 51, 913. (b) J. R. Sheats, H. Antoniadis, M. Hueschen,W. Leonard, J. Miller, R. Moon, D. Roitman, A. Stocking, *Science*. **1996**, 273, 884.

(5) (a) Sapp, S. A.; Sotzing, G. A.; Reynolds, J. R. *Chem. Mater*. **1998**, 10, 2101. (b) Kumar, A.; Welsh, D. M.; Morvant, M. C.; Piroux, F.; Abboud, K. A.; Reynolds, J. R. *Chem. Mater.* **1998**, 10, 896.

(6) (a) Thompson, B. C.; Schottland, P.; Zong, K.; Reynolds, J. R. *Chem. Mater*. **2000**, 12, 1563. (b) Thompson, B. C.; Schottland, P.; Sonmez, G.; Reynolds, J. R. *Synth. Met*. **2001**, 119, 333.

(7) (a) Skotheim, T. A.; Elsenbaumer, R. L.; Reynolds, J. R. *Handbook of Conducting Polymers*, 2nd ed.; Marcel Dekker: New York, **1998**. (b) Nalwa, H. S. *Handbook of Organic Conductive Molecules and Polymers*; John Wiley and Sons: New York, **1997**. (c) Sonmez, G.; Schwendeman, I.; Schottland, P.; Zong, K.; Reynolds, J. R. *Macromolecules*. **2003**, 36, 639. (d) Schwendeman, I.; Hickman, R.; Sonmez, G.; Schottland, P.; Zong, K.; Welsh, D.; Reynolds, J. R. *Chem. Mater*. **2002**, 14, 3118.

(8) Decher, G.; Hong, J. D.; Schmitt, J. *Thin Solid Films*. **1992**, 210/ 211, 831.

(9) J. Cho, K. Char, J. D Hong, K.B. Lee. *Adv. Mater*. **2001**, 13, 14, 1076.

(10) (a) Dean M. DeLongchamp, Mark Kastantin, Paula T. Hammond, *Chem. Mater*. **2003**, 15, 1575. (b) Dean M. DeLongchamp, Paula T. Hammond, *Adv .Mater*, **2001**, 13, 19, 1455. (c) Dean M. DeLongchamp, Paula T. Hammond, *Chem. Mater*. **2004**, 16, 4799. (d) C. A. Cutler, M. Bouguettaya, J. R. Reynolds. *Adv .Mater*. **2002**, 14, 9, 684.

(11) (a) D, Laurent ; J, Schlenoff, *Langumuir*. **1997**, 13, 1552. (b) J, Sclenoff, *Adv. Mater* **1998**, 10, 347.

(12) M, Thelakkat. *Macomol. Mater. Eng*. **2002**, 287, 442.

(13) M. Behl, E. Hattemer, M. Brehmer, R. Zentel. *Macromol. Chem. Phys*. **2002**, 203, 503.

(14) K. Choi, R. Mruk, A. Moussa, A. M. Jonas, R. Zentel. *Macromolecules*. **2005**, 38, 9124.

(15) C. Lambert, G. Nöll. *Angew. Chem. Int. Ed*. **1998**, 37, 15. 2107.

(16) K.S. Ahn, Y.C. Nah, J.H. Yum, Y.-E. Sung, *Jpn. J. Appl. Phys*. **2002**,41 , L212.

(17) K. Bange, T. Gambke, *Adv. Mater.* **1990**, 2, 10.

(18) W. A. Gazotti, G. C. Miceli, A. Geri, A. Berlin, M. A. De Paoli. *Adv. Mater.* **1998**, 10, 18, 1522.

6. Vacuum-deposited Triarylamine Thin-Film and Its Structure and Electronic Properties.*

6.1. Introduction

Organic semiconductors and conjugated polymers are currently of wide interest for applications in electronic and optoelectronic devices including light-emitting diodes,[1-5] thin film transistors,[6-10] photovoltaic cells[11-14] and electrochromic devices.[15,16] Conjugated polymers have the advantages of allowing an easy and low-cost manufacture of large-area displays using solution-processing of film-forming polymers. The triarylamine moiety – mostly in polymeric form- widely used as a hole-transporting material due to the electron-donating nature of the nitrogen atom in LEDs.[17, 18] Under the influence of an electric field, the positive charge is transported by a hopping mechanism and drift mobilities up to 10^{-3} cm^2/(V•s) are possible.[19]

Usually polymer thin films are prepared from organic materials in solution by solution-dipping or spin-coating method onto transparent conductive oxide (TCO)-coated glasses. Although excellent results were achieved by this way, there are a number of problems that can arise. It can be difficult to find suitable solvents to prepare thin films (50-400 nm) that are free from pinholes. Moreover, if there are suitable solvents without any pinholes on the surface, mutually exclusive solvents for the different polymer layers in a multilayer device are also difficult to engineer. As a next problem, oxygen and other contaminants (e.g. dust) are difficult to exclude from the solutions used to make films and solvent is not fully removed from the films after deposition. They can cause the formation of voids and chemical reactivity with the electrodes and finally minimize the device performance. At this point, dry process such as vapor deposition under vacuum condition can be the perfect candidate to deposit the polymer films for LEDs. Vapor deposition method provides a clean environment; it is solvent free and well suited to sequential depositions in hetero-structured multilayer system. Moreover, the device fabrication by vacuum deposition method allows a whole processing in the same run without vacuum breaking from the polymer materials to the metal upper electrode. Since polymers generally cannot be vaporized without decomposition, the vapor deposition method has been explored for sublimation of low-molecular-weight dyes[20] and oligomers[21, 22] but only a very limited number of polymers.

On the other hand: many polymers decompose to oligomers at elevated temperatures.[23-25] Thus polymers may act as precursors for oligomers, which can be vaporized. Such evaporated oligomers could benefit from the advantages described above and they may give more stable amorphous structures compared to low-molar-weight materials. We now found that a triarylamine polymer, which was intentionally made for the layer-by-layer (LBL) assembly by solution-dipping or spin-coating method as anionic polymer, can be vaporized. During the evaporation process, this polymer undergoes imidization at elevated temperatures, afterwards, giving rise to high quality thin films for LEDs.

6.2. Results and discussion

As hole transporting functional moiety, the p-type triarylamine polymers were synthesized by the synthetic route described elsewhere[26] (see Experimental Part). The chemical structures of the polymers are shown below.

Scheme 6.1. Triarylamine Polymers **P1-P2** and precursor PPV.

P1   P2

precursor PPV   PPV
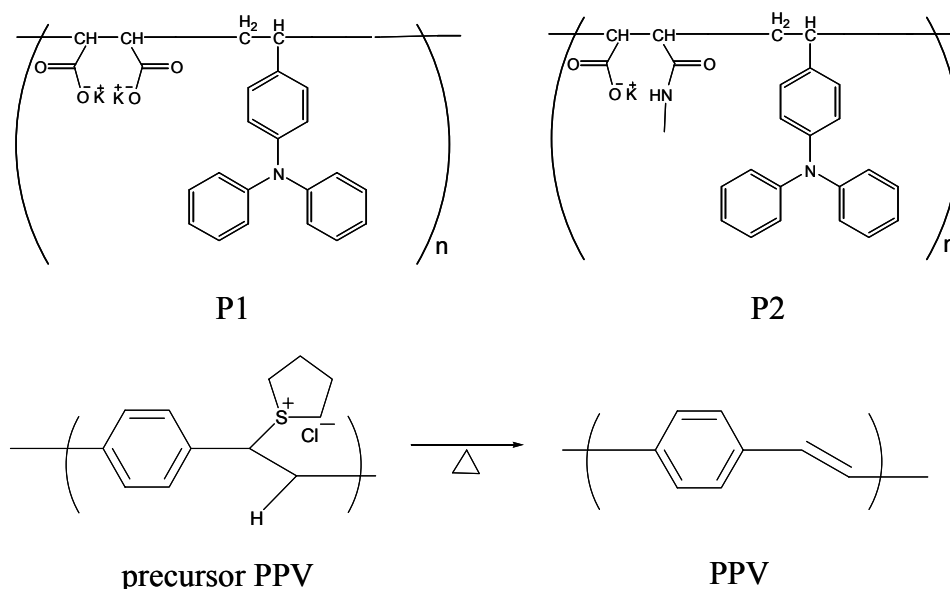
Due to their negative charges, the synthesized polymers **P1-P2** are suitable for the LBL self-assembly deposition from polymer solutions using the spin-coating technique with oppositely charged cationic precursor poly(phenylenevinylene) (PPV). Since the first report of Decher and coworkers in the early 1990s, there have been numerous reports on the LBL assembly based on the electrostatic attraction between polycations and polyanions.[27] The LBL technique can form a variety of ultra-thin interfacial layers and create films comprised of semi-interpenetrated bilayers of polycations and polyanions. Moreover, the film thickness can be easily controlled at the molecular level and a multilayer architecture does indeed make it possible to realize significant improvements in the device performance.[28]

The optical properties of **P1** and **P2** were investigated by UV/VIS and photoluminescence (PL) spectroscopy as shown in Figure 6.1(a) and Table 6.1 in THF:H_2O = 5:1 mixture solvents. They show the maximum of the π-π* absorbance of the conjugated triarylamine polymers at about 300 nm. For the solid state behavior of the polymers, thin mono-layer films of **P1** and **P2** were assembled on quartz substrates by spin-coating method and spectroscopy measurements were also done. A slightly bathochromic shift occurs, because of the formation of intermolecular excimers originated from interchain interaction in the film state. All results are summarized in Table 6.1.
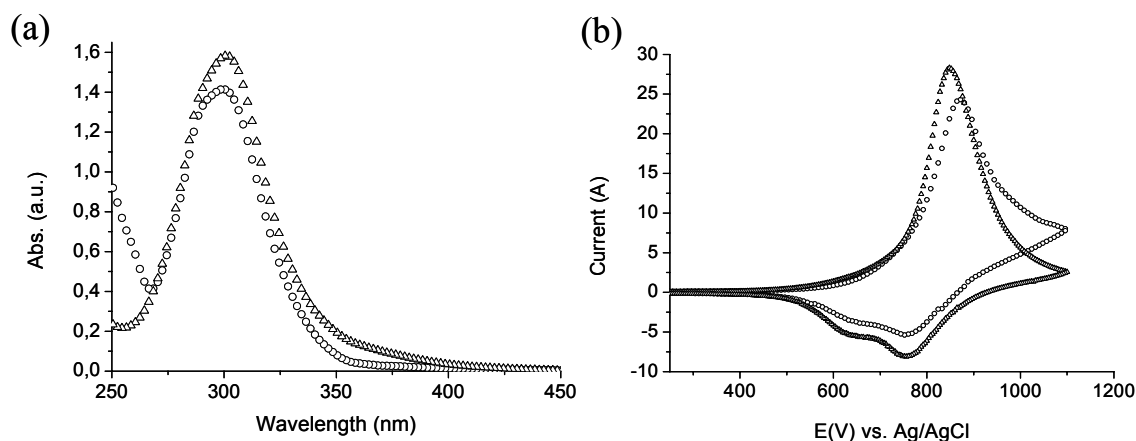
Figure 6.1. (a) UV/VIS spectra of triarylamine polymers **P1** and **P2** in solution of THF:H_2O = 5:1 mixture solvents. (b) Cyclic voltammograms of **P1** (○) and **P2** (Δ) on Pt-working electrode (with 0.1 M TBABF$_4$) at a scan rate of 20 mV/s, between 0 V and +1.1 V.

Following the optical measurements, the electrochemical properties of the **P1-P2** were evaluated using cyclic voltammetry (CV). All CV data were obtained using a three-electrode cell in an electrolyte of 0.1 M tetrabutylammonium tetrafluoroborate (TBABF$_4$) in acetonitrile using ferrocene as the internal standard. For these investigations, thin mono-layer **P1-P2** films were coated on Pt-working electrodes from the polymer solutions in THF:H$_2$O = 5:1 mixture solvents.[26] The scan for cyclic voltammograms of **P1** and **P2** was made anodically, proceeding from 0 V to +1.1 V. Upon oxidation of the films, the oxidation peak (E$_{ox}$) of **P1** appears at 871 mV and the oxidation peak of **P2** appears at 847 mV (see figure 6.1(b)). These values are characteristics for the triarylamine moieties in polymers. The difference of the oxidation potentials between **P1** and **P2** is presumably a consequence of changes in packing resulting from 1 or 2 ionic groups per repeating unit. As the potential gets reversed from +1.1 V to 0 V, two reversible reduction waves (E$_{red'}$) can be observed identically for the two polymers. The **P1** film has two peaks at 753mV and 646 mV and the **P2** film also has two peaks at 760 mV and 634 mV. The first peak at 753 or 760 mV corresponds to the reduction of the triarylamine radical-cation. The second peak at 646 or 634 mV can be attributed to the reduction of the oxidized dimer, which is formed from the radical-cations during the first oxidation cycle. Generally unsubstituted triarylamines undergo dimerization and the resulting dimers show both a reduced oxidation potential and an increased charge carrier mobility.[19] In addition, the formation of the dimer is a key factor to achieve stable films both with respect to mechanical stability (no dissolution due to the crosslinking) and chemical stability (more stable radical cations of the dimer). Concerning the use of hole transporting materials in devices, optimized energy band gap (E$_g$) of the polymers, which are defined with both the HOMO (highest occupied molecular orbital) and the LUMO (lowest unoccupied molecular orbital) levels, are necessary. Based on the optical and electrochemical data, each of the energy levels can be calculated and all values are listed in Table 6.1.

Table 6.1. Optical and electrochemical properties and energy levels of the **P1** and **P2**.

Polymers	UV/vis λ_{max} solution (nm)	UV/vis λ_{max} film (nm)	$E_g{}^a$ (eV)	PL λ_{max} solution (nm)	PL λ_{max} film (nm)	E_{ox} (mV)	E_{red}' (mV)	HOMO[b] (eV)	LUMO[c] (eV)
P1	299	308	3.04	455	462	871	753, 646	5.27	2.23
P2	301	305	3.03	460	460	847	760, 634	5.25	2.22

[a] Band gaps were calculated from the onset of the UV/VIS absorption spectra.

[b] HOMO levels were converted from the measured oxidation potentials assuming the absolute energy level of ferrocene to be -4.8 eV.[29]

[c] LUMO levels were estimated from the HOMO levels and energy gaps.

Due to the same triarylamine functionality, there is no significant difference in the HOMO and LUMO levels between the polymers **P1** and **P2**. According to the calculation, **P1** and **P2** possess low enough HOMO levels at -5.25~ -5.27 eV compared to the energy level of the ITO anode at -4.8 eV. It indicates that holes generated from the ITO anode can be effectively transported to the **P1** or **P2** layer. The calculated energy band diagram of the polymers is presented in Figure 6.2, suggesting that they are promising as hole transporting (p-type) materials in polymer LEDs.
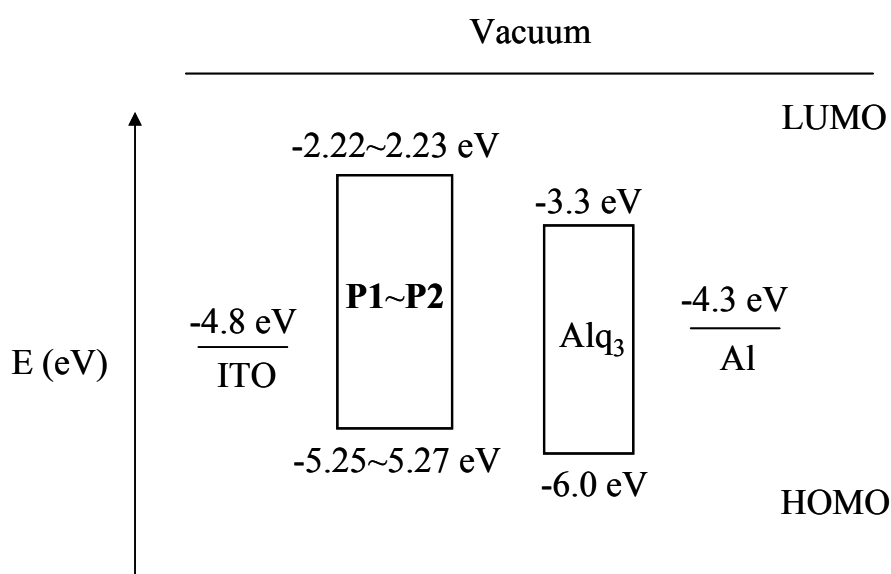
Figure 6.2. Energy band diagram of **P1** and **P2**.

Thin film LEDs based on multi-bilayer combinations of the conjugated poly(phenylene vinylene) (PPV) and different polyanions have been fabricated by the LBL molecular-level processing scheme.[30, 31] We have used this concept to prepare multilayer thin films (spin-coating variant of LBL method) from combinations of **P1-P2** and the precursor PPV (Scheme 6.1) and the fabricated multilayers were grown constantly in thickness. These films were fabricated with alternatively 20 or 40 bilayers of **P1-P2** and precursor PPV polycation solutions. The thermal conversion of the precursor PPV to the conjugated form of PPV was effected by heating the (**P1-P2**/precursor PPV)$_n$ films from room temperature to 180 °C, holding at that temperature for 10 h, and then allowing the samples to cool back down to room temperature over another 4 h period, all under dynamic vacuum conditions.

For an application with the fabricated multilayer films, we have fabricated simple devices with the configuration of ITO/(**P1-P2**/PPV)n films/LiF/ Al. Figure 6.3 shows the light intensity-voltage and relative device efficiencies plots of LEDs using thin films as hole transporting and light emitting layers. The turn-on voltages of (**P1**/PPV)$_{20}$ and (**P2**/PPV)$_{20}$ devices are found to be about 2.8 V and 2.2 V. The thicker (**P1**/PPV)$_{40}$ and (**P2**/PPV)$_{40}$ devices show about 6.4 V and 3.8 V of the turn-on voltages. Interestingly, the (**P1-P2**/PPV)$_{40}$ devices show dramatically increased turn-on voltages compared to the (**P1-P2**/PPV)$_{20}$ devices. We believe that this thickness dependent behavior can be explained -besides the usual thickness dependence due to constant field strength- by a thickness dependent conversion of the precursor PPV, which gets more limited with increasing thickness. In Figure 6.3(b), the light intensity characteristics of **P1-P2**/PPV films with 20-40 bilayers show the same thickness dependency and especially there is relatively large gap between (**P1**/PPV)$_{40}$ and (**P2**/PPV)$_{40}$ films. In order to improve the device characteristics, we have tried different conversion temperatures, because the thermal conversion of the precursor PPV was done at 180 °C. Thereby we found by accident that **P2** can be vaporized well at higher temperatures. Heating polymer **P2** to temperature slightly above 300 °C leads to a vaporization of **P2** and a constant growth of an organic film on the substrate. This vaporized material will be called **P2 vap.** in the following.

(a)

(b)
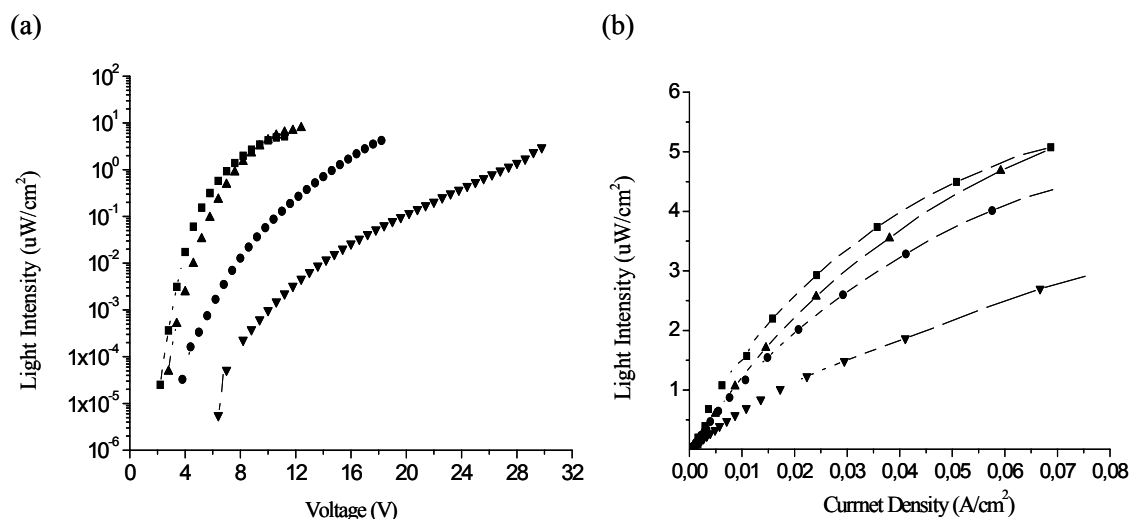
Figure 6.3. Light intensity-voltage and relative device efficiencies plots obtained from LEDs of ITO(**P1-P2**/PPV)$_n$/LiF/Al. Symbol represents the number of **P1** or **P2**/PPV bilayers: (■) (**P2**/PPV)$_{20}$, (▲) (**P1**/PPV)$_{20}$, (●) (**P2**/PPV)$_{40}$ and (▼) (**P1**/PPV)$_{40}$.

Although very little amount of evaporated material was available, we succeeded in analyzing the chemical structure of the organic film (**P2 vap.**) formed on the substrate by ^{1}H NMR and FT-IR spectroscopy. ^{1}H NMR shows that, in the deposited material, all functional groups are still present: the triarylamine (7.23~7.02 ppm in CD$_2$Cl$_2$), as well as the methyl group on the nitrogen of the comonomer (1.66 ppm in CD$_2$Cl$_2$, see Experimental section). FT-IR measurements show differences before and after vacuum deposition process (see Figure 6.4(a)). For the parent polymer (**P2**), a sharp carboxylate peak at 1586 cm^{-1} and a relatively weak amide peak at 1641 cm^{-1} are observed. After vacuum deposition (**P2 vap.**), the an amide peak has disappeared and replaced by a strong new peak at 1702 cm^{-1} , which can be assigned to the imide bond. Such a reaction is expectable since imidization (figure 6.4(c)) of amide–acid at higher temperatures is a classical reaction.[32, 33] The imidization explains also the different thermal behaviors between **P1** and **P2** during the heating process, because **P1**, which has two carboxylate groups at the comonomer unit, cannot form an imide. As a result, it stays an ionic polymer, of which fragments can hardly vaporize. On the contrary, **P2** looses its ionic character during imidization and fragments can more easily vaporize.
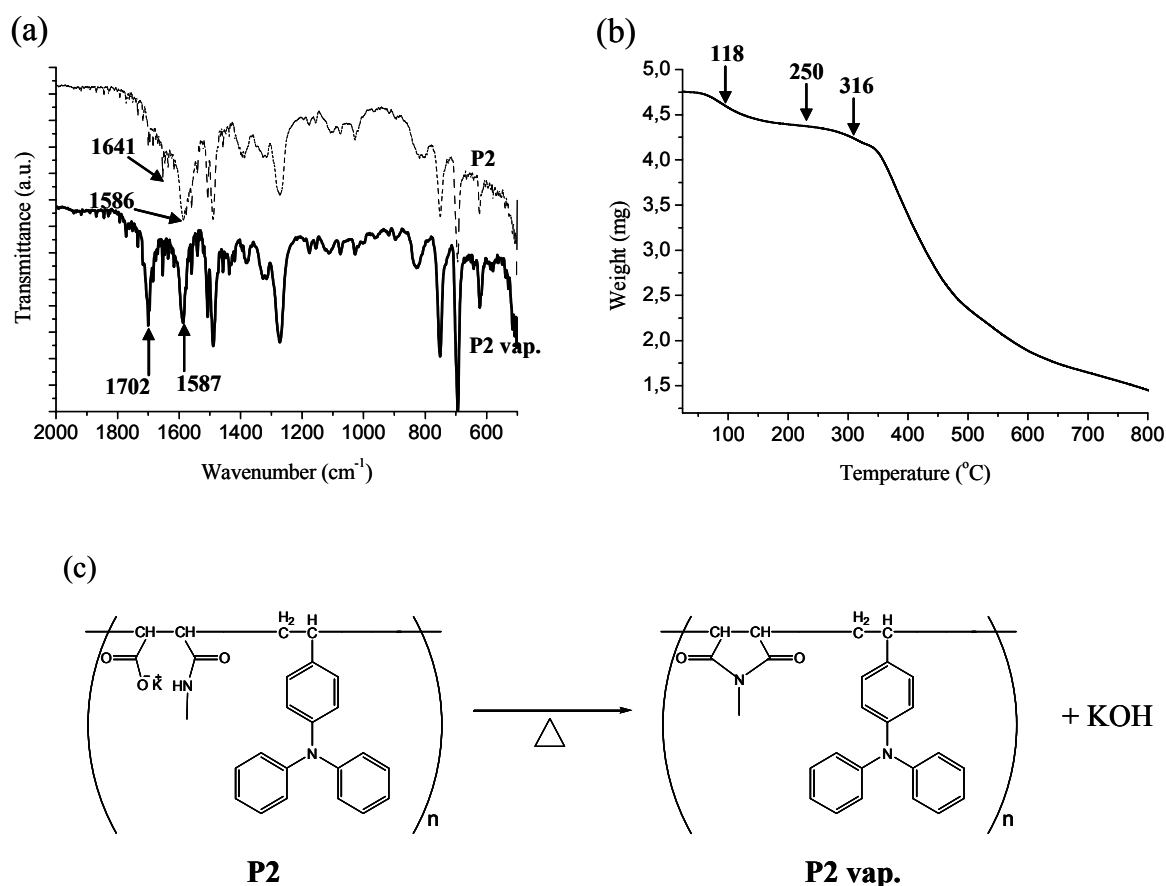
Figure 6.4. (a) The IR spectra of **P2** before and after (**P2 vap.**) the vacuum deposition process (b) TGA thermogram of **P2**. (c) The estimated secondary reaction from **P2** to **P2 vap.**

To study the chemical processes during the heat treatment of **P2**, a thermo-gravimetric (TGA) measurement was carried out under dried nitrogen gas. Figure 6.4(b) shows the three-step weight loss as a result. The first step appears below 118 °C and involves a small weight loss. It can be attributed to the evaporation of DMF and H_2O molecules used as solvents during the synthesis and purification. The second step occurs over the range 118 ~ 250 °C and involves a relatively small weight loss. This small weight loss is most likely due to traces of water formed as a byproduct of the imide-ring. Although the imidization is the major reaction, it cannot lead to a large weight loss, because KOH is formed during the reaction of potassium carboxylate with the amide group. When the temperature is raised above 320 °C, the most significant weight loss occurs. It is due to the degradation of the imidized polymer chains. From the TGA result, we conclude that in the heating run, **P2** is partially degraded above

320 °C and it leads to oligomeric structure with all subunits in tact. This assumption is in agreement with the GPC-measurements of the evaporated material. For the deposited oligomers of **P2 vap.,** an Mw of 2100 is found, which is much smaller than the Mw of the parent **P2** (151 000, see Experimental Part).

From deposited films of oligomeric **P2 vap.** we have fabricated simple LEDs with the configuration of ITO / vacuum deposited **P2 vap.** film / Alq$_3$ / LiF / Al. Figure 6.5(a) and 6.5(b) show the external EL quantum efficiency (η_{ext}) and the luminous efficiency-current density (J) characteristics of LEDs using a vacuum deposited **P2 vap.** film as a hole transporting layer. A maximum η_{ext} of 0.48 % was obtained at a current density of $J = 31$ mA/cm^2 and a maximum luminous efficiency of 1.6 cd/A was found at the same current density. Therefore, the insertion of the **P2 vap.** layer in the device increases the quantum efficiency (Q_E) and luminous efficiency. Moreover, these values are highly improved compared to the values of multilayer device with the configuration of ITO/(**P1-P2**/PPV)$_n$ films/Alq$_3$/LiF/ Al.
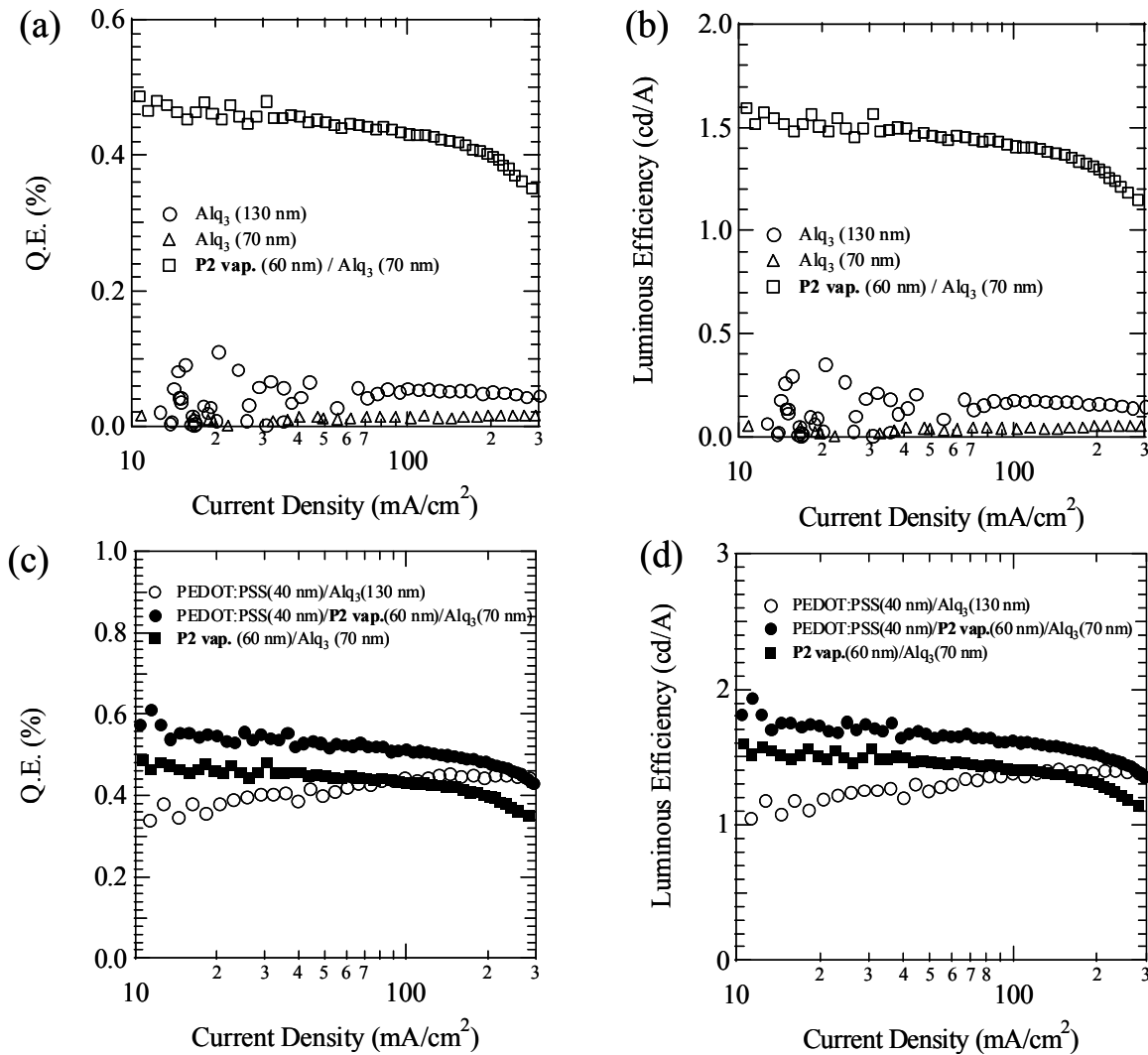
Figure 6.5. (a) The external EL quantum efficiency (η_{ext})-current density (J) characteristics (b) luminous efficiency-current density (J) characteristics of LEDs using a vacuum deposited **P2 vap.** film as a hole transporting layer. (c) external EL quantum efficiency (η_{ext})-current density (J) characteristics (d) luminous efficiency-current density (J) characteristics of LEDs using the configuration with PEDOT: PSS layer as a hole injection layer.

Since there is a small energy gap between the ITO (-4.8 eV) and the **P2** polymer (-5.25~ -5.27 eV), a barrier for hole injection results. In order to further enhance the device performance, the insertion of a PEDOT: PSS (-5.1 eV) layer as a hole injection layer in the devices can optimize the energy band gap. Figure 6.5(c) and 6.5(d) show the external EL quantum efficiency (η_{ext})–luminous efficiency-current density (J) characteristics of the devices with the

configuration of ITO / PEDOT: PSS (HIL)/vacuum deposited **P2 vap.** film (HTL) / Alq$_3$ / LiF / Al. As a result, a maximum η_{ext} of 0.55 % is obtained at a current density of $J = 36$ mA/cm^2 and a maximum luminous efficiency of 1.8 cd/A is found at the same current density. These characteristics suggest that the quantum efficiency and the luminous efficiency can be further improved with PEDOT: PSS layer as a hole injection layer in **P2 vap.** devices.

6.3. Conclusion

In summary, we presented the successful fabrication of a thin film of semiconducting oligomers from triarylamine polymers by the vacuum deposition method. As hole transporting materials, the p-type triarylamine polymers were synthesized by radical polymerization. The anionic polymers are suitable for the LBL assembly with oppositely charged polycations. We have fabricated a simple multilayer device using the fabricated multilayer film; however, the characteristics were not comparable to the values of the state of the art system. Interestingly, we found that **P2**, which has one carboxylate and one amide groups can be imidized during heat treatment and degrades to oligomers. As one of the potential applications, the vacuum deposited films were used in LEDs as hole transporting layers. The external EL quantum efficiency (η_{ext}) and the luminous efficiency-current density (J) characteristics of these devices showed dramatic improvements, indicating that the **P2 vap.** film is promising as a hole transporting layer. Therefore, we conclude that polymers, which decompose to oligomers at elevated temperatures, can be deposited as high quality films by the vacuum deposition process.

6.4. Experimental

^{1}H NMR spectra were measured on a Bruker 300 MHz FT spectrometer. FT-IR spectra were measured on a Bruker Vector 22 FT-IR spectrometer with a Harrick ATR unit. Gel permeation chromatography (GPC) at RT was used to determine the molecular weight with THF as eluent. For this purpose, Jasco PU-1580 pump, Autosampler AS 1555, UV-detector UV 1575 and RI-detector RI 1530 were used. (Wyatt light scattering, MZ-Gel SDplus10^2, 10^4 Å and 10^6 Å). To evaluate the data, universal calibration based on polystyrene standards was

used. UV/VIS absorption spectra were taken with a Shimadzu UV- 2102 PC spectrometer and photoluminescence (PL) spectra were taken with a Fluoromax-II fluorometer (ISA). All electrochemical tests were performed using an Autolab PGSTAT30 (Eco Chemie) Potentiostat/Galvanostat. Pt-wire and Ag/AgCl electrodes were used as the counter and reference electrodes. Polymer films coated on ITO substrates were used as the working electrodes and 0.1 M tetrabutylammonium tetrafluoroborate (TBABF$_4$) in acetonitrile was used as the electrolyte. The substrates were treated by UV ozone ambient condition of a UVO cleaner, UVO-42 and for spin-coating; a Convac ST146 spin-coater was used.

Preparation of triarylamine polyelmer P1-P2 and their multilayer build-up.

The synthesis of the polymers started with the radical copolymerization of maleic anhydride and triarylamine monomers and the multilayer build-up of polymers **P1-P2** are described elsewhere[26] in more detail. To determine the molecular weight, the resulting alternating copolymer was analyzed by GPC with THF as eluent; a Mn : 98720 g/mol , Mw : 150900 g/mol and polydispersity index (PDI) (Mw/Mn) : 1.53 were found. After treatment of the potassium hydroxide or alkyl amine solution, the **P1** and **P2** are composed with two different moieties; one part is the two carboxylate groups derived from the maleic anhydride for **P1** or only one carboxylate group and amide group derived from maleic anhydride and one amine solution for **P2** and the other part is triarylamine.

P1: ^{1}H NMR (CD$_2$Cl$_2$, 300 MHz): δ = 6.97 (14H, arom H), 1.66 (5H, main chain)
    IR (ATR): 1586 (CO) cm^{-1}

P2: ^{1}H NMR (CD$_2$Cl$_2$, 300 MHz): δ = 6.93 (14H, arom H), 2.47 (5H, main chain), 1.82 (3H, NH-CH$_3$)
    IR (ATR): 1641 cm^{-1} (amide bond), 1585 (CO) cm^{-1}

P2 vap.: ^{1}H NMR (CD$_2$Cl$_2$, 300 MHz): δ = 7.23 (4H, arom H), 7.02 (10H, arom H), 2.93 (5H, main chain), 1.54 (3H, N-CH$_3$)
    IR (ATR): 1702 cm^{-1} (imide bond), 1587 (CO) cm^{-1}
    Mn: 1448 g/mol, Mw: 2079 g/mol, PDI (Mw/Mn): 1.43

The optical and electrochemical properties of the **P1** and **P2** in Table 6.1 were obtained based on the UV/VIS spectra and CV data. The HOMO and LUMO levels calculated according to an empirical formula, E_{HOMO} = -e (E_{ox} + 4.4) (eV) and E_{LUMO} = -e (E_{red} + 4.4) (eV).[29] Band gaps were calculated from the onset of the UV/VIS absorption spectra (λ = 1240 /V).

P2 vap. film fabrication by vacuum deposition method.

For the devices with **P2 vap.** films, the ITO substrate (sheet resistance of about 10 $\Omega/\square$, 150 nm thick) was cleaned ultrasonically in organic solvents (isopropyl alcohol, acetone, and methanol) and rinsed in de-ionized (DI) water. It was dried in an oven kept at 100 ℃ for more than 30 min. The device was fabricated with the successive vacuum deposition of **P2**, Alq_3, LiF, and aluminum (Al), under a vacuum (< 3 x 10^{-6} Torr) without breaking vacuum. The deposition rates for organic layers were about 0.1~0.15 nm/sec and about 0.3nm/sec for Al. The active area of the OLED, defined by the overlap of the ITO and the Al cathode, was 1.96 mm^2. High conducting PEDOT: PSS (Baytron PAI 4083) was spin-coated (4000 rpm) with thickness 40 nm after passing a 0.5 μm filter. And then the film was dried at vacuum oven in 120 ℃ over 30 min. The current-voltage-luminance (I-V-L) characteristics were measured with a Keithley 236 source-measure unit and a Keithley 2000 multimeter equipped with a PMT through an ARC 275 monochromator. The luminous efficiency was estimated by measuring the EL emission intensity with the calibrated Si photodiode placed at the normal angle to the device surface and assuming that the device is a Lambertian source.

6.5. References

(1) Tang, C. W.; Van Slyke, S. A. *Appl. Phys. Lett*. **1987**, 51, 913.

(2) Kolosov, S.; Adamovich, V.; Djurovich, P.; Thompson, M. E.; Adachi, C. *J. Am. Chem. Soc*. **2002**, 124, 9945.

(3) Baldo, M. A.; O'Brien, D. F.; You, Y.; Shoustikov, A.; Sibley, S.; Thompson, M. E.; Forrest, S.R. *Nature* **1998**, 395, 151.

(4) Shirota, Y.; Kinoshita, M.; Noda, T.; Okumoto, K.; Ohara, T. *J. Am. Chem. Soc*. **2000**, 122, 11021.

(5) Mitschke, U.; Bauerle, P. *J. Mater. Chem*. **2000**, 10, 1471.

(6) Katz, H. E.; Bao, Z. *J. Phys. Chem. B*. **2000**, 104, 671.

(7) Katz, H. E.; Bao, Z.; Gilat, S. L. *Acc. Chem. Res*. **2001**, 14, 359.

(8) Dimitrakopoulos, C. D.; Malenfant, P. R. L. *Adv. Mater*. **2002**, 14, 99.

(9) Horowitz, G. *Adv. Mater*. **1998**, 10, 365.

(10) Sirringhaus,H.; Tessler, N.; Friend, R. H. *Science* **1998**, 280, 1741.

(11) Brabec, C. J.; Sariciftci, N. S.; Hummelen, J. C. *Adv. Funct. Mater*. **2001**, 11, 15.

(12) Yu, G.; Gao, J.; Hummelen, J. C.; Wudl, F.; Heeger, A. J. *Science* **1995**, 267, 1969.

(13) Antoniadis, H.; Hsieh, B. R.; Abkowitz, M. A.; Jenekhe, S. A.; Stolka, M. *Synth. Met*. **1994**, 62, 265.

(14) Jenekhe, S. A.; Yi, S. *Appl. Phys. Lett*. **2000**, 77, 2635.

(15) Sapp, S. A.; Sotzing, G. A.; Reynolds, J. R. *Chem. Mater*. **1998**, 10, 2101.

(16) Kumar, A.; Welsh, D. M.; Morvant, M. C.; Piroux, F.; Abboud, K. A.; Reynolds, J. R. *Chem. Mater*. **1998**, 10, 896.

(17) Adachi C, Tsutsui T, Saito S, *Appl. Phys. Lett*. **1989**, 55, 1489

(18) Adachi C, Tokito S, Tsutsui T, Saito S. *Jpn. J. Appl. Phys*. **1988**, 27, L269

(19) M, Thelakkat. *Macomol. Mater. Eng*. **2002**, 287, 442.

(20) Han, E.; Do, L.; Yamamoto, N.; Fujihira, M. *Mol. Cryst. Liq. Cryst*. **1996**, 280, 349.

(21) De Leeuw, D. M.; Lous, E. J. *Synth. Met*. **1994**, 65, 45.

(22) Garnier., F.; Yassar, A.; Hajlaoui, R.; Horowitz, G.; Deloffre, F.; Servet, B.; Ries, S.; Alnot, P. *J. Am. Chem. Soc*. **1993**, 115, 8716.

(23) K. Miyashita, M. Kaneko. *Synth. Met*. **1995**, 68, 161.

(24) S. Kobayashi, Y. Haga. *Synth. Met*. **1997**, 87, 31.

(25) C. H. Lee, G. W. Kang, J. W. Jeon, W. J. Song, C. Seoul. *Thin Solid Films* **2000**, 363, 306.

(26) K. Choi, R. Zentel, *Macromol. Chem. Phys*. **2006**, accepted.

(27) (a) Decher, G.; Hong, J. D.; Schmitt, J. *Thin Solid Films* **1992**, 210/ 211, 831. (b) Ferreirat, M.; Rubner, M. F. *Macromolecules* **1995**, 28, 7107. (c) Park, S. Y.; Rubner, M. F.; Mayes, A. M. *Langmuir* **2002**, 18, 9600.

(28) A. Berlin, G Zotti, *Macromol. Rapid Commun*. **2000**, 21, 301.

(29) Liu, Y.; Liu, M. S.; Jen, A. K.-Y. *Acta. Polym*. **1999**, 50, 105.

(30) A. C. Fou, O. Onitsuka, M. Ferreira, M. F. Rubner, *J. Appl. Phys*. **1996**, 79 (10), 15, 7501.

(31) O. Onitsuka, A. C. Fou, M. Ferreira, B. R. Hsieh, M. F. Rubner, *J. Appl. Phys*. **1996**, 80 (7), 4067.

(32) L. Huang, Y. Shi, L. Chen, X. Jin, R. Liu, M. A. Winnik, *J. Polym. Sci. Part A: Polym. Chem.* **2000**, 38, 730.

(33) N. T. Karangu, M. E. Rezac, H. W. Beckham, *Chem. Mater*. **1998**, 10, 567.

7. Summary and Conclusions

The presented study describes novel layer-by-layer (LBL) self-assembly method with synthesized functional polymers. The LBL method is one of the most simplest self-assembly techniques to approach nanotechnology at nano-scale film thickness. In addition, the ionic self-assembly method provides an elegant way of controlling the composition of the resulting assemblies. Newly synthesized cationic and anionic LC amphotropic ionomers, p-type and n-type semiconducting polyelectrolytes with triarylamine, oxadiazole, thiadiazole and triazine moieties were used as proper polyelectrolytes for the LBL assembly.

First, the multilayers were fabricated by various LBL methods such as solution-dipping and spin-coating methods with the amphotoropic LC ionomers, which show both thermotropic phases in bulk and lyotropic phases in concentrated solution. We have investigated the internal structure of the LBL assembly fabricated by both methods and they showed different physical phenomena on a molecular level. The multilayers deposited by the solution-dipping method possessed the order parameter closed to that of real liquid crystalline monodomains, and the mesogens of the LC ionomers were oriented perpendicular to the substrate. On the other hand, the spin-coating method gave much thicker films that possessed less internal order. The differences between the solution-dipped and spin-coated samples can be rationalized by the different deposition mechanism.

The newly synthesized semiconducting ionic polymers with triarylamine, oxadiazole, thiadiazole and triazine moieties have outstanding electrochemical properties as electron- or hole-transporting materials. They were examined optically and electrochemically by UV/VIS spectroscopy, photoluminescence spectroscopy and cyclic voltammetry. Based on the optical and electrochemical data, each of the energy levels was calculated and all values suggested that they are favorably promising as hole- (p-type) or electron-(n-type) transport materials in devices. Concerning the making of the polymer films for the devices, LBL assembly was introduced, that is ideal processing technique to prepare thin polymer film composites with fine control over morphology and composition. Nano-scale control of the structure of organic/polymeric materials is a prerequisite to the fabrication of sophisticated functional devices. As the potential applications, the fabricated semiconducting polymer thin films were used as simple electrochromic films.

The electroactive triarylamine polymers have unique properties which are easy oxidizability and its ability to transport positive charge centers via the radical cation species. Furthermore, the triarylamines are anodically coloring electrochromic species within the LBL film. Due to the dimerization of the triarylamine, fabricated thin films were electrochemically and mechanically stabilized. Electrochemical and electrochromic characterizations of assembled films revealed that the LBL films with triarylamine polymers give rise to high contrast ratio and fast switching electrochromic films. This is a result of the thin nano-scale film formed by the LBL technique in combination with the high charge carrier mobility of triarylamine dimers.

We have also presented the successful fabrication of a thin film of semiconducting oligomers from triarylamine polymers by the vacuum deposition method. The anionic polymers were originally designed for the LBL assembly with oppositely charged polycations; however, the device characteristics of the multilayer films were not comparable to the values of the state of the art system. In order to make thin films, we have introduced a vacuum deposition method. Usually polymer thin films are prepared from solution by solution-dipping or spin-coating method and the vapor deposition method has been explored only for low-molecular weight materials. During the vacuum deposition process, a secondary reaction is occurrs and the triarylamine polymer is degraded to oligomers at elevated temperatures. Such evaporated oligomers could give more stable amorphous structures compared to low molar mass materials. As one of the potential applications, the fabricated films were used in light emitting devices as hole transporting layers. The external EL quantum efficiency (η_{ext}) and the luminous efficiency-current density (J) characteristics of these devices showed dramatic improvements in device characteristics, indicating that the vacuum deposited film is promising as a hole transporting layer. We conclude that polymers, which decompose to oligomers at elevated temperatures, can be deposited as high quality films by the vacuum deposition process.

8. Methods and Instrumentation

8.1. Surface plasmon resonance spectroscopy (SPR)

At an interface between two transparent media of different refractive index (glass and water), light coming from the side of higher refractive index is partly reflected and partly refracted. Above a certain critical angle of incidence, no light is refracted across the interface, and total internal reflection is observed. While incident light is totally reflected the electromagnetic field component penetrates a short (tens of nanometers) distance into a medium of a lower refractive index creating an exponentially detenuating evanescent wave. If the interface between the media is coated with a thin layer of metal (gold), and light is monochromatic and p-polarized, the intensity of the reflected light is reduced at a specific incident angle producing a sharp shadow (called surface plasmon resonance) due to the resonance energy transfer between evanescent wave and surface plasmons. The resonance conditions are influenced by the material adsorbed onto the thin metal film. Satisfactory linear relationship is found between resonance energy and mass concentration of biochemically relevant molecules such as proteins, sugars and DNA.

The Surface Plasmon Resonance spectroscopy[1] is a versatile tool to measure the thickness of thin films adsorbed onto a metal surface. The method is based on electrons which have the ability to move nearly free as electron gas and thus they are completely disconnected from the atomic nucleus. This property is related to metals with a complete d-shell, having valence electrons in s- or p-orbitals like gold or silver. Under these circumstances the electrons are able to relay vibrations, i. e. the charge density like the gas particles in air. These fluctuations of the charge density are called plasmon. They show characteristic vibration energy:

$$E_p = \hbar \cdot \omega_P = \hbar \cdot \sqrt{\frac{4\pi\eta e^2}{\varepsilon\varepsilon_0 m_e}}$$

η = electron concentration

m_e = electron mass

$\varepsilon, \varepsilon_0$ = dielectric constants

As the vibrational energy acts as an electromagnetic wave the electrons can be excited by radiation.
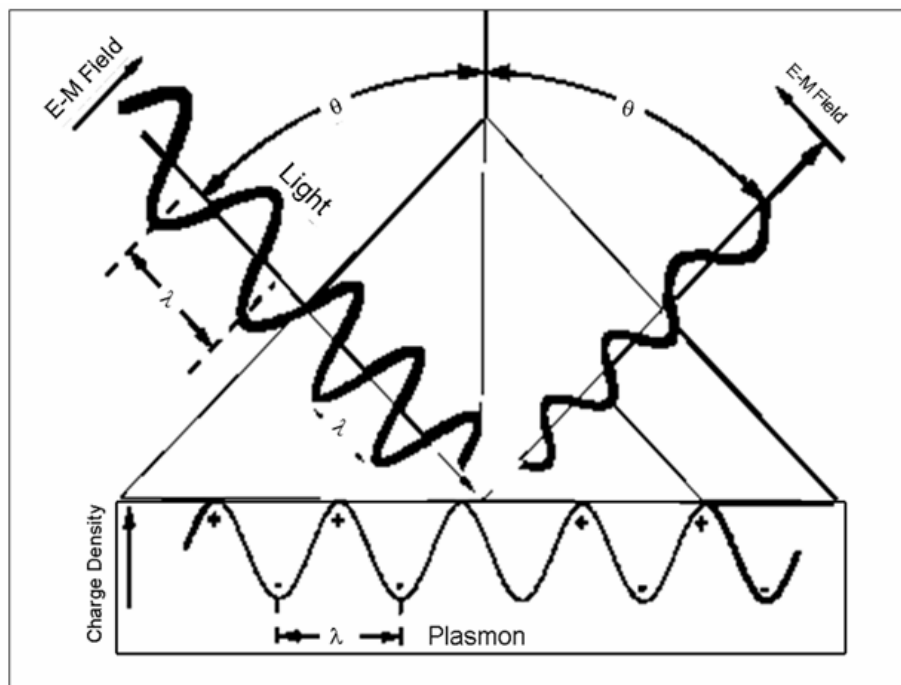
Figure 8.1.1. Kretschmann configuration of the plasmon resoncance.

The excitation of the plasmon is possible at a metal-dielectric interface by a monochromatic light beam, normally by a Helium-Neon laser and can be understood as a longitudinal propagation of the surface plasmon at the interface. Therefore, it is surface selective as well as a surface sensitive method. It is observed as a deep minimum in the p-polarised reflected light as the angle-of-incidence is incremented. The amplitude of the vibration is exponentially debilitated into the interior of the metal with a penetration depth of about ~100 nm. To measure the film thickness at a gold surface the most convenient configuration for plasmon resonance is the Kretschmann configuration (Figure 8.1.1).[2] The plasmon is measured at the interface between a dielectric material and the gold, where the light comes from a medium with a higher refractive index to penetrate a material with a lower refractive index. The Snellius equation of refraction is valid (Figure 8.1.1):

$$\frac{\sin \alpha}{\sin \beta} = \frac{n_2}{n_1}$$

The phenomen of total reflection is observed by the transition of light from an optically dense material to a less dense material. In this case β is $> 90°$. At critical angle of $\alpha_T = \alpha$, β is $90°$ and thus $\sin \beta = 1$. The refraction equation results in:

$$\sin \alpha_T = \frac{n_2}{n_1}$$

At this critical angle total reflections of the light beam occur. Thus the plasmon spectra show a maximum (Figure 8.1.2). If α increases more, a small part of the incident light beam energy passes through the boundary layer between glass and gold. This so called evanescent wave couples with the plasmon and at a certain angle a maximum of energy is absorbed resulting in a minimum in the spectrum.
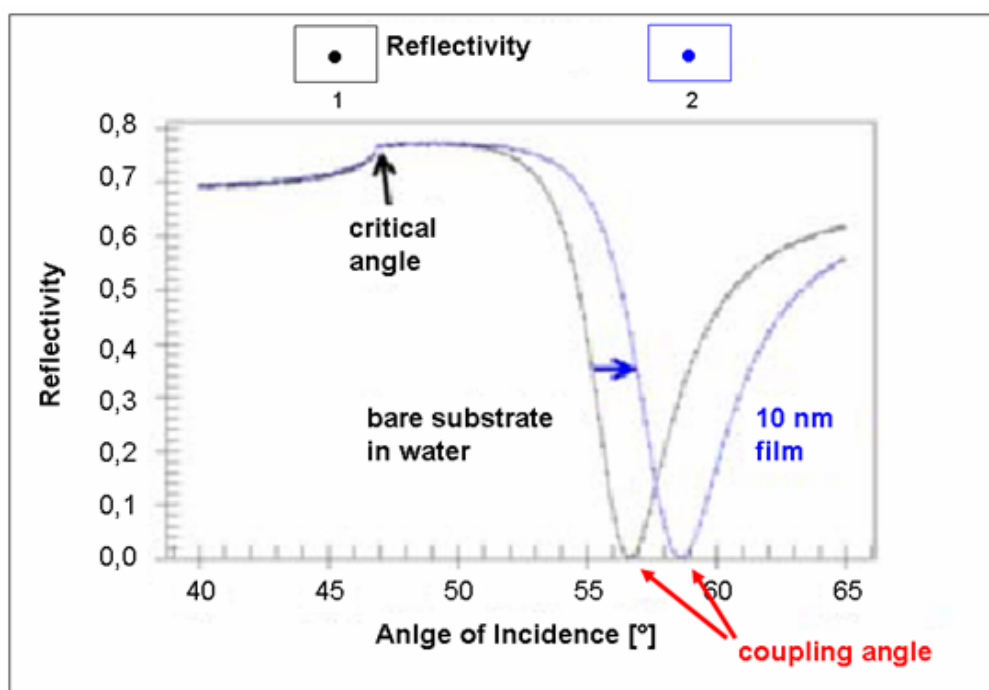
Figure 8.1.2. Plasmon spectrum from bare gold (black line) and with a substrate on the gold surface (blue line).

This coupling angle indicates the point of the highest light absorption by the plasmon, i. e. the collective oscillation of the electrons with the light. The value of the experiment is that the exact angle for the plasmon resonance peak is extremely sensitive to any thin film on the metal surface even for a monolayer consisting of organic molecules. So the minimum position of the peek can be used to determine the thickness and density. The theoretical characterization of these phenomena is completely understood and the thickness of the layer can be inferred from the angle shift between spectra taken from the clean gold surface and from the gold surface with an absorbed layer by simulation with programs like WINSPALL.[3]

One of the important advantages of the SPR analysis is the quite good time resolution since the surface plasmon can be generated and measured in a short time. Thus real time analysis can be made as in kinetic measurements of the absorption of a solute like proteins.

For this PhD thesis, all measurements were done using a spectrometer in the Kretschmann-configuration purchased from Resonant Probes GmbH (Goslar).[4] A graphical description of the complete equipment is shown in Figure 8.1.3.
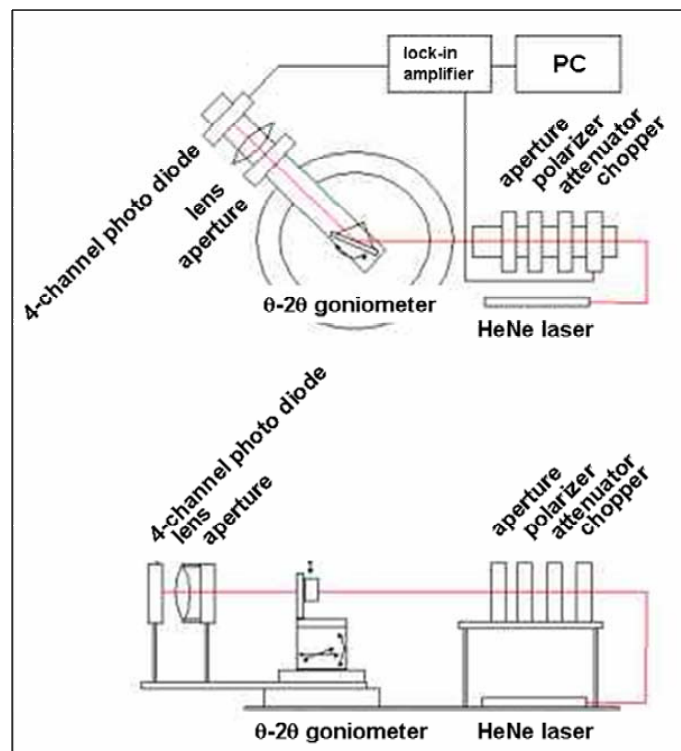
Figure 8.1.3. Kretschmann set-up of a surface plasmon spectrometer.

8.2. Atomic force microscopy (AFM)

All scanning techniques which use a sharp tip moving over the surface of a sample in a raster scan are summarized under the name scanning probe microscopy (SPM).[5,6] Binnig, Rohrer, and Gerber invented in 1982 the scanning tunnelling microscope (STM), the first type of SPM. They won the Nobel Prize in 1986. This method based on electron tunnelling, i.e. an electrical current that flows between two conductors that are separated by very short distances at Angstrom scale. This tunnelling current depends exponentially on the distance between the two conductors. By monitoring the current over each point of the surface of the sample, the electronic topography of the surface is recorded. Thus there are two distinguishable modes of operation:

i) **Constant Height Mode**: When the distance between tip and samples is kept constant current is recorded over each point giving the electronic properties of the sample;

ii) **Constant Current Mode**: When the current is kept constant during the scan the topography of the substrate surface is recorded.

This microscopic method is restricted to conductive substrates but permits atomic information not from an average over many atoms, but over atom by atom.

The complementary technique to the STM is the atomic force microscopy (AFM). With this instrument also non-conducting materials can be investigated. It was invented by Binnig, Quate and Gerber in 1986. The AFM uses a cantilever with a sharp tip moving over the surface of the sample in a raster scan. The cantilever bends in response to the force between the tip and the sample surface. Most of the AFMs employ an optical lever technique for detecting the bending of the cantilever. The light from a laser is reflected from the cantilever onto a split photo-diode. By measuring the aberration of the signal, and changes in the bending of the cantilever, (as the cantilever obeys Hooke´s Law for small displacements,) the interaction force between the tip and the sample can be determined (Figure 8.2.1). The displacement of the tip or sample is performed by an extremely precise positioning device made from piezo-electric ceramics with a resolution of sub-angstrom.

There are principally three different classes of interaction between tip and sample: contact mode, tapping mode, and non-contact mode.

1) Contact mode signifies a close contact between tip and sample during scanning progress. Close contact mean that the tip approach to the surface that the inter-molecular repulsive force become positive and producing large lateral forces on the sample and the tip is dragged over the surface.(Figure 8.2.2)

2) The tapping mode is used by poorly immobilized or soft samples. By operating in air or other gases, the cantilever oscillates at its resonant frequency and is positioned above the surface. It only taps the surface for a very small part of its oscillation period. Thus it has a short time contact with sample surface. This decrease dramatically the lateral force as the tip scans over the surface.

3) The third mode of measuring is the non-contact mode. The cantilever oscillates above the surface at such a distance that there is no lateral force which means that it is no longer in the repulsive regime of the inter-molecular force curve.
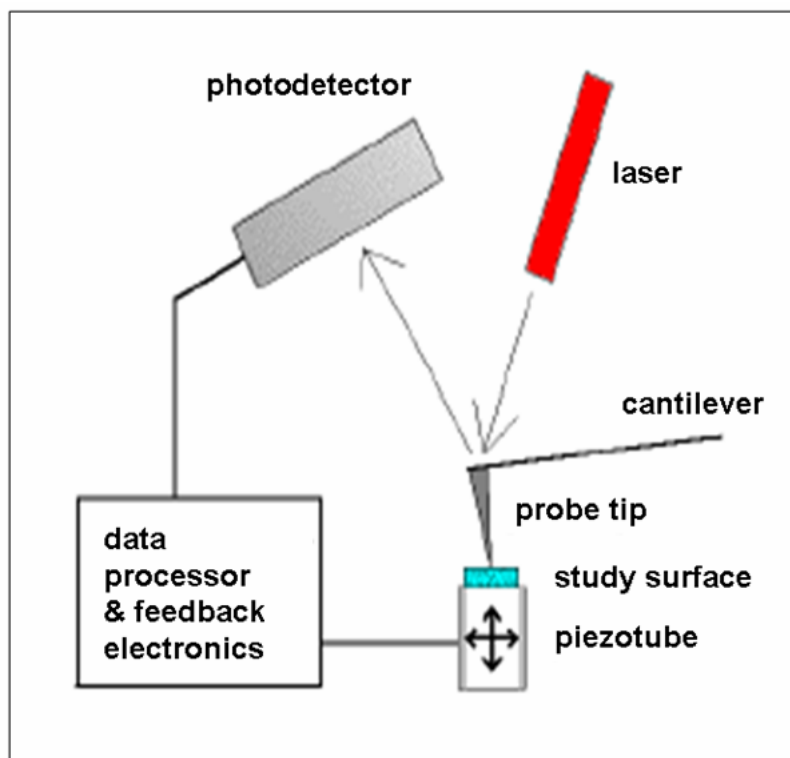
Figure 8.2.1. Schematic illustration of the measurement technique by an Atomic Force Microscope.

Apart from the study of topography with high resolution and interactions between the tip and the surface of nearly every material, AFM also can be applied for nanomechanic studies employing the AFM tip to produce indents in a specimen or for friction measurements by scratching the tip over the surface. The great advantage of all SPM techniques is the ability to do time-resolved investigations down to atomic or near-atomic processes in all materials.
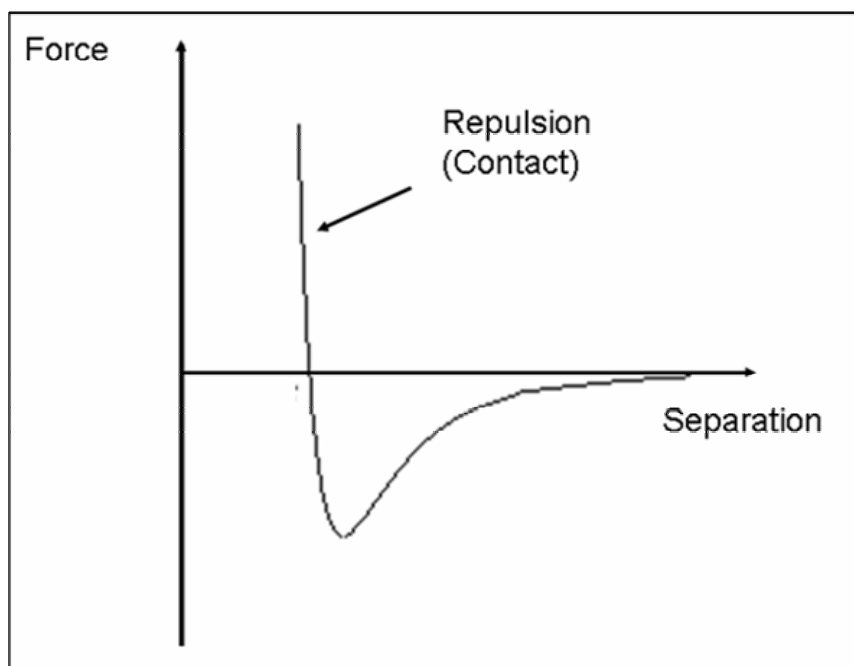
Figure 8.2.2. Inter-molecular force curve.

In this Ph.D. thesis, samples were imaged at room temperature with a commercial SFM (Nanoscope IIIa, Digital Instruments, Santa Barbara, California) employing Tapping ModeTM using rectangular silicon cantilevers (Nanosensors, 125μm long, 30μm wide, 4μm thick) with an integrated tip, a nominal spring constant of 42 N m^{-1}, and a resonance frequency of 330 kHz. To control and enhance the range of the attractive interaction regime the instrument was equipped with a special active feedback circuit, called Q-control (Nanoanalytics, Germany).

8.3. Cyclic Voltammetry (CV)

Cyclic voltammetry is a kind of potentiodynamic electrochemical measurement. Being a specific type of voltammetry, it is used for studying the redox properties of chemicals and interfacial structures. For the majority of experiments the electroactive species is in the form of a solution.

The three-electrode method is the most widely used because the electrical potential of reference does not change easily during the measurement. This method uses a reference electrode, working electrode, and counter electrode (also called the secondary or auxiliary electrode). Electrolyte is usually added to the test solution to ensure sufficient conductivity. The combination of the solvent, electrolyte and specific working electrode material determines the range of the potential. The practical set-up for measurement is shown in Figure 8.3.1.
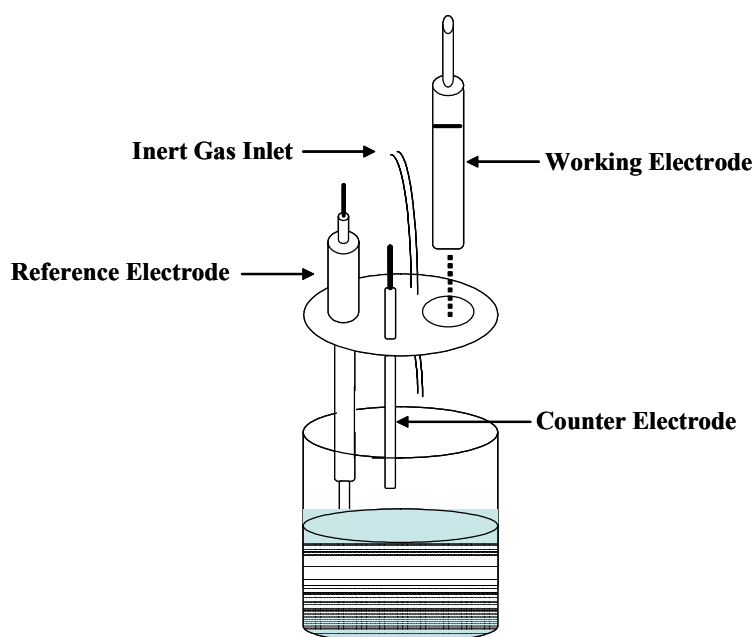
Figure 8.3.1. Electrochemical cell for cyclic voltammetry.

The potential is measured between the reference electrode and the working electrode and the current is measured between the working electrode and the counterelectrode. This data is then

plotted as current (i) vs. potential (E) (Figure 8.3.2(a)). As the waveform shows (Figure 8.3.2(b)), the forward scan produces a current peak for any analytes that can be reduced through the range of the potential scan. The current will increase as the potential reaches the reduction potential of the analyte, but then falls off as the concentration of the analyte is depleted close to the electrode surface. As the applied potential is reversed, it will reach a potential that will reoxidize the product formed in the first reduction reaction, and produce a current of reverse polarity from the forward scan. This oxidation peak will usually have a similar shape to the reduction peak. As a result, information about the redox potential and electrochemical reaction rates of the compounds is obtained.[7]
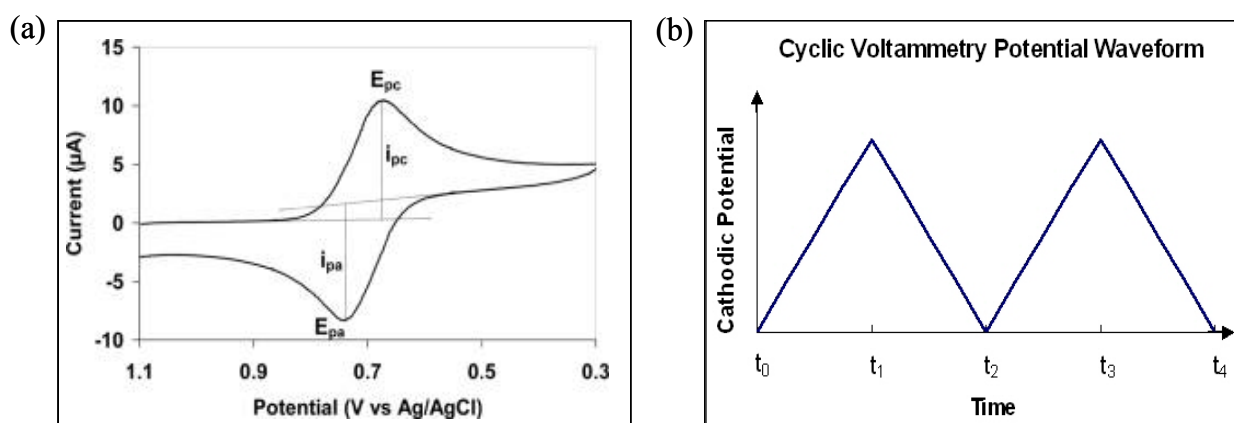
Figure 8.3.2. (a) Typical cyclic voltammogram showing the important peak parameters. (b) Cyclic voltammetry waveform.

If a redox system remains in equilibrium throughout the potential scan, the redox process is said to be reversible (equilibrium requires that the surface concentrations of O and R are maintained at the values required by the Nernst equation). The following parameter values are used to characterize the cyclic voltammogram of a reversible process:

a) the peak potential separation ΔE_p (= E_{pc} - E_{pa}) = 58/n mV at all scan rates at 25 $^{\circ}$C.

b) the peak current ratio = i_{pa}/i_{pc} = 1 at all scan rates

c) the peak current function $i_p/v^{1/2}$ (n = scan rate) is independent of v (see equation for peak current)

The peak current is given by the equation:

$$i_p = 2.69 \times 10^5 n^{3/2} ACD^{1/2} v^{1/2}$$

where: n = number of electrons transferred/molecule

A = electrode surface area (cm^2)

C = concentration (mol cm^{-3})

D = diffusion coefficient ($cm^2 s^{-1}$)

In this dissertation, the electrochemically measured redox behaviour can be analyzed to estimate the ionisation potential I_p (oxidation) and electron affinity E_a (reduction). This knowledge about the energy levels of the polymer materials allows a useful first approximation for the design of organic light emitting devices or diodes. A necessary requirement is to know the energy levels of the polymers to understand the device operation and, in particular, the physics of charge-carrier injection, transport and radiative recombination, with the goal of improving electroluminescence efficiency.

For this reason it is necessary to relate the electrochemical potentials to the vacuum for which I_p and E_a are defined. An empirical relationship has been proposed by Brédas et al.[8] on the basis of a detailed comparison between valence-effective Hamiltonian calculations and experimental measurements. The expectation is that:

$$I_p = (E'_{ox} + 4.4) \text{ eV}$$
$$E_a = (E'_{red} + 4.4) \text{ eV}$$

where E'_{ox} and E'_{red} are the onset potentials for oxidation and reduction relative to an Ag/AgCl reference electrode, respectively. These potentials are clearly defined in Figure 8.3.2(a) by the step changes in cell current. The use of onset potentials rather than peaks gives values that represent the minimum I_p and maximum E_a for the inhomogeneous ensemble of polymer chains present in a typical sample.[9]

In this Ph.D. thesis, samples were measured using an Autolab PGSTAT30 (Eco Chemie) Potentiostat/Galvanostat. Pt-wire and Ag/AgCl were used as the counter and reference electrodes, respectively. Polymer films coated on ITO-coated glass and carbon glassy electrode were used as the working electrodes and 0.1 M tetrabutylammonium tetrafluoroborate (TBABF$_4$) in acetonitrile was used as the electrolyte.

8.4. References

(1) (a) W. Knoll, *MRS Bulletin*, **1991**, *16,* 29. (b) A. Janshoff, H. J. Galla, C. Steinem, *Angew. Chem.* **2000**, *112*, 4164. (c) H. Raether, *"Surface Plasmons on Smooth and Rough Surfaces and on Gratings"*, Tracts in Modern Physics, Springer Verlag, Berlin, **1988**. (d) E. Burstein, W. P. Chen, Y. J. Chen, A. Hartstein, *J. Vac. Sci. Technol.*, **1974**, *11*, 1004. (e) B. Rothenhäusler, C. Duschl, W. Knoll, *Thin Solid Films*, **1988**, *159***,** 323.

(2) E. Kretschmann, *Z. Physik.* **1971**, *241*, 313.

(3) http://www.mpip-mainz.mpg.de/documents/akkn/index.html.

(4) http://www.resonant-probes.de

(5) D. Sarid, *Scanning Force Microscopy*, Oxford Series in Optical and Imaging Sciences, Oxford University Press, New York, **1994**.

(6) R. Wiesendanger, *Scanning probe microscopy: analytical Methods*, Springer, Berlin, **1998**.

(7) (a) David K. Gosser, Jr. "Cyclic Voltammetry, simulation and analysis of reaction mechanism', WILEY-VCH, 1993. (b) Nawaz, Tahir. *Ph.D. Thesis* Mainz, Germany, **2006**.

(8) J. L. Brédas, R. Silby, D. S. Boudreaux, R. R. Chance, J. Am. Chem. Soc. 1983, 105, 6555.

(9) S. Janietz, S. Anlauf, A. Wedel, *Macromol. Chem. Phys*. **2002**, 203, 433.

9. Appendix

9. 1. List of Figures

Figure 1.2.3. The electro- and photo-active building blocks for LBL assembly. (a) CuTsPc, (b) tpps$_4$, (c) CoTsPc, (d) PyC$_6$BPC$_6$Py, (e) NC$_6$BPC$_6$N, (f) PVP-Os, (g) PSS, (h) PAPSAH, (i) DAR, (j) PAH, (k) PAA, (l) SNAN, (m) BST and (n) Pr.

Figure 1.3.1. (a) Schematic representation of an absorption/ transmission-type device. (b) Percent transmittance spectra of an absorption/transmission electrochromic device composed of the complementary polymers PProDOT-Me$_2$ and N-PrSPProDOP. (J. R. Reynolds, *Chem. Mater.* **2004**, 16, 4401)

Figure 1.3.2. (a) Spectroelectrochemistry of (PXV/PEDOT:SPS)$_{40}$. Spectra were taken from 0.5 V to -0.9 V. (b) Potential step absorptometry of PXV/PEDOT:SPS films. Films of 20-, 30-, 40-, 50-, and 60-layer pairs were tested, corresponding to plots (a)-(e), respectively.

Figure 1.3.3. (a) Multilayer structure of OLED. (b) Electron and hole recombination process.

Figure 1.3.4. Light–voltage and current–voltage curves obtained from light emitting devices of ITO / (SPS/PPV)$_{20}$ / Al(top), ITO / (PMA/PPV)$_{20}$ / Al(middle), and ITO / (SPS/PPV)$_5$ / (PMA/PPV)$_{15}$ / Al (bottom).

Figure 3.1. Polarizing microscopy image of (a) A thermotropic phase of **P1** (163 °C) and (b) a lyotropic phase of **P3b** (50 °C) with ethylene glycol.

Figure 3.2. (a) Molecular model structure with distance of **P2** by using Chem 3D Ultra 7.0. (b) X-ray scattering diagram of **P1** (homopolymer) and **P2** (anionic LC ionomer) in bulk state (using Ni-filtered Cu KR radiation, λ = 1.54 Å). (c) Schematic representation of the smectic bulk structure of **P1** and (d) **P2**. (e) Interdigitated layer structure present in the multilayer.

Figure 3.3. Multilayer build-up from LC-ionomer **P2**. (a) UV/VIS spectra measured during the multilayer build-up of **P2** and PCM by solution-dipping. (b) Growth of the solution-dipping films at 267 nm. (c) Comparison of the growth of the multilayer films assembled by solution-dipping (●) and spin-coating (▲)

Figure 3.4. Tapping mode AFM images of 12 double layers of **P2** and PCM multilayer films prepared by (a) The solution-dipping method and (b) The spin-coating method

Figure 3.5. (a) Angular dependent SPR curves after different deposition cycles of the LC polymer **P2** and PCM by the solution-dipping method. (b) The film thickness according to the number of bilayers.

Figure 3.6. (a) X-ray reflectivity of different multilayer films: (a-1) basis double layer prepared with PEI and PAMPS; (a-2) 16 bilayers sample with **P2**/PCM prepared by the solution-dipping method; (a-3) annealed solution-dipping sample for 12 h

at 150 °C; (a-4) 16 bilayers sample with **P2**/PCM prepared by the spin-coating method. k_{z0} is the vertical component of the incident photons in a vacuum. (b) Patterson function of samples shown in (a). In (a) and (b), the curves are shifted vertically for clarity.

Figure 3.7. (a) Geometry scheme for the angular dependent UV/VIS measurement with unpolarized light, i.e., light polarized within the paper plane and perpendicular. Note that the absorption of light polarized perpendicular to the paper plane should not vary while changing the angle Θ. (b) Results of angular dependent UV/VIS measurement of 12 bilayers consisting of **P2** and PCM prepared by the solution-dipping method and (c) By the spin-coating method. For comparison of the both spectra the absorption perpendicular to the substrate A⊥ was subtracted. ▲: primary data; ●: after thickness correction by factor *d*.

Figure 4.1. (a) UV/VIS spectra of triarylamine, oxadiazole, thiadiazole, and triazine polymers **P1-P8** in solution of THF: H_2O = 5:1 mixture solvents (b) Cyclic Voltammograms of multilayer films from **P1-P8** at a scan rate of 20 mV/s. (onset: reduction behaviors of **P5-P8**, in detail procedure of the multilayer build-up will discuss later).

Figure 4.2. Energy band diagram of **P1-P8**.

Figure 4.3. (a) Multilayer build-up from **P1**/PCM film (Inset: The growth of the multilayer films assembled by the spin-coating method at 308 nm). (b) Multilayer build-up from **P5**/**P8** film (Inset: The growth of the multilayer films assembled by the spin-coating method at 299 nm)

Figure 4.4. Multilayer build-up from **P1**/PCM. (a) Cyclic Voltammograms of sequential bilayer deposition, from 2-10 bilayer, at a scan rate of 20 mV/s, between 0 V and +1.6 V. (b) The peak current vs. the number of bilayer deposited on ITO-coated glass substrate.

Figure 5.1. Cyclic voltammograms of triarylamine polymers measured on Pt-working electrode (with 0.1 M TBABF$_4$) at 20 mV/s. (a) Unsubstituted triarylamine polymer, **P1** (b) p-substituted triarylamine polymer, **P3**.

Figure 5.2. Multilayer build-up from a **P1**/PCM film (a) The growth of the multilayer films assembled by the spin-coating method at 308 nm (b) Cyclic voltammograms of sequential bilayer deposition, from 2-10 bilayers, at a scan rate of 20 mV/s, between 0 V and +1.6 V (Inset: The peak current vs. the number of bilayer deposited on ITO-coated glass).

9. 2. List of Schemes

Scheme 3.1. Synthesis of the Mesogen-Containing Primary Amine.

Scheme 3.2. Structures of Mesogen-Containing Polymers (s: Smectic Phase; i: Isotropic Phase).

Scheme 4.1. Synthetic route to the p-type and n-type semiconducting polyelectrolytes **P1-P8**.

Scheme 5.1. Synthetic route to the electrochromic Polyanions **P1-P4**.

Scheme 6.1. Triarylamine Polymers **P1-P2** and precursor PPV.

9. 3. List of Tables

9. 4. List of Abbreviations

AFM	Atomic force microscopy
Al	Aluminum
Alq$_3$	Aluminum tris(8-hydroxyquinoline)
Ag / AgCl	Silver-Silver chloride
a.u.	Arbitrary units
Å	Angstrom
A$_{ll}$	"parallel absorbance" (UV/VIS sepctroscopy)
A$_\perp$	"perpendicular absorbance" (UV/VIS sepctroscopy)
CE	Coloration efficiency
cm	Centimeter
CV	Cyclic voltammetry
d	Layer thickness (X-ray reflexion)
d	Correction factor (angle dependent UV/VIS sepctroscopy)
δ	Chemical shift (NMR-Spectroscopy)
DSC	Differential scanning calorimetry
DMF	N,N-Dimethylformamide
DMSO	Dimethylsulfoxid
EL	Elecroluminescence
eV	Electron volt
E$_g$	Energy band gap
E$_{ox}$	Oxidation potential (Cyclic voltammetry)
E$_{red}$	Reduction potential (Cyclic voltammetry)
ECs	Electrochromics
ESA	Electrostatic self-assembly
ETL	Electron transport layer
GPC	Gel permeation chromatography
HOMO	Highest Occupied Molecular Orbital
HTL	Hole transport layer
h	Hour
i	Isotropic Phase
ITO	Indium tin oxide

IR	Infrared (-Spectroscopy)
J	Coupling constant (NMR-Spectroscopy)
J	Luminous efficiency-current density (OLED)
k	Crystalline Phase
λ	Wavelength
LUMO	Lowest Unoccupied Molecular Orbitals
LBL	Layer-by-layer
LC	Liquid crystalline
Mn	Molecular weight, number average
Mw	Molecular weight, weight average
min	Minute
M	mol/l
ml	Milliliter
NMR	Nuclear magnetic resonance
NLO	Nonlinear optical device
nm	Nanometer
NMP	N-methylbutylactam
OLED	Organic light emitting diode
ΔOD	Optical density
PAMPS	Poly(2-acryloylamino-2-methylpropyl sulfonate sodium salt)
PCM	Poly(choline methacrylate)
PEI	Poly(ethylene imine)
PEDOT	Poly(3,4-ethylenedioxythiophene)
PAA	Poly(allylamine)
PDI	Polydispersity index
PPV	Poly(phenylenevinylene)
PSS	Poly(styrenesulfonate)
PL	Photoluminescence
ppm	„parts per million" (NMR-Spectroscopy)
Pt-wire	Platinum-wire electrode
Q$_E$	Quantum efficiency (OLED)
RT	Room temperature
s	Smectic Phase
s	Second

S	Order parameter
SPR	Surface plasmon resonance
TBABF$_4$	Tetrabutylammonium tetrafluoroborate
TGA	Termogravimetric analysis
TLC	Thin layer chromatography
t	Deposition time
θ	Incident angle (X-ray reflexion)
THF	Tetrahydrofuran
ΔT	Transmittance differences
UV/VIS	Ultraviolet-visible (-spectroscopy)
XRR	X-ray reflectometry

Curriculum vitae

Personal Data

Name	Kyungsun Choi
Date of Birth	12.06.1978
Place of Birth	Seoul, Korea
Marital status	single

Education und experience

March. 1985 – February 1991	Myungwon Elementary School
	Seoul, Korea
March. 1991 – February 1994	Myungil women's Middle School
	Seoul, Korea
March. 1994 – February 1997	Myungil women's High School
	Seoul, Korea
March. 1997 – February 2001	Chung-Ang University
	Seoul, Korea
	B.S. Chemistry
March. 2001 – February 2003	Seoul National University
	Seoul, Korea
	M.S. Organic Chemistry
June. 2003 – present	Institute of Organic Chemistry
	Johannes Gutenberg University
	Mainz, Germany
	Promotion in Chemistry